Genetic analysis and *in vivo* imaging of vascular development in the zebrafish

Genetische analyse en *in vivo* visualisatie van de vaatontwikkeling in de zebravis
(met een samenvatting in het Nederlands)

Proefschrift

ter verkrijging van de graad van doctor aan de Universiteit Utrecht op gezag van de rector magnificus, prof.dr. J.C. Stoof., ingevolge het besluit van het college voor promoties in het openbaar te verdedigen op woensdag 18 november 2009 des morgens te 10.30 uur

door

Jeroen Bussmann

geboren op 6 september 1981
te Eindhoven

Promotor: Prof. Dr. H.C. Clevers

Co-promotor: Prof. Dr. S.Schulte-Merker

The research described in this thesis was performed at the Hubrecht Institute of the Royal Netherlands Academy of Arts and Sciences (KNAW), within the framework of the Graduate School of Cancer Genomics and Developmental Biology in Utrecht, the Netherlands.
This work was financially supported by the Stichting Vrienden van het Hubrecht and a PhD followship from the Boehringer Ingelheim Fonds.

Contents

Chapter 1	General Introduction	5
Chapter 2	*ccm1* Cell Autonomously Regulates Endothelial Cellular Morphogenesis and Vascular Tubulogenesis in zebrafish	19
Chapter 3	Early Endocardial Morphogenesis Requires *tal1*	33
Chapter 4	*In vivo* Imaging of Endothelial Diversity in Transgenic Zebrafish	55
Chapter 5	*ccbe1* is Required for Embryonic Lymphangiogenesis and Venous Sprouting	71
Chapter 6	General Discussion	81
	References	87
	Samenvatting	93
	Dankwoord	96
	Curriculum Vitae	98
	List of Publications	99

Chapter 1

General Introduction

Abstract

The circulatory system is one of the major organ systems required for maintaining homeostasis in humans. It's main functions are the transport of nutrients, gases, signaling molecules and cells to and from tissues to maintain an array of body parameters including tissue oxygen levels, temperature, and to help fight diseases. The circulatory system consists of two major components distributing two types of body fluids. The first is the cardiovascular system, consisting of the heart, the blood and blood vessels (arteries and veins) which distributes blood. The second is the lymphatic system, consisting of lymph, lymph nodes and lymphatic vessels which distributes lymph. Both systems consist of an extensive tree-like network of tubes, lined by a specialized cell-type, the endothelial cells.

Malformation or malfunction of the blood or lymphatic network contributes to the pathogenesis of many diseases. For example, insufficient blood supply due to vessel blockage can cause ischemia as occurs during a heart attack or stroke. Also, tumors attract blood vessels for their oxygen and nutrient supply and can infiltrate the lymphatic vessels to metastasize to lymph nodes. Since the adult blood and lymphatic endothelial networks are largely quiescent and get activated only in pathological situations, the ability to promote or reduce their growth is an attractive mechanism to interfere with disease progression with little effect on normal physiology.

During recent years, the zebrafish has emerged as an important and instructive model organism for studying development of the vertebrate circulatory system. The excellent optical transparency of the zebrafish embryo allows direct visualization of blood and lymphatic vessels as they develop *in vivo*. Because of the small size of zebrafish embryos, enough oxygen is received through passive diffusion to continue to survive and develop a relatively normal vascular network in the complete absence of blood circulation. The large brood sizes and short generation time combined with a high tolerance for heterozygous mutations permits the use of genetic screens to identify genes that are required for vascular development. Since many of the genes essential for embryonic vascular development are required for the activation of vessel growth in adult pathology, identifying new genes involved in vascular development, or understanding the interactions between known genes will allow the development of new drugs that target these genes in order to inhibit or promote vessel formation.

Here, the architecture of the zebrafish circulatory system during embryonic development will be described briefly. An overview will be provided of the methods that are used to analyse the development of the circulatory system in the zebrafish. Finally, a summary

will be given of the genes that are required for zebrafish vascular development, identified from forward genetic screens.

Anatomy of the zebrafish circulatory system

In this section, a brief overview of the development of the circulatory system will be given. Special emphasis will be placed on the early development of the blood vascular endothelium.

Initial stages in the formation of the blood vessel system

The endothelial cells that line all blood vessels originate during gastrulation, and as in other vertebrates arise from the lateral plate mesoderm [1]. During early developmental stages these presumptive endothelial cells are commonly referred to as angioblasts. The angioblasts in the early zebrafish embryo are located in two domains: the posterior angioblasts that will give rise to the trunk and tail vasculature and the anterior angioblasts that will give rise to the head vasculature. In a process called vasculogenesis – the *de novo* formation of blood vessels - the posterior angioblasts form the first blood vessels of the embryo: the dorsal aorta (DA), the posterior cardinal vein (PCV) and the duct of Cuvier (DC). At the same time, the anterior angioblasts give rise to the first head vessels, the lateral dorsal aortas (LDA) and the first aortic arches (AA1), which connect the first blood vessels to the heart. As the heart starts to beat, the LDAs grow posterior and connect to the DA to establish the first circulatory loop in the embryo (around 24 hours post fertilization, hpf). Blood cells can now be seen to circulate from the heart, through the aortic arches into the LDA and later the DA. In the tip of the tail, the blood cells make a U-turn into the PCV, which returns the blood back to the heart through the DC. The connection between the DC and the heart over the yolk is initially not lined by endothelial cells (Figure 1A).
The second circulatory loop that arises around 28hpf provides blood supply to the head. From the first aortic arch, vessels form anteriorly to give rise to the primitive internal carotid artery (PICA) which connects to the first head vein, the primordial mid- and hindbrain channel (PMBC and PHBC). This vein connects to the Duct of Cuvier and directs blood back from the head to the heart.

The trunk blood vessels

The two initial circulatory loops arise largely through vasculogenesis from angioblasts. After these are established, the remainder of the blood vascular system arises mainly through angiogenesis – the formation of blood vessels from pre-existing vessels, usually

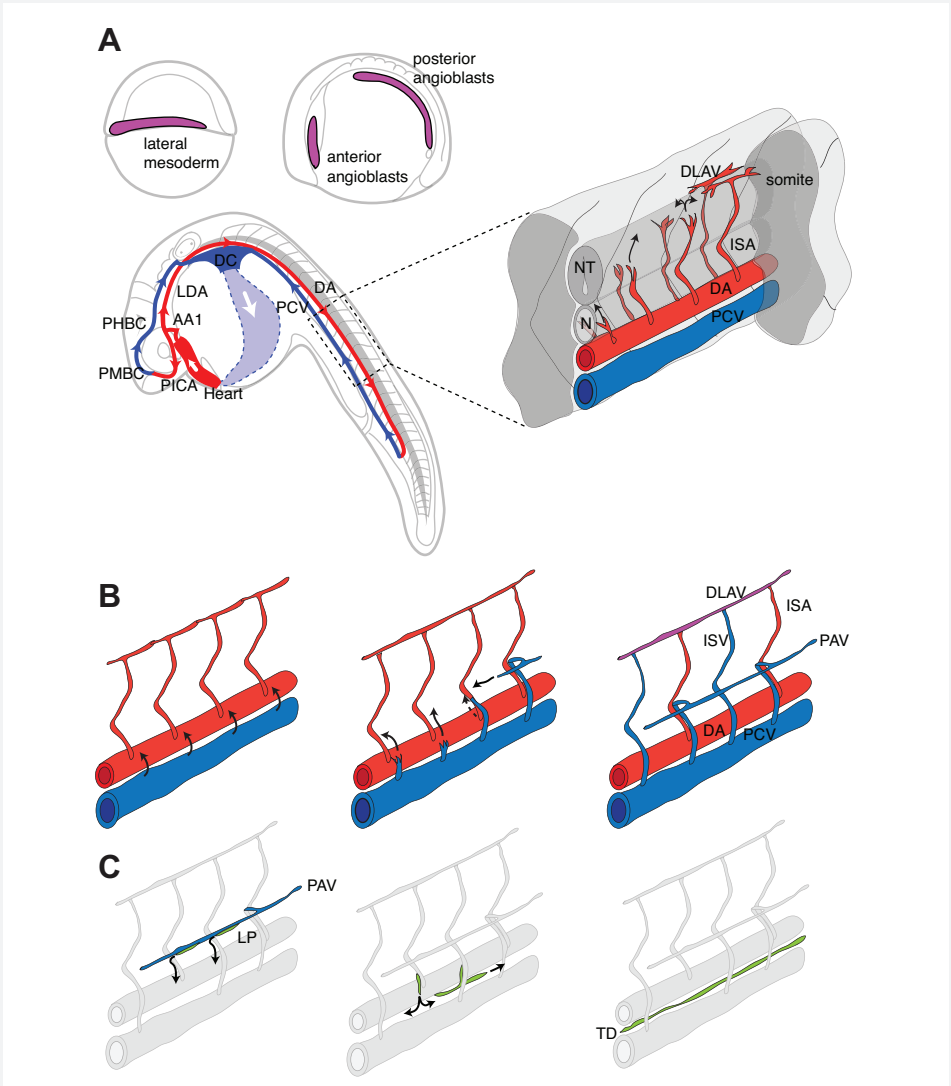

Figure 1. Angiogenesis and lymphangiogenesis in the zebrafish embryo. A. Vasculogenesis and primary angiogenesis (5-36hpf). Endothelial cells originate from precursors in the lateral mesoderm at 5 hpf (Top left). These precursors are separated in two populations at 12hpf (middle), which migrate to the midline and form the first vessels of the zebrafish embryo (bottom). During primary angiogenesis, sprouts emerge from the dorsal aorta (DA) and form the first vascular network in the trunk (bottom right). **B.** Secondary angiogenesis (36-60hpf). Sprouts emerge from the posterior cardinal vein (PCV) and either form a connection with a pre-existing intersegmental vessel, or form the parachordal vessel (PAV). **C.** Lymphangiogenesis (60-96hpf). The first lymphatic precursors (LP) emerge from the parachordal vessel and migrate along an intersegmental blood vessel to form the first lymphatic vessel in the trunk, the thoracic duct (TD).

associated with sprouting of endothelial cells. A good example of angiogenic sprouting can be seen in the trunk and tail [2]. Here, sprouts emerge bilaterally from the DA at every somite, or segment to form the intersegmental arteries (ISAs). These grow to the dorsal side of the embryo, T-branch and connect to each other to form the dorsal longitudinal anastomotic vessel (DLAV) (Figure 1B). This process is defined as primary angiogenesis – the sprouting of arterial blood vessels - and results in a network composed entirely out of arteries. This network is not very efficient in providing equal blood flow through every segment. Therefore, it is remodeled by venous angiogenic sprouts emerging from the PCV in a process called secondary angiogenesis – the sprouting of venous blood vessels. These sprouts emerge from the PCV at every segment in the trunk, but only every second one connects to an ISA. This connection results in the detachment of the ISA from the DA at its most basal part, and consequently, the ISA is converted into an intersegmental vein (ISV). The angiogenic sprouts from the PCV that do not connect to the ISAs have been suggested to form a different vessel, the parachordal vessel (PAV). The trunk vascular network has become an important model system for the visualization of angiogenic sprouting, since it is very simple, involving only 3 to 4 cells per intersegmental vessel, allows easy imaging and is very stereotypic, allowing quantitative analysis of angiogenesis *in vivo*.

The lymphatic vascular system

The existence of a lymphatic vascular system in fish has been a subject of much debate. Morphological studies in the 18th century suggested the existence of lymphatic vessels in fish [3], but these observations have been challenged by the characterization of a so-called secondary vascular system [4]. Direct connections between presumed lymphatic vessels and the arteries of the blood vascular system, combined with the observation of erythrocytes circulating through these vessels [5] have led to suggestion that fish do not possess a functional lymphatic system. The relationships between the secondary vascular system and the lymphatic system of higher vertebrates have been unclear. Recently however, the embryonic development of the first lymphatic vessel in the zebrafish, the thoracic duct (TD) has been described [6,7]. Formation of the TD shares morphological characteristics and molecular requirements with the development of the mammalian TD. Moreover, this vessel is functionally defined as a lymphatic vessel, since it serves to absorb macromolecules from the interstitium.

The TD develops in a process called lymphangiogenesis from cells that have been reported to bud from the PAV and to migrate along intersegmental vessels ventrally to the dorsal aorta (Figure 1C) [6]. Here, extensive proliferation and migration combined with fusion of various TD fragments leads to the formation of a patent TD. Lymphatic vessels also arise in the head, connect to the TD and drain lymph into the jugular vein. The mammalian

lymphatic system also drains into the jugular vein, lending further support to the existence of an evolutionary conserved lymphatic system in fish.

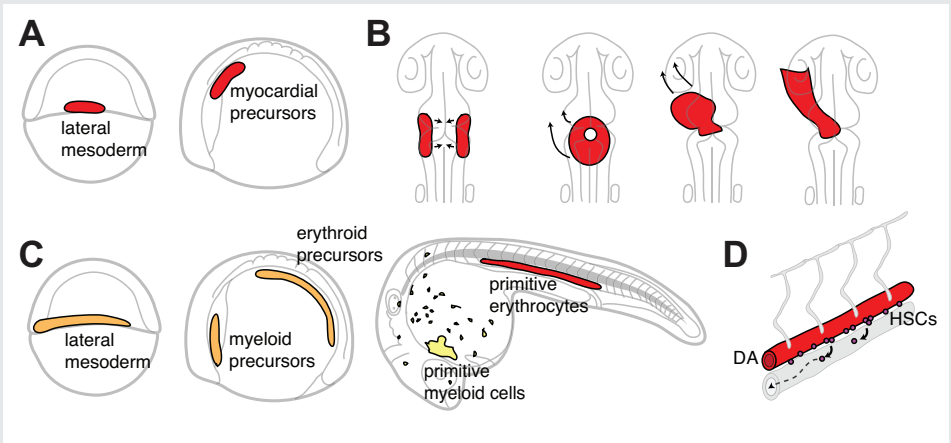

Figure 2. Formation of the heart and blood in the zebrafish embryo. A. Myocardial precursors originate from the lateral plate mesoderm at 5hpf (left) and form bilateral precursors at 12hpf (right). **B.** These precursor populations migrate to the midline to form a disc, and then start migrating to the left side of the embryo to form the primary heart tube. **C.** Blood precursors originate from the same locations within the lateral mesoderm as the angioblasts (left). The anterior population at 12hpf (middle) will give rise to myeloid cells at 24hpf (right), while the posterior population will give rise to erythroid cells. **D.** The hematopoietic stem cells (HSCs) that give rise to the blood cells of the larval and adult zebrafish arise from the ventral wall of the dorsal aorta , from which they enter the circulation and migrate to the various hematopoietic organs of the zebrafish.

The heart

Initially, the heart is composed of only two cell types, an inner endothelial layer called the endocardium, and an outer muscular layer called the myocardium. The myocardium arises from the lateral mesoderm, between the anterior and posterior angioblast precursors. These bilateral myocardial populations migrate to the midline and fuse to form a cardiac disc. After fusion, the cardiac dis elongates and rotates to the left to form a simple tube (Figure 2A). This tube starts to contract rhythmically at 22hpf, and functions as a suction pump. The opening of blood vessel lumens around this stages leads to the establishment of blood circulation around 24hpf [8]. The interactions between the endocardium and myocardium result in the formation of heart valves at the boundaries of the heart chambers [9], but other than that, little is known about the early development of the endocardium in the zebrafish.

The blood cells

During development, blood formation occurs in two separate waves. The first wave, called primitive hematopoiesis, gives rise to a transient population of erythroid and myeloid cells that provide oxygenation and antimicrobial defense to the early embryo [10]. Primitive hematopoietic precursors arise from the same cell populations in the lateral mesoderm that also give rise to the endothelial cells and recent fate-mapping studies have established that they are indeed derived from a common progenitor [11]. Similar to the angioblasts, the primitive hematopoietic precursors are divided in an anterior and a posterior domain. The anterior domain gives rise exclusively to primitive myeloid cells, whereas the posterior domain only gives rise to primitive erythroid cells. The second wave, definitive hematopoiesis, is associated with the development of the first multipotent hematopoietic stem cells (HSCs). These specialized cells give rise to all of the diverse adult blood types. In the zebrafish, as in other vertebrates, the first cells with definitive hematopoietic potential are associated with the ventral wall of the dorsal aorta. HSCs in the zebrafish enter the circulatory system through the PCV from which they migrate to the various hematopoietic organs [12](Figure 2B).

Methods to analyze the zebrafish circulatory system

Since the zebrafish is optically transparent, the heart and circulating blood cells can be directly observed. Therefore, several observations can be made *in vivo* via conventional light microscopy. The vasculature can be easily visualized in fixed embryos by taking advantage of the high endogenous alkaline phosphatase (AP) activity of zebrafish endothelial cells. Detection of marker gene expression through RNA *in situ* hybridization allows the identification of separate endothelial lineages [13].

In order to visualize the circulatory system more specifically, various techniques have been developed. Traditionally, angiography has been widely used in the morphological analysis of the circulatory system. Dyes can be injected into a vessel and are quickly distributed throughout the vascular system. By using a fluorescent dye, this approach can be combined with confocal microscopy to obtain a high-resolution 3-dimensional image of the vascular system. This method has been used in the zebrafish to obtain a complete morphological description of blood vascular development [14]. More recently, this method has been adapted to visualize the zebrafish lymphatic system [6,7].

Although angiography is a powerful method, it has several inherent limitations. Angiography only permits visualization of the vessel lumen, but not of the endothelial cells, and therefore sprouting, migration and formation of cellular connections remain undetectable. Also, lumen formation only occurs after correct vascular connections have been

Table 1. Overview of zebrafish transgenic lines for visualizing the circulatory system.

Construct	Lines generated	Expression	Other expression
fli1a promoter	*fli1a:gfp* [15] *fli1a:nls-gfp* [19]	All endothelial cells	pharyngeal mesoderm
kdrl promoter	*kdrl:gfp* [20,21,22] *kdrl:mem-rfp* [23] *kdrl:nls-gfp* [24]	All endothelial cells*	hindbrain
lmo2 promoter	*lmo2:gfp* [25] *lmo2:rfp* [25]	All endothelial cells	erythrocytes
Mouse *tie2* promoter	*tie2:gfp* [26]	All endothelial cells, heart valves	-
gata1 promoter	*gata1:gfp* [27] *gata1:rfp* [28]	-	erythrocytes
myl7 promoter	*myl7:gfp* [29] *myl7:rfp* [30]	-	myocardium
spi1 promoter	*spi1:gfp* [31]	-	myeloid cells

*not expressed in lymphatic endothelial cells (see Chapter 5)

established. In addition, because the dyes employed are cleared from the system relatively rapidly, this method is not suitable to visualize vessel development over time. To get aruound these limitations, several transgenic zebrafish lines have been developed that allow direct visualization of the different cellular lineages that comprise the circulatory system (Table 1). In general these lines employ a promoter fragment of a marker gene that is expressed in a given cellular lineage to drive the expression of a fluorescent protein [green or red fluorescent protein (GFP/RFP)]. For example, the endothelial-restricted *fli1a* and *kdrl* promoters have been used to specifically label endothelial cells throughout the embryo [15,16]. This represents the first vertebrate system in which vascular development can be visualized at the cellular level in a developing embryo, and has led to important observations on general mechanisms of vascular development, such as the formation of a vascular lumen [17] , and the lineage relation of hematopoietic and vascular endothelial cells [11].

Other lineages that can be visualized include the myocardium of the heart, red blood cells and the definitive hematopoietic stem cells. By combining various lines, the developing endothelial cells can be observed in relation to other tissues. For example, the combination of *kdrl:gfp* and *gata1:rfp* allows the simultaneous visualization of endothelial and circulating red blood cells, which can be used to identify forming, but not yet functional blood vessels [18].

Genetic analysis of vascular development

The ability to perform large-scale forward genetic screens is one of the prime advantages of the zebrafish as a vertebrate model system. The main reasons for this opportunity are the large number of animals that can be maintained at relatively low cost, the large numbers of progeny that are obtained and the external embryonic development. Large-scale mutagenesis screens have already resulted in the identification of thousands of genes involved in various aspects of development [32,33]. The most widely used method to create randomly mutated genomic DNA is treatment of adult males with N-ethyl-N-nitrosourea (ENU). This results in heterozygous mutations in spermatogonial stem cells, which are transmitted to the next generation. Two rounds of crossing are set up, which results in the generation of homozygous mutant embryos, which can be screened for visible phenotypes. The next step is the positional cloning of the induced point mutations, which is still a very time-consuming process. Several zebrafish mutants with defects in vascular development have been identified in forward genetic screens that use light microscopy to identify morphological phenotypes More recently, several targeted screens have been performed that use transgenic lines (*fli1a:gfp* and *kdrl:gfp*) or detection of AP activity to specifically screen for defects in vascular development [34-36] (See Table 2). These screens were large-scale efforts in which mutants were identified with defects in the development of the vascular system. Subsequent analysis of the recovered mutant phenotypes allowed the characterization of several phenotypic classes, which allowed the genetic analysis of several aspects of vascular development. Several of these classes are discussed below.

Arteriovenous differentiation

One of the largest phenotypic classes identified in forward genetic screens is the class with defects in the differentiation of arteries and veins. Although it was previously thought that the formation of arteries or veins was mainly regulated by blood flow patterns, it has become clear that at least the initial separation of arterial and venous endothelial cells occurs prior to the onset of blood circulation, and that this is regulated genetically [1]. Identification of the genes affected in several zebrafish mutants has allowed the identification of the signaling pathways involved. More specifically, genes involved in the Hedgehog, the vascular endothelial growth factor (VEGF) and the Delta/Notch signaling pathways have been found to be required for arteriovenous differentiation. All three pathways involve signaling by a ligand (Sonic Hedgehog, VEGF-A and Delta-like proteins) to a transmembrane receptor (Patched/Smoothened, VEGF-receptors and Notch proteins, respectively) and subsequent regulation of transcription (Gli, Ets/Fox and Su(H) transcription factors, respectively). Epistasis experiments have shown a relatively linear pathway, in which *shh*

Table 2. Overview of cloned zebrafish vascular mutants

Phenotypic class and affected gene	#	SM	Phenotypes	Reference
A/V differentiation and angiogenesis				
Signal peptide, CUB domain, EGF-like 2 (scube2)	4	M	Defects in A/V differentiation and angioblast migration	[33]
Gli-kruppel family member 2a (gli2a)	4	M, K	Defects in A/V differentiation and angioblast migration	[33,35,37]
Sonic hedgehog a (shha)	6	M	Defects in A/V differentiation and angioblast migration	[33,37]
Smoothened (smo)	8	M	Defects in A/V differentiation and angioblast migration	[50]
Phospholipase C gamma 1 (plcg1)	9	F	Defects in A/V differentiation	[32,34,38]
Kinase insert domain receptor-like (kdrl)	5	A, F	Reduced angiogenesis	[36,38]
Hairy/enhancer of split with YRPW motif 2 (hey2)	2	M	Defects in A/V differentiation	[32,51,52]
Delta-like 4 (dll4)	1	M	Excessive angiogenesis	[53]
Mind bomb (mib)	7	M	Defects in A/V differentiation, excessive angiogenesis	[39,53,54]
Vessel patterning				
Plexin D1 (plxnd1)	5	M, K, F	Disorganized vessel patterning	[35,38,41,55]
unc-45 homolog A (unc45a)	1	M	Defects in gill vascular patterning	[33,43]
Seryl-tRNA synthetase (sars)	4	K	Defects in gill vascular patterning	[18,35,56]
EC proliferation				
Activin A receptor type II-like (acvrl1)	3	M, K, F	Increased EC number	[19,35]
Vessel stability				
Integrin-linked kinase (ilk)	2	M	Vessel instability, hemorrhage	[46]
Rho guanine nucleotide exchange factor 7b (rhogef7b)	2	M	Vessel instability, hemorrhage	[32,48]
p21-associated kinase 2a (pak2a)	1	M	Vessel instability, hemorrhage	[47,48]
EC survival				
Baculoviral IAP repeat containing protein 2 (birc2)	2	K	Increased endothelial apoptosis	[35,49]

#: number of identified alleles; SM: screening method (M: light microscopy, K: *kdrl:gfp* transgenic line, F: *fli1a:gfp* transgenic line); A/V: arteriovenous

expression from the midline induces the expression of *vegfa* in the somitic mesoderm. *Vegfa* in turn regulates the migration of angioblasts and expression of Notch pathway genes in endothelial cells leading to the differentiation of arterial and venous ECs [37]. Interestingly, VEGF and Notch signaling also have an opposing role in regulating sprouting angiogenesis, also identified in mutants. Whereas VEGF signaling inhibition leads to a

reduction of angiogenesis [38] the opposite is the case for inhibition of Notch signaling, which leads to an increase in angiogenesis [39]. This suggests combined regulation of arteriovenous differentiation and sprouting angiogenesis [40].

Vessel patterning and proliferation

Several mutants have been identified with defects in vessel patterning. Trunk intersegmental vessels, for example follow tightly regulated paths along the somite boundaries. In mutants for the *plexinD1* gene this patterning is disturbed [41]. PlexinD1 is a receptor for the Semaphorin class of extracellular ligands. Semaphorins are repellants that guide blood vessels by pathway exclusion. Regulation of vascular patterning by Semaphorin/Plexin signaling appears a general mechanism in several vascular beds [42]. In contrast, some of the mutants have restricted defects in gill vascular development [18,43].

The formation of new blood vessels through angiogenesis is usually associated with endothelial cell proliferation. A mutation in the zebrafish ortholog of *activin-receptor receptor like 1 (acvrl1)* indicated that endothelial cell proliferation is tightly regulated [19]. Endothelial cell number is increased in *acvrl1* mutants, implicating *BMP9/10* signaling [44] through *acvrl1* as a restrictive factor for endothelial proliferation. *ACVRL1* is mutated in the human disease hereditary hemorrhagic telangiectasia type II, and the mutants provide a zebrafish model for this disease [45].

Vessel stability and survival

The vertebrate circulatory system is closed and completely lined with endothelial cells. Disruption of the endothelial layer has dramatic consequences, as it exposes the basement membrane leading to the activation of the coagulation pathway. Alternatively, vessel disruption can cause bleeding (hemorrhage). Several mutants have been identified that show bleedings in various parts of the embryo. Usually, this is associated with vessel instability. The small caliber vessels in the brain are especially sensitive to vessel instability, causing the accumulation of erythrocytes in the brain ventricles. Three genes that when mutated cause this phenotype have been identified so far: *integrin-linked kinase (ilk)* [46], *p21 associated kinase 2a (pak2a)* [47] and *rho guanine exchange factor 7 (arhgef7)* [48]. These genes are involved in the regulation of cell-adhesion and cytoskeleton reorganization. Alternatively, vessel disruption can be caused by endothelial cell death. Mutation of the apoptosis regulator *baculoviral IAP repeat-containing 2* causes an increase in endothelial apoptosis and vessel disruption [49].

This overview of genes involved in vascular development in the zebrafish only includes mutants for which the causative gene has been identified. In this thesis, positional clon-

ing and analysis of 3 additional mutant zebrafish lines are described. Using a combination of *in vivo* imaging and genetics, several novel insights into the development of the circulatory system are provided.

Outline of this Thesis

In **Chapter 2**, we report the identification and characterization of the zebrafish mutant *t26458*. These mutants display dilation of blood vessels throughout the embryo. We show that the phenotype is due to a mutation in *cavernous cerebral malformation 1 (ccm1)*. This gene is associated with a human syndrome, which presents as a cerebral hemorrhage and dilated-vessel phenotype at multiple sites throughout the body. We show that the *ccm1* gene acts cell-autonomously in endothelial cells and is not associated with defects in arteriovenous differentiation.

In **Chapter 3**, we report the identification and characterization of the zebrafish mutant *t21384*. These mutants have a defect in arterial differentiation and hematopoiesis. The mutant phenotype is due to a mutation in *T-cell acute leukemia 1 (tal1)*. Over- or misexpression of *tal1* is a frequent cause of leukemia in humans. We show that *tal1* has an additional role during heart development. Development of the inner lining of the heart (the endocardium) is severely perturbed, and is associated with defects in cardiac morphogenesis.

In **Chapter 4**, we report the generation of a transgenic zebrafish line based on regulatory elements of the zebrafish VEGF receptor *flt1 (flt1^{enh}:rfp)*. This line differentially labels arterial, venous and lymphatic endothelial cells in embryonic and adult zebrafish. Interestingly, a fourth vessel type is identified in adults (lymph-arteries) with distinct *flt1^{enh}:rfp* expression levels. Lymph-arteries possibly represent the afferent component of the lymphatic vasculature in lower vertebrates.

In **Chapter 5**, we report the identification and characterization of the zebrafish mutant *full-of-fluid*. These mutants lack lymphatic vessels and have a defect in venous angiogenic sprouting. We show that the phenotype is due to a mutation in *collagen and calcium-binding EGF domain containing protein 1(ccbe1)*. This gene has no previous described role in (lymph) vascular development, and presents a novel candidate gene for human syndromes associated with defects in lymphangiogenesis. The transgenic lines described in chapter 4 are used to visualize lymphatic development in wildtype and mutant zebrafish.

This thesis is concluded in **Chapter 6** with a general discussion on the evolution of the vertebrate circulatory system

Chapter 2

ccm1 cell autonomously regulates endothelial cellular morphogenesis and vascular tubulogenesis in zebrafish

Benjamin M. Hogan[1], Jeroen Bussmann[1], Hartwig Wolburg[2] and Stefan Schulte-Merker[1]

Human Molecular Genetics 17(16): 2424-32 (2008)

[1]Hubrecht Institute, Developmental Biology and Stem Cell Research, Utrecht, The Netherlands
[2]Institut für Pathologie, Tübingen, Germany

Abstract

Cerebral cavernous malformations (CCMs) are a prevalent class of vascular anomalies characterized by thin-walled clusters of malformed blood vessels in the brain. Heritable forms are caused by mutations in CCM1, CCM2 and CCM3, but despite the importance of these factors in vascular biology, an understanding of their molecular and cellular functions remains elusive. Here we describe the characterization of a zebrafish embryonic model of CCM. Loss of *ccm1* in zebrafish embryos leads to severe and progressive dilation of major vessels, despite normal endothelial cell fate and number. Vascular dilation in *ccm1* mutants is accompanied by progressive spreading of endothelial cells and thinning of vessel walls despite ultrastructurally normal cell–cell contacts. Zebrafish *ccm2* mutants display comparable vascular defects. Finally, we show that *ccm1* function is cell autonomous, suggesting that it is endothelial cellular morphogenesis that is regulated by CCM proteins during development and pathogenesis.

Introduction

Cerebral cavernous malformation (CCM) is a prevalent disease characterized by enlarged thin-walled capillary clusters in the brain. Familial CCM is inherited as an autosomal dominant trait and in some populations can account for up to 50% of clinical presentation. Loss of function mutations in three genes, CCM1, CCM2 or CCM3, have been demonstrated to be responsible for familial CCM [57].

In vitro studies have shown that the three CCM proteins associate with each other in the same complex, which is associated with the cytoskeleton as well as with components of signal transduction pathways and the cell junctions [58-65]. Although *in vivo* analysis has been limited, Ccm1-deficient mice display vascular dilation phenotypes that strongly resemble the human disease. The dilations in Ccm1-deficient mice are associated with the loss of arterial gene expression and increased endothelial mitosis, suggesting that changes in cell fate or proliferation may contribute to CCM phenotypes and pathogenesis [66]. The zebrafish dilated-heart mutants *santa* and *valentine* have recently been shown to correspond to *ccm1* and *ccm2*, respectively [67], but a thorough analysis of the mutant vasculature remains to be reported and these mutants have yet to yield genuine mechanistic insights into CCM function.

Here we describe in detail the vascular phenotypes associated with the loss of Ccm1 in zebrafish. Zebrafish *ccm1* mutants display conserved progressive dilations of embryonic vessels, resembling both the murine and human CCM phenotypes. In contrast to previous findings in the mouse, these conserved vascular dilation phenotypes can occur independent of changes in cell number or cell fate. Vascular dilations are associated with specific

changes in cell shape although endothelial cell–cell contacts appear normal. Furthermore, *ccm1*, *ccm2* and *ccm1/2* double mutants displayed indistinguishable vascular phenotypes, implicating a conserved functional relationship. Finally, we demonstrate that the function of *ccm1* is autonomous to endothelial cells. This study identifies zebrafish *ccm1* as an endothelial specific regulator of cellular morphogenesis, implicating specific endothelial cellular morphogenesis defects in the dilation of CCM deficient vessels during development and pathogenesis.

Materials and methods

Zebrafish

All zebrafish strains were maintained in the Hubrecht Institute using standard husbandry conditions. Animal experiments were approved by the Animal Experimentation Committee of the Royal Netherlands Academy of Arts and Sciences (DEC). The *ccm1*^{t26458} allele was isolated in a genetic screen for ENU-induced mutations affecting vascular development [36]. Transgenic lines used were TG(*fli1a:gfp*)^{y1}, TG(*fli1a:nls-gfp*)^{y7} and TG(*kdrl:gfp*)^{s843} [15,19,21] (also known as *flk1*, *kdra* or *vegfr4,* see Ch.4). *ccm2*^{hi296} insertional mutants have been previously identified [68] and were a generous gift from Adam Amsterdam and Nancy Hopkins.

Meiotic Mapping and Sequencing

Bioinformatics construction of the genomic region and synteny analysis was performed using the Ensembl database (http://www.ensembl.org), release 44, April 2007. The chromosomal location of the *t26457* mutation was identified using standard simple sequence length polymorphism mapping. Subsequent genotyping of *ccm1*^{t26457} mutants was performed on individual embryos using the PCR primers: ccm1_ex5_fw and ccm1_ex5_rev. DNA sequencing was performed with the ccm1_ex5_fw primer.

Morpholino Oligos

The *ccm1* start codon targeting morpholino olgionucleotide (MO) was injected at a concentration of 1.25 ng/embryo. The *silent heart* MO [53] was injected at a concentration of 1 ng/embryo.

Whole-Mount In Situ Hybridization and Immunohistochemistry

In situ hybridization and immunohistochemistry using anti-GFP antibody (Torrey Pines Biolabs, http://www.chemokine.com/) were performed as previously described [69]. Cell counts in immuno-stained embryos were normalized between wt and mutant embryos by focusing on the region encompassed from the first SIV endothelial cell immediately posterior to the pectoral fin tip to the region where the yolk extension meets the yolk ball. Previously described probes used for in situ hybridization were: *notch3* [54], *dll4* [39,53], *hey2* [52], *ephrinB2* [54], *flt4* [70] and *dab2* [71]. *ccm1* probe was synthesized by first cloning a PCR fragment amplified from cDNA with primers EcoRI_ccm1_fw and XhoI_ccm1_rev into the EcoRI and XhoI sites of the pCS2+ vector [72] followed by in vitro transcription of RNA with T7 RNA polymerase (Promega) from EcoRI digested plasmid DNA. Vibratome sections were cut to a thickness of 250 µm using a HM650V vibratome (Microm). Filamentous actin was visualized with rhodamine phalloidin counter staining (Fluka) by incubation overnight at a 1/1000 dilution in phosphate buffered saline. Samples were mounted and imaged in Aquamount (BDH laboratory supplies).

Imaging

Embryos were mounted in 0.25% agarose in a six-well culture plate with a cover slip replacing the bottom of each well. Imaging was performed with a Leica TCS SP confocal microscope (Leica Microsystems, http://www.

leica-microsystems.com/) using a 10x or 40x objective with digital zoom. Scale is given as image width in the absence of distinct morphological features. The timelapse analysis was compiled using ImageJ software. Time points were recorded every 20 min for 24 h. A heated stage maintained the embryos at approximately 28.5°C. Movies of 3D reconstructions were made using the Volocity software package (Improvision). Analysis of *fli1a:nls-gfp* vessels including cell counting, distance to nearest neighbor and dorsal–ventral extent calculation was aided by the Volocity software package (Improvision) for object recognition, 3D reconstruction and distance calculations. Diameter calculations were made based on combined GFP z-stack and light (DIC) images to best observe the venous lumen. Cell counts in the PCV and CV using the *fli1a:nls-gfp* strain were normalized by imaging equivalent regions of each vessel and counting cells in a region of each vessel spanning three somite widths. Embryos for electron microscopy were fixed in 2.5% glutaraldehyde in 0.2 M cacodylate buffer.

Transplantation and microinjections

Transplantation was performed essentially as previously described [73]. Briefly, wild-type donor embryos of the genotype *fli1a:gfp* or *kdrl:gfp* were injected with 70 kDa Tetramethyl Rhodamine (TAMRA) (Molecular Probes) at the one cell stage and utilized as donors at pre-dome stages. Approximately 10–20 cells were transferred from donor to recipient embryos with recipient embryos utilized between sphere and 30% epiboly stages. Genotypes were inferred from phenotype at 48 h. Analysis of cell shape in mosaic mutant and wild-type vessels was performed using DNA injections of a construct consisting of approximately 6.5 kb of the previously described *kdrl* promoter [21] driving the expression of *tdTomato* [74] and flanked by I-SceI meganuclease recognition sites.

Results

The Vascular Morphogenesis Mutant t26458 Encodes ccm1/krit1

In a large-scale forward genetic screen [36], we identified a mutant which displayed normal vascular patterning but dramatic and completely penetrant vascular morphogenesis defects. This mutant failed to initiate circulation and starting from 32 hours post fertilization (h), dilation was observed in the primordial midbrain channel (PMBC) (Figure 1A,B) and the heart, with the caudal vein (CV) also showing severe morphogenesis defects and apparent dilation (not shown). At 50 h, severe prominent dilation of the sub-intestinal vessels (SIVs), dilation of the posterior cardinal vein (PCV) in the region dorsal to the sub intestinal vessels, as well as aberrant morphogenesis and dilation of the CV were observed in mutants (Figure 1C–H). Severe heart and vascular dilation was also observable using standard histological approaches (Supplementary Figure 1). Genetic mapping localized the mutation to a region containing 9 genes (Supplementary Figure 1). One gene in this region, *krit1/ccm1*, had been previously associated with vascular dilation phenotypes [57,66]. Sequencing of *ccm1* identified a cytosine to adenosine transversion mutating a tyrosine into a premature stop codon at a position corresponding to amino acid 237 of the protein (Figure 1I). In contrast to two previously reported alleles, which led to a small in frame deletion and a C-terminal premature stop codon retaining most functional domains [67], this mutant protein would lack almost all known functional domains (Figure 1I). The injection of a morpholino (MO) targeted to the *ccm1* start codon recapitulated the phenotypes observed, whereas the injection of a *silent heart* targeting MO [75], which inhibited

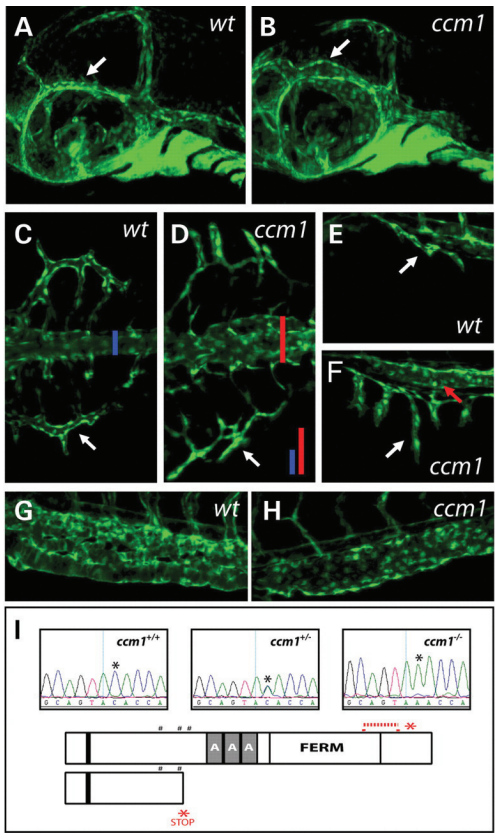

Figure 1. Phenotypes of *ccm1* mutants in the *fli1a:gfp* transgenic background analysed by confocal imaging. A,B. The PMBC (arrow) is dilated in ccm1 mutant but not wild-type embryos at 32 h. **C,D.** The SIVs (arrows) and trunk vasculature (coloured bars in C and D) are dilated and spread in *ccm1* but not wild-type embryos viewed dorsally at 50h. **E,F.** *ccm1* mutants viewed laterally reveal overgrown, dilated SIVs (white arrow) and dilated PCV (red arrow) by comparison with wild-type embryos. **G,H.** The CV is a single dilated tube in *ccm1* mutants at 50 h by comparison with the highly organized plexus of a wild-type CV. **I.** Sequence chromatograms (upper) spanning the *ccm1* mutation indicate representative wild-type, heterozygous and mutant samples (mutation indicated by asterisk). Predicted mutant *ccm1* protein (lower) is truncated by a premature stop codon (asterisk) lacking ankyrin repeats and the FERM domain. Previously reported zebrafish alleles [22] (upper) removed a small region of the FERM domain (hashed bar) and truncated a C-terminal fragment (asterisk). The black bar close to the N-terminus indicates the conserved nuclear localization signal and the # indicates NPXY motifs.

circulation, did not lead to vascular dilations, demonstrating that the vascular phenotypes are caused by the loss of *ccm1* and not loss of circulation (Supplementary Figure 1).

ccm2 Mutants Display Identical Phenotypes to ccm1 Mutants

We next examined a previously identified retroviral insertional mutant for *ccm2* with the insertion located 162 base pairs into the first intron of the *ccm2* gene [68]. By analysis in the *fli1a:gfp* background, we found that the vascular and heart dilation phenotype was variable in this line (Figure 2A and data not shown). The phenotypic variability in heart dilation associated with this allele was different from previously described alleles (*ccm2*^{m201}) which did not show an intermediate phenotype, indicating that our allele is a hypomorphic allele of *ccm2* [67]. *ccm2*^{hi296} mutants displayed mild or severe vascular phenotypes, with severe vascular dilation and morphogenesis defects from 48 h identical to those observed in *ccm1* mutants (Figure 2B-E). Although early defects of the CV (comparable to

ccm1 mutant phenotypes) were apparent, dilation of the PMBC was variable, apparently reduced and not clearly quantifiable in these hypomorphic mutants (data not shown). In addition, we produced double mutants for *ccm1* and *ccm2*^{hi296} and examined their vasculature. We found that the dilation of embryonic vessels in double mutants was indistinguishable from *ccm1* or severe *ccm2*^{hi296} mutants (data not shown). This phenotypic similarity and double mutant epistasis correlate with the biochemical analysis placing CCM proteins within the same complex and demonstrates non-redundant and essential functions for both *ccm1* and *ccm2*.

Arteriovenous Fates and Cell Number Are Normal in ccm1 Mutants

Analysis of *Ccm1*-deficient mice has suggested that CCM vascular dilations are associated with altered arterial fate and increased endothelial mitosis [66]. Zebrafish *santa* mutants have been recently identified in a separate screen for vascular defects and a cursory analysis of the phenotype identified increased *tie2* expression in mutant vessels leading to the suggestion that endothelial cell number is also increased [35]. Incongruously, the number of endocardial cells, which are endothelial in origin, is reportedly unchanged in *santa* mutants [67].

To determine if altered cell fate or altered proliferation were responsible for CCM phenotypes, we carefully examined both in mutants. We found no difference between *ccm1* mutant and wild-type embryos for the expression of *notch3, dll4, hey2, ephrinB2, flt4* and *dab2* at both 24 and 32 h (preceding and concurrent with the first phenotypes) (Figure 3A-D, Supplementary Figure 2). We also analyzed large clutches of embryos produced from double heterozygote's for *ccm1* and *ccm2* for the expression of *ephrinB2* and *flt4* and observed no change in expression (at 32 h, $n = 118/118$ embryos displayed normal expression of *ephrinB2* and $n = 67/67$ embryos displayed normal expression of *flt4*). Furthermore, we observed normal development of the dorsal aorta and intersomitic vessels, indicating

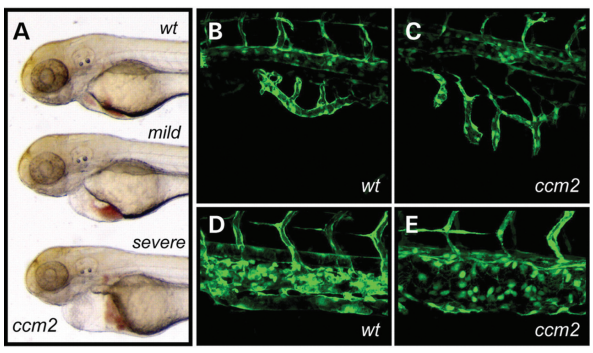

Figure 2. A *ccm2*^{hi296} mutants display either mild heart dilation (middle) or severe heart dilation (bottom) compared with wild-type siblings (top). **B,C.** Lateral views of the SIVs of wild-type (B) and severe *ccm2*^{hi296} (C) mutants visualized using a fli1a:gfp background at 48 h. **D,E.** Wild-type (D) and severe *ccm2*^{hi296} (E) mutant CV phenotypes visualized using a *fli1a:gfp* background at 48 h.

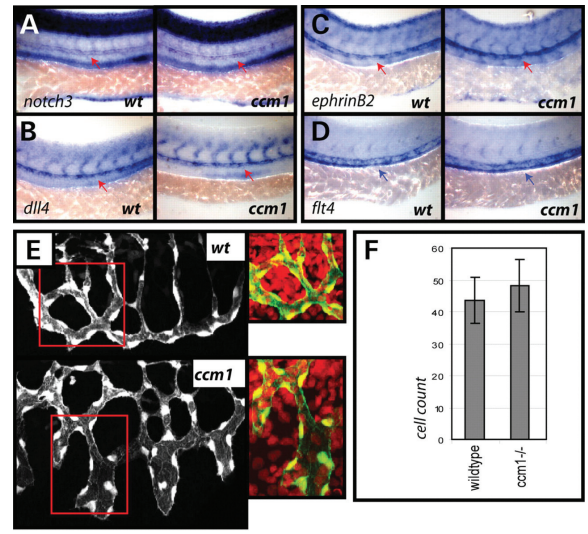

Figure 3. A–D. Arterial and venous markers are expressed normally in the trunk of individually genotyped *ccm1* mutant embryos viewed laterally at 24 h (full analysis Supplementary Figure 2) **A.** *notch3* expression in representative mutant and sibling embryos. **B.** *dll4* expression in representative mutant and sibling embryos. **C.** *ephrinB2a* expression in representative mutant and sibling embryos. **D.** *flt4* expression in representative mutant and sibling embryos. Red arrows indicate arterial expression, blue arrows indicate venous expression. **E,F.** Cell counts of endothelial cells in wholemount wild-type and ccm1 mutant SIVs using anti-GFP staining and nuclear counter-stain (DAPI) at 72 h (E). No significant difference in cell number was observed between mutant (n=10) and sibling (n=10) SIVs counted (F).

that arterial fates were normal in *ccm1, ccm2* and *ccm1/2* double mutants. To investigate cell number in mutant vessels, we focused on the SIVs due to their prominent mutant phenotype and their relative isolation over the yolk, away from other embryonic tissues which might impede on accurate cell counting. We directly counted the number of endothelial cells in the SIV in mutant and sibling vessels using an anti-GFP antibody counter-stained for individual endothelial cell nuclei (DAPI) at 72 h. We observed no significant difference in the number of cells between mutant and sibling embryos (Figure 3E,F). We also saw no difference in cell number using the *fli1a:nls-gfp* transgenic line to count cells in the SIV [SIV at 58 h: wt = 33 ± 3; *ccm1* = 35 ± 5 (mean±SD; $P = 0.402$ by Student's *t*-test; $n = 5$)]. Determination of cell number in the PCV and CV is hampered by the transient presence of variable numbers of haemopoietic stem cells which seed and differentiate in both the PCV and CV [76] and express the marker gene *fli1a*. However, cell counts in equivalent regions of these vessels revealed no indication of an increase in the number of *fli1a:nls-gfp* positive nuclei in 2, 3 and 4 dpf mutants compared with wild-type (2 dpf PCV: wt = 52 ± 9.5; *ccm1* = 43.8 ± 7.5, 2 dpf CV: wt = 95 ± 10.2; *ccm1* = 83 ± 12, 3 dpf PCV: wt = 67.8 ± 4.1; *ccm1* = 56.8 ± 4, 3 dpf CV: wt = 87.8 ± 7; *ccm1* = 85 ± 10.1, 4 dpf PCV: wt = 68.6 ± 4.6; *ccm1* = 63.2 ± 3.4, n = 5 for all time-points and genotypes). Furthermore, we observed no change in PCNA (*in situ* hybridization at 24 h), phosphorylated histone (immunohistochemistry at 24 and 32 h) or

BrdU incorporation (24 and 32 h) in wholemount stainings (data not shown). Collectively, these data indicate that increased endothelial cell number and proliferation do not contribute to the vascular dilation phenotype observed.

Vascular Dilation is Associated With Progressive Dilation and Cell Spreading But Normal Cell–cell Contact

To better understand the defects observed, we examined dilation and morphogenesis of the SIVs using live confocal timelapse imaging in the nuclear localized *fli1a:nls-gfp* transgenic line [19]. We found that between 34 and 58 h, the dilation of mutant SIVs was associated with an apparent progressive and dynamic spreading of endothelial cells over the embryonic yolk (Figure 4A,B; Supplementary Movies 1,2). This defect was not a secondary

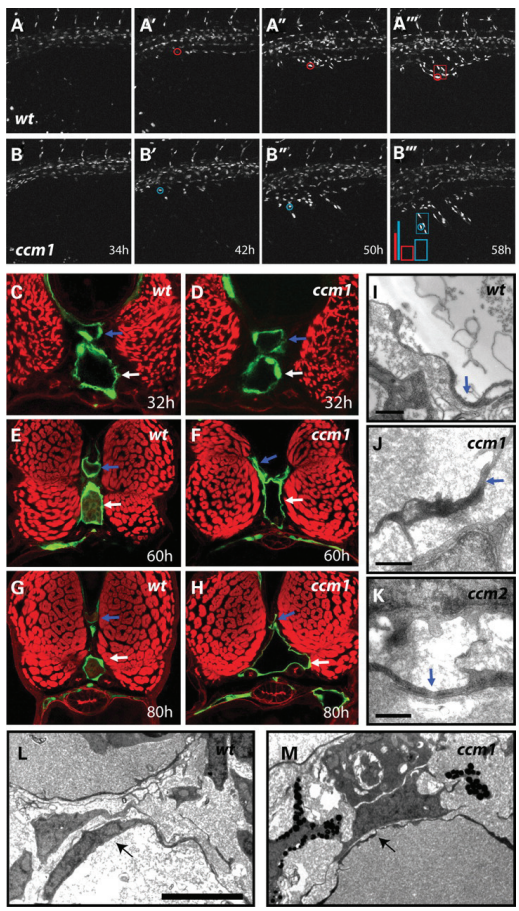

Figure 4. A,B. Timelapse imaging of the SIVs of *fli1a:nuclear-gfp* wild-type and *ccm1* mutant embryos over a 24 h period (34–58 h). Coloured bars track dorsal-ventral movement of the individual cells indicated by the circles. Coloured boxes indicate the spread of four nuclei at the ventral edge of each SIV [(A–A''') wild-type sibling, (B–B''') *ccm1* mutant, image width=375 µm). n = 3 analysed for each genotype. **C–H.** Progressive dilation and vessel wall thinning in *ccm1* mutant vessels. Equivalent confocal stacks of vibratome sections of wild-type (C, E, G) and *ccm1* mutant (D, F, H) vessels in fli1a:gfp animals counterstained with rhodamine phalloidin at the indicated time-points (blue arrow=DA, white arrow=PCV, n > 8 analysed for each time-point). **I–K.** Visualization of cell–cell junctions in the PCV of wild-type (I) *ccm1* mutant (J) and *ccm2* mutant (severe phenotype) (K) embryos using electron microscopy at 48 h. Blue arrows indicate junctions. Scale=0.5 µm. **L,M.** EM analysis of the PCV (arrow) in the trunk of both wt (L) and ccm1 mutant (M) animals confirms thinning of the endothelial wall in mutants at 48h. Scalebar =5 µm, equivalent magnification was used for both (A) and (B).

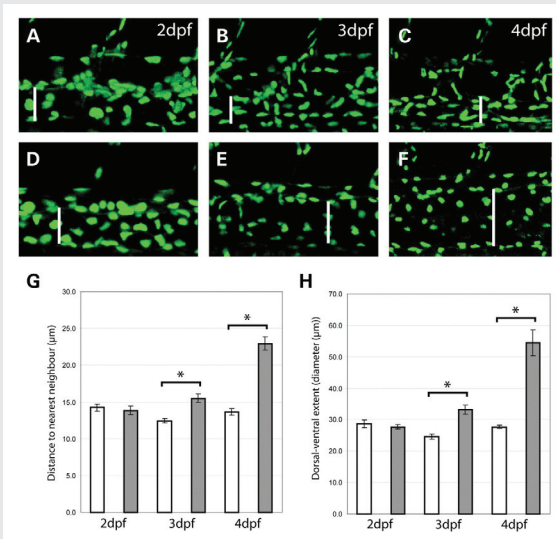

Figure 5. A–F. Representative lateral views of z-stack projections through the trunk vasculature in *fli1a:nuclear-gfp* animals between 2 somites immediately anterior to the cloaca at 2, 3 and 4 dpf. (A–C) Wild-type and (D–F) mutant. White bars indicate the dorsal–ventral extent (diameter) of the PCV at each time-point (determination of diameter aided by transmitted light images). **G.** Column graphical summary of distance in µm between nearest neighbouring nuclei in the PCV at 2 and 4 dpf. Mean±SEM. *=P<0.01. White bars indicate wild-type values and grey bars indicate mutant values.

effect of loss of circulation, as *silent heart* MO injected embryos [75], with no observable circulation, develop constricted SIVs (Supplementary Figure 3). We next compared vascular dilation in the trunk of *ccm1* mutants with wild-type siblings at 32, 60 and 80 h. While the diameter of the PCV was not increased in mutants compared with siblings at 32 h, mutant PCV dilation was prominent at 60 h, and at 80 h mutant PCVs were vastly dilated with a dramatic thinning of vessel walls (Figure 4C-H). Importantly, these observations suggest that *ccm1* mutant vascular dilations likely occur due to progressive thinning and spreading of endothelial cells during vascular morphogenesis. Intuitive explanations for such cellular morphogenesis defects could be altered cell junctions and cell–cell adhesion leading to spreading and dilation or, alternatively, the morphogenesis defects may be inherent to the mutant endothelial cells themselves and independent of their contacts with neighboring cells. Using electron microscopy to examine endothelial cells within the PCV in *ccm1* and *ccm2* (severe phenotype) mutant vessels at 48 h, we observed no obvious ultrastructural remodeling of cell junctions despite marked thinning of the vessel wall in mutants (Figure 4I-M). These data suggest that cell-shape changes occur independent of any obvious changes in endothelial cell–cell contact.

Given that CCM in humans almost exclusively presents in the vasculature of the brain, we examined the morphology and ultrastructure of the brain vasculature at 72 h, a time-point prior to general necrosis and death but when later cranial phenotypes were apparent. We examined the secondary vessels that form via angiogenesis and permeate the brain as they most resemble those present throughout the mammalian CNS and we found that they were extremely abnormal and failed to lumenize in *ccm1* mutants. These defects were

most likely due to the failure to initiate circulation as *silent heart* MO injected embryos displayed apparently identical defects (Supplementary Figure 3). This phenotype precludes a thorough analysis of lumenized mutant secondary vessels Supplementary Figure 4). However, an analysis of the ultrastructure of these highly abnormal *ccm1* mutant brain vessels did identify endothelial junctions (Supplementary Figure 4).

Quantitation of Progressive Venous Dilations in ccm1 Mutants

To quantitate endothelial cell spreading and dilation, we next analyzed *ccm1* mutants using the *fli1a:nuclear-gfp* transgenic line at 2, 3 and 4 dpf. We focused on the PCV due to its simple, predictable morphology in wild-type and mutant embryos. We used three-dimensional GFP and transmitted light z-stack images to measure vessel diameter as well as the

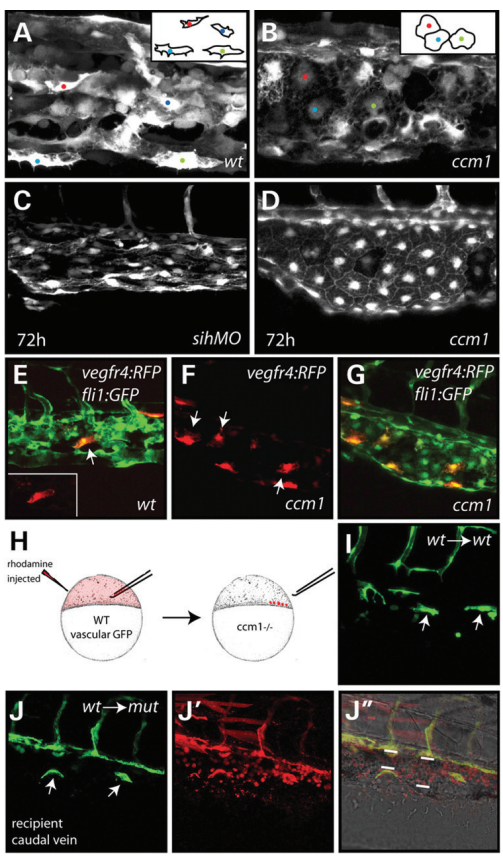

Figure 6. A,B. Morphology of endothelial cells in the CV of wild-type and *ccm1* mutant embryos at 48 h (image width=188 µm, cartoon inset indicates approximate morphology of cells). **C,D.** Comparison of *ccm1* mutant (D) and *sih* MO injected (C) CVs viewed laterally at 72 h. *sih* MO injected but not *ccm1* mutant CVs contain elongated endothelial cells (for full analysis, see Supplementary Figure 5). **E–G.** Analysis of endothelial cell shape in the CV by mosaic labeling of endothelial cells upon injection of DNA encoding *kdrl:rfp* in the *fli1a:gfp* background. Individually labeled, wild-type endothelial cells take up an elongated endothelial morphology (E), whereas individually labeled mutant cells show a typical spread morphology (F and G). (E) and (G) show merged GFP and RFP z-stack images, (F) shows isolated mutant endothelial cells in an RFP z-stack image. Inset in (E) is an isolated, elongated wild-type endothelial cell from an RFP z-stack. Arrowheads indicate isolated cells at the lateral surface of each vessel. **H.** Summary of transplantation approach. Rhodamine-labeled cells were transplanted from pre-dome stage *fli1a:gfp* or *kdrl:gfp* transgenic wild-type embryos into clutches from GFP negative *ccm1* carriers (25% mutant). **I,J.** Transplanted wild-type cell morphology in the CV of wild-type (I) and mutant (J) embryos at 48h [GFP indicates transplanted endothelial cells (I and J), rhodamine indicates all transplanted cells (J'), arrows indicate individual elongated cells in the CV, bars in J" indicate vascular diameter).

distance between nearest neighboring nuclei within each PCV. Quantitation of approximate vessel diameter (based on the dorsal–ventral extent of the lateral surface of the PCV) indicated that dilation progressed over time in mutants with no quantifiable difference observed at 48 h, but a significant increase of approximately 8.5 μm ($P = 0.00085$) at 72 h, and of 26.7 μm ($P = 2 \times 10^{-4}$) at 4 dpf (Figure 5). Quantitation of cell spreading was based on multiple measurements of the distance between nearest neighboring endothelial nuclei located in the same plane of the vessel and at equivalent locations between somites immediately anterior to the cloaca. Measurements were taken between wild-type and mutant vessels and indicated that the spreading of endothelial cells was progressive over developmental time with no quantifiable difference observed in this region of the PCV at 48 h, but a significant increase of approximately 3 μm ($P = 1.19 \times 10^{-5}$) at 72 h, and of 9.3 μm ($P = 4.6 \times 10^{-14}$) at 4 dpf (Figure 5). Interestingly, the ratio of vascular diameter to distance between nearest neighbors remained virtually unchanged throughout the analysis, providing an independent measurement indicating that cell-number changes are unlikely to contribute to dilation. These data indicate that progressive, quantifiable, cellular spreading and vascular dilation underpin the *ccm1* phenotype.

ccm1 is Required Cell Autonomously for the Regulation of Endothelial Cell Shape

All three *Ccm* genes are expressed broadly during development, making it unclear whether CCMs function in endothelial or surrounding tissues [77-79] (Supplementary Figure 5). In order to formally determine whether *ccm1* function is cell autonomous to the endothelium, we aimed to perform transplantation assays. We transplanted wild-type *kdrl:gfp* or *fli1a:gfp* cells into non-transgenic *ccm1* mutant recipient embryos and found that wild-type cells were capable of forming a wild-type elongated morphology in multiple vessels in mutant host embryos (Figure 6). To better understand morphology in mutant vessels, we focused on mutant cells in the region of the CV and found that they appeared distinctly and uniformly spread in appearance, whereas wild-type cells were elongated forming the CV plexus (Figure 6A,B; Supplementary Movies 3,4). This cell spreading in the CV was specific as endothelial cells are elongated in *silent heart* MO injected CVs (Figure 6C,D). We counted the relative number of elongated and spread cells in the lateral wall of the CV in *silent heart* MO injected and *ccm1* mutant embryos and found that mutant vessels never displayed elongated cells at 72 h (Supplementary Figure 6). We also injected DNA encoding *kdrl* promoter driven *tdTomato* into *ccm1* mutant and sibling embryos and counted the number of isolated elongated cells versus isolated spread cells in the lateral wall of the CV in mosaic animals (Figure 6E-G). We found no elongated cells in mutant embryos although we did observe spread cells in wild-type CVs (Supplementary Figure

6). isolated transplanted wild-type endothelial cells in an otherwise mutant CV were capable of marked elongation and could even constrict dilated mutant vessels (Figure 6; Supplementary Figure 6G). Reciprocal transplantations of mutant cells into wild-type embryos would not be interpretable in this assay given the occasional presence of spread cell morphologies in wild-type CVs. This ability of wild-type cells in a mutant environment to independently elongate and to influence the mutant phenotype demonstrates that *ccm1* functions autonomously within endothelial cells.

Discussion

Understanding CCM Phenotypes Using Embryonic Zebrafish Vessels

Human mutations in CCM1, CCM2 and CCM3 cause cavernous malformations, but despite the importance of these genes in the etiology of this disease, very little is known about their molecular and cellular functions. A genetically tractable *in vivo* model allowing genetic, molecular and cellular dissection of the effects of loss of CCMs will greatly aid our understanding in this field. The zebrafish vascular phenotypes associated with the loss of *ccm1* and *ccm2* described here are strikingly similar to those associated with the loss of the CCM genes in mice and humans. In particular, the hypomorphic allele of *ccm2* will be of use for performing MO-based reverse genetic or pharmacological modifier screens which can be used to identify phenotypically relevant genetic or chemical interactors in the CCM pathway.

Here, we show that CCM phenotypes can occur *in vivo*, despite normal endothelial cell fate, normal endothelial proliferation and in the presence of ultrastructurally normal cell–cell contacts. The fact that zebrafish mutant embryos show no alterations in arterial-venous specification or endothelial proliferation, challenges findings in mice [66] and warrants further analysis of the murine phenotype. Given that circulation through forming vessels has been shown to be necessary for their normal expression of arterial marker genes in the chick [80], it seems plausible that the loss of arterial gene expression in Ccm1 knockout mice may be secondary to a loss of circulation. We also show here that the progressive vascular dilation phenotype is associated with specific thinning of vessel walls concurrent with the broadening and spreading of endothelial cells. This requirement for *ccm1* in defining endothelial cell morphology is specific and intrinsic to endothelial cells themselves and not to surrounding or supporting cells because transplanted wild-type endothelial cells in an otherwise mutant vessel establish their wild-type elongated morphology and influence the structure of the surrounding mutant vessel.

Our findings complement recent *in vitro* findings, which demonstrate that the CCM complex associates with cytoskeletal elements, signal transduction components and junctions

[58-65]. The presence of the CCM complex on the cytoskeleton and at the cell junctions, combined with the *in vivo* analysis described here, point towards a working model to explain CCM function during development and pathogenesis. We suggest that CCMs, acting within endothelial cells, at the interface between the cytoskeleton and the cell junctions, primarily regulate endothelial cellular morphogenesis and thereby vascular tubular morphogenesis and that this occurs downstream of normal differentiation events. Further studies focused on the role of CCM family protein function at the sub-cellular level are now required to fully elucidate the mechanism by which they regulate the morphogenesis of endothelial cells and vascular tubes.

Acknowledgements

The *t26458* allele was discovered thanks to the Tubingen 2000 Screen Consortium. We would like to thank Nancy Hopkins and Adam Amsterdam for supplying the *ccm2* mutant line, Gabi Frommer-Kästle for expert assistance with electron microscopy, Merlijn Witte and Josi Peterson-Maduro for technical assistance, Terhi Kärpänen for the *kdrl:tdTomato* construct and Kelly Smith, T. Kärpänen and Andy Oates for critical reading of the manuscript.

Supplementary Information

Supplementary information, including 6 figures and 4 movies, can be found online at http://hmg.oxfordjournals.org/cgi/content/full/ddn142/DC1.

Supplementary Table 1. DNA Oligo Sequences

Name	Sequence
ccm1_ex5_fw	CCACAAGCGTAACGTAAATG
ccm1_ex5_rev	ATCTATGGACGCAATGCAG
EcoRI_ccm1_fw	GCGCGAATTCACCATGGGAAACCAAGAGCTAGAGGAGG
XhoI_ccm1_rev	GCGCCTCGAGTTACCCATACGCATATTTATCAGAC

Supplementary Table 2. Morpholino Oligo Sequences

Name	Sequence
ccm1	CTCCTCTAGCTCTTGGTTTCCCATC
sih	CATGTTTGCTCTGATCTGACACGCA

Chapter 3

Early endocardial morphogenesis requires *tal1*

Jeroen Bussmann[1], Jeroen Bakkers[1,2], Stefan Schulte-Merker[1]

PLoS Genetics: 3(8): e140 (2007)

[1]Hubrecht Institute, Developmental Biology and Stem Cell Research, Utrecht, The Netherlands
[2]Interuniversity Cardiology Institute of the Netherlands, Utrecht, The Netherlands

Abstract

The primitive heart tube is composed of an outer myocardial and an inner endocardial layer that will give rise to the cardiac valves and septa. Specification and differentiation of these two cell layers are among the earliest events in heart development, but the embryonic origins and genetic regulation of early endocardial development remain largely undefined. We have analyzed early endocardial development in the zebrafish using time-lapse confocal microscopy and show that the endocardium seems to originate from a region in the lateral plate mesoderm that will give rise to hematopoietic cells of the primitive myeloid lineage. Endocardial precursors appear to rapidly migrate to the site of heart tube formation, where they arrive prior to the bilateral myocardial primordia. Analysis of a newly discovered zebrafish *tal1* mutant showed an additional and previously undescribed role of this transcription factor during the development of the endocardium. In *tal1* mutant embryos, endocardial precursors are specified, but migration is severely defective and endocardial cells aggregate at the ventricular pole of the heart. We further show that the initial fusion of the bilateral myocardial precursor populations occurs independently of the endocardium and *tal1* function. Our results suggest early separation of the two components of the primitive heart tube and imply *tal1* as an indispensable component of the molecular hierarchy that controls endocardium morphogenesis.

Introduction

The primitive heart tube is the first functional organ in the vertebrate embryo and is composed of a myocardial tube lined by an inner endothelial layer called the endocardium. Significant progress has been made towards elucidating the morphogenetic events and transcriptional control underlying patterning of the myocardium [81]. However, the morphogenetic events and the transcription factors involved in early development of the endocardium remain largely undefined. In fact, the specific embryonic origin of the future endocardial cells and their relationship with the future myocardial cells is still unclear [82].

Results obtained using in vitro differentiation of embryonic stem cells [83] and analysis of different mesodermal or cardiac cell lines [84,85] suggest the development of both cardiac lineages from bipotential progenitors during heart field formation and, indeed, bipotential cells have been identified in the early mouse embryo at a single-cell level [83]. However, lineage tracing experiments in the avian embryo have shown restricted myocardial or endocardial potential of precardiac cells, with both types of precursors inter-

mingled during their migration towards the site of the primitive heart tube [86]. A similar sequestration of endocardial and myocardial cells is observed in the zebrafish where cells at late blastula stages give rise to both endocardial and myocardial cells [87]. These cells also give rise to the head vasculature and an anterior population of hematopoietic cells of the primitive myeloid lineage and become restricted in their potential to form either endocardium or myocardium during early gastrulation stages [88].

After endocardial and myocardial precursors have been specified, complex morphogenetic movements occur that shape the primitive heart tube. Again, most studies have focused on the morphogenesis of the myocardium. One of the early markers of myocardial differentiation is the transcription factor *nkx2.5*, expression of which is detected in the zebrafish in bilateral populations starting at the ten-somite stage [89]. Subsequently, these bilateral myocardial fields merge in the midline at the 18-somite stage, with the first contacts occurring in a relative posterior position [90]. The myocardial precursors posterior to the first junction as well as the most anterior portions then come in contact with each other, creating a ring with a central circle devoid of myocardial cells that has been suggested to contain the endocardial precursors [90,91]. Around these stages, expression of cardiac contractile genes, such as such as cardiac myosin light chain (*myl7*), starts [92]. Finally, myocardial cells move to the left, and during a complex and poorly understood process, convert the myocardial disc into the primitive heart tube [90].

The basic helix-loop-helix (bHLH) transcription factor Scl/Tal1, hereafter referred to as Tal1, an oncogene originally identified in childhood leukemias, is expressed in endothelial, endocardial and hematopoietic, but not myocardial cells during early murine development [93]. Tal1 forms a transcriptional complex containing Lmo2 to regulate expression of target genes. Gain of function of Tal1 in combination with Lmo2 leads to an expansion of endothelial and hematopoietic cells at the expense of other nonaxial mesodermal components, including myocardial precursors [94], suggesting an important role for these genes during endocardial/myocardial specification and differentiation. Gene targeting studies in the mouse have revealed that Tal1 is essential for the formation of all blood lineages. Tal1 loss of function also leads to considerably less well-defined defects during endothelial development [95,96,97]. Knockdown of *tal1* in zebrafish showed a conserved function in generating hematopoietic cells. In addition, *tal1* knockdown embryos display defects during arterial versus venous differentiation [98-100].

Here, we analyze early endocardial morphogenesis in the zebrafish, and show that the endocardium appears to arise from the anterior lateral plate mesoderm, from a region that will give rise to hematopoietic cells of the primitive myeloid lineage. From there, presumptive pre-endocardial cells seem to rapidly migrate posterior and towards the midline, where they are later joined by the bilateral myocardial primordia. The myocardial primordia then fuse over the endocardial layer to form the disc that subsequently gives

rise to the primitive heart tube. We show that *tal1* has an additional and previously undescribed role in endocardial development. In *tal1* mutants, migration of endocardial but not myocardial precursors is defective, leading to severe outflow tract stenosis and defects in the formation of the primitive heart tube. Our results suggest a separate origin for the two components of the primitive heart tube and show an indispensable role for Tal1 during endocardial morphogenesis.

Materials and Methods

Zebrafish

All zebrafish strains were maintained in the Hubrecht Institute using standard husbandry conditions. Animal experiments were approved by the Animal Experimentation Committee of the Royal Netherlands Academy of Arts and Sciences (DEC). The *tal1*^{t21384} allele was isolated in a genetic screen for ENU-induced mutations affecting vascular development [36]. The transgenic line *TG(fli1a:gfp)*^{y1} [15] was obtained from Brant Weinstein (Bethesda, Maryland). The transgenic line *TG(kdrl:gfp)*^{s843} [35] was obtained from Didier Stainier (San Fransisco, California).

Meiotic Mapping and Sequencing

The *t21384* mutation was positioned on Chromosome 22 using standard simple sequence length polymorphism mapping. For sequencing of the *tal1* gene, genomic DNA was extracted from 12 wild-type (wt) and 12 mutant *tal1*^{t21384} embryos. The three coding exons of the zebrafish *tal1* gene were PCR amplified and sequenced on both strands. A mutation in the third coding exon was confirmed in a panel of 580 single mutant and 53 single sibling embryos using PCR with primers tal1_ex3_ fw and tal1_ex3_rev and sequenced using primer tal1_ex3_seq.

Full-Length Sequence of kdr, flt1 and flt4

We used an unidirectionally cloned, oligo dT-primed SMART cDNA library constructed from 2- and 3-day old zebrafish larvae using Advantage2 DNA Polymerase Mix (Clontech). Primers used for identification of *kdr*, *flt1* and *flt4* 3′ and 5′ ends are available upon request.

Phylogenetic and Synteny Analysis

The MEGA3 package was used for phylogenetic analysis [84]. Amino acid sequences were aligned with ClustalW (the resulting alignment is available upon request) and a phylogenetic tree was constructed using a neighbor-joining algorithm. The resulting tree was testing using 1,000 bootstrap resamplings. Pairwise distances were calculated with the PAM substitution matrix. Identification of vertebrate VEGF receptors was performed using the Ensembl database, release 44, April 2007.

Whole-Mount In Situ Hybridization and Immunohistochemistry

Single and double in situ hybridizations were performed essentially as described [101], except that labeled probes were purified using NucleoSpin RNA clean-up columns (Machery-Nagel) and embryos were transferred to 15-mm Costar Netwells (Corning) after hybridization. The substrate used in the second color-reaction was INT ([4-iodophenyl]-3-[4-nitrophenyl]-5-phenyl-tetrazolium chloride) (Roche Applied Science). Previously described probes used were *tal1, gata1, spi1, runx1, hey2, flk1/kdrl, ephrinb2a, dab2, nkx2.5, amhc* and *cmlc2* [52,54,89,92,102-108]. Probes for *flt4, kdr* and *flt1* were transcribed from the 5′ part of the respective cDNAs that code for the extracellular domain of the proteins. Immunohistochemistry using anti-GFP (Torrey Pines Biolabs) and anti-tropomyosin (CH1; Sigma) antibodies was performed as described [109]. Secondary antibodies were

Alexa^{555}-anti-rabbit and Alexa^{647}-anti-mouse (Invitrogen).

mRNA Injections

Full length *tal1* mRNA was transcribed from linearized plasmids using the mMessage-mMachine kit (Ambion) as described [98]. mRNA injections were done in a volume of 1 nl at the one-cell stage in Milli-Q water (Millipore) at a concentration of 20 pg/embryo.

Time-Lapse Analysis

Embryos were mounted in 0.25% agarose in a six-well culture plate with a cover slip replacing the bottom of each well and imaged with a Leica TCS SP confocal microscope (Leica Microsystems) using a 40× dry objective (*kdrl:gfp*) or 10× dry objective with 2× digital zoom (*fli1a:gfp*). Maximal z-projections of 40–50 slices at 4 µm per slice were compiled using ImageJ software. Time points were recorded every 5 min (*fli1a:gfp*) or 7.5 min (*kdrl:gfp*) for 6–8 h. A heated stage was employed to keep the embryos at approximately 28.5 °C.

Results

A Truncating Mutation in Zebrafish tal1

In a large-scale forward genetic screen [36], we identified a mutant (*t21384*) that showed a severe reduction in endothelial alkaline phosphatase activity at 4 d post fertilization, particularly in the region of the dorsal aorta. Until 26 h post fertilization (hpf), the general morphology of mutant embryos was indistinguishable from that of their wt siblings. At this time however, the pericardium became edematous (Figure 1A), even though heartbeat was initiated normally. No erythrocytes were observed and embryos consequently lacked circulation. To identify the molecular lesion responsible for the *t21384* phenotype, we used simple sequence length polymorphism mapping to position the mutation on Chromosome 22. Single embryo mapping using a limited number of mutant embryos (n = 96) positioned the mutation at 28.0 cM (+/− 0.5 cM), between simple sequence length polymorphism markers z21515 and z938, closely linked to the *tal1* gene (27.89 cM). The combination of endothelial and hematopoietic defects seen in *t21384* mutants had also been observed in mouse Tal1 knockouts [95], as well as in a morpholino knockdown of *tal1* in zebrafish [98-100]. Therefore, *tal1* was a very likely candidate gene. Sequencing of the three coding exons of the zebrafish *tal1* gene in mutant and sibling embryos revealed an A to T transversion in the third and final coding exon (Figure 1B). The mutation resulted in a K to ochre nonsense mutation at position 183 of the protein. The resulting putative protein had a deletion of the highly conserved bHLH domain, including the DNA binding basic region (Figure 1C).

Using this SNP, we also examined the degree of linkage and observed no recombinants for this mutation in 580 mutant embryos tested (genetic distance < 0.09 cM). In genotyping embryos after in situ hybridization or immunohistochemistry, we have never observed a mutant genotype in a sibling embryo. We conclude that the phenotype is fully penetrant

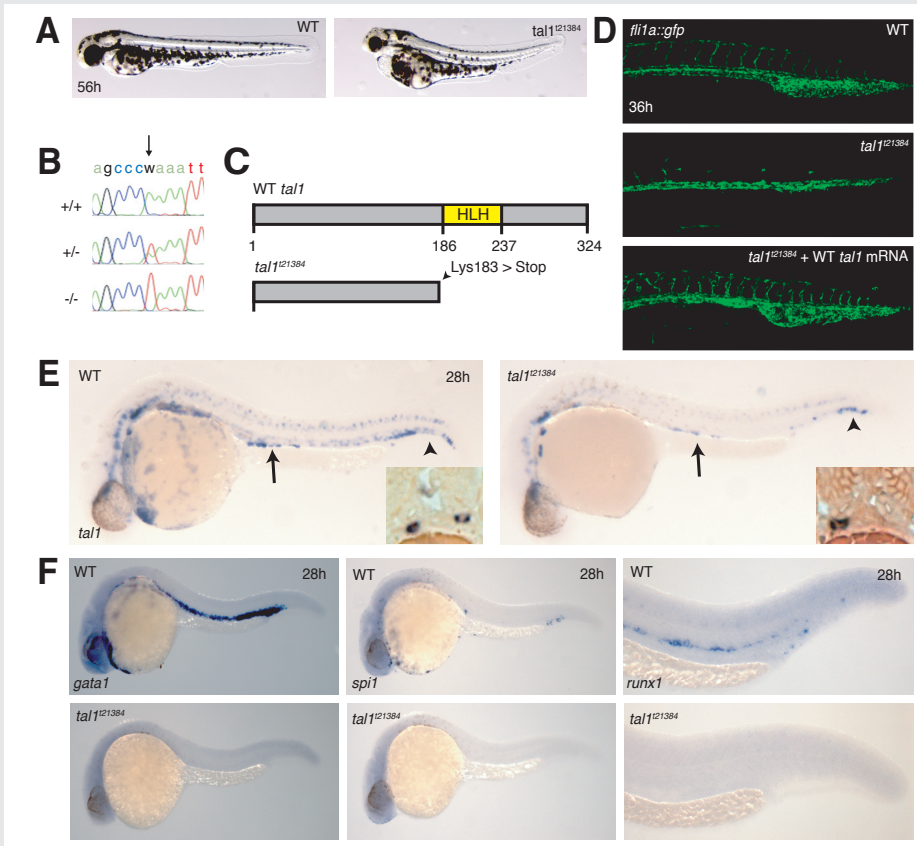

Figure 1. A Truncating Mutation in the Zebrafish *tal1* Gene. A. Live micrographs of wt and *tal1*^{t21384} mutant embryos at 56h. Mutant embryos have slightly curved tails, smaller eyes, and pericardial edema. **B.** Electropherograms of wt (+/+), heterozygous (+/–) and *tal1*^{t21384} homozygous genomic DNA from bp 7–17 of the third *tal1* coding exon. The A to T transversion (arrow) mutates lysine 183 to an ochre (TAA) stop codon (K183X). **C.** Schematic diagram of the primary Tal1 protein structure. The DNA-binding bHLH domain is indicated in yellow. The *tal1*^{t21384} mutation deletes the Tal1 protein C terminus including the complete helix-loop-helix domain. **D.** The *tal1*^{t21384} mutation leads to severe defects in intersomitic vessel formation at 36 hpf, visualized in a *fli1a:gfp* transgenic background. Early endothelial pattering can be rescued by injecting 20 pg wt *tal1* mRNA into mutant embryos. **E.** Loss of *tal1* expression in *tal1*^{t21384} mutant embryos. *In situ* hybridization for *tal1* shows a loss of *tal1* expression in erythroid cells and a reduction of *tal1* expression in the spinal chord. *tal1* expression is retained at normal levels in some hematopoietic/endothelial progenitor cells in the tail (arrowheads) and in some mesenchymal cells of unknown nature just dorsal to the yolk extension (arrows). These bilateral cell populations lie ventral to the pronephric tubules and lateral to the gut endoderm (insets). Also note the loss of *tal1* expression in the ventral wall of the dorsal aorta containing, in wt embryos, the definitive hematopoietic stem cells. **F.** Loss of hematopoiesis in *tal1*^{t21384} mutant embryos. In situ hybridization for hematopoietic markers at 26 hpf shows a loss of primitive erythroid cells (*gata1*), primitive myeloid cells (*pu.1*), and definitive hematopoietic stem cells (*runx1*).

(see also Figure 2). To further confirm that the mutation of *tal1* was the defect underlying the *t21384* mutant phenotype, we forced expression of *tal1* by injecting 20 pg of capped wt mRNA into embryos from a cross between heterozygous individuals carrying the *fli1a:gfp* transgene to visualize endothelial cells. In uninjected mutant embryos, vascular patterning was severely affected, leading to a loss of intersomitic vessels. The defect in vascular patterning was rescued by injection of wt *tal1* mRNA (Figure 1D), as was the hematopoietic and the endocardial defect.

Although the *t21384* mutation resided in the final coding exon of the *tal1* gene, and therefore the mRNA was unlikely to be subjected to nonsense-mediated decay [110], we observed reduced expression of *tal1* mRNA at 28 hpf, as revealed by *in situ* hybridization (Figure 1E). Expression of *tal1* was retained in the ventral mesenchyme of the tail, a region that has been hypothesized to contain hematopoietic progenitors [102]. In addition, we consistently observed a bilateral population of *tal1* expressing cells above the yolk extension. These cells resided in the mesenchyme ventral to the pronephric tubule and lateral to the developing gut tube (Figure 1E, inset).

To confirm the loss of hematopoietic lineages, we performed *in situ* hybridization for genes that are required for the formation of the two major primitive hematopoietic lineages in the early embryo as well as those that are required for the formation of definitive hematopoietic stem cells. Consistent with data obtained by morpholino injection [98,99,100], we showed that the development of the primitive erythroid lineage (*gata1*) as well as the formation of definitive hematopoietic stem cells (*runx1*) was lost. Similarly, development of the primitive myeloid lineage was severely affected (Figure 1F), although some *spi1* expressing cells were observed in the head at 28 h (unpublished data).

Based on the tight linkage, the stop codon in the *tal1* gene, and the rescue of all phenotypic aspects in mutant embryos through injection of wt mRNA, we conclude that *t21384* encodes *tal1* and hereafter refer to the mutant allele as $tal1^{t21384}$.

tal1 Mutants Display Defects in Early Endocardial Development

In addition to the defects observed in the hematopoietic and endothelial lineages (Figure 1D and see below), we observed in $tal1^{t21384}$ mutants a strong defect in the morphogenesis of the heart that has not been previously described in the zebrafish or mouse. Although myocardial differentiation does not appear to be affected and heartbeat is initiated normally, the endocardial cells in the $tal1^{t21384}$ mutants do not form a single cell layer lining the myocardium, and do not form atrial endocardium. Instead, endocardial cells aggregate at the arterial pole of the heart, leading to complete ventricular stenosis (Figure 2A,B). Later, concentric growth of the myocardium is defective and no heart valves are formed, consistent with an important role for the endocardium in these processes [30,111]. This pheno-

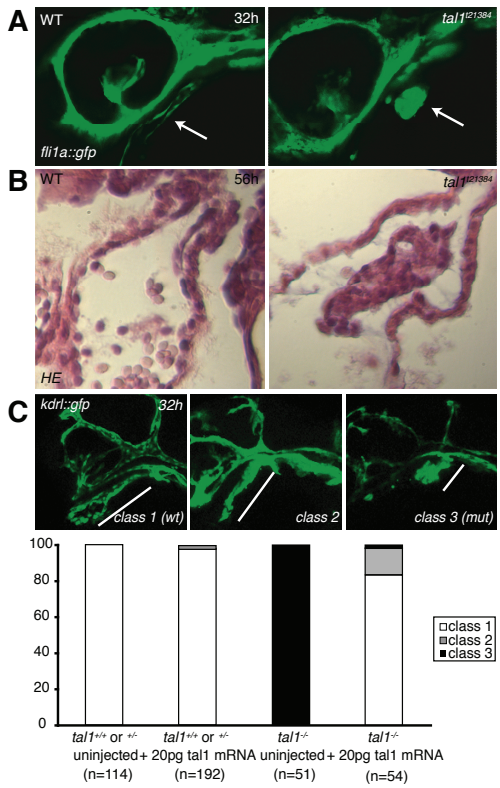

Figure 2. Defects in Endocardial Development in *tal1*^{t21384} Mutants A. Confocal images of the head region from embryos transgenic for *fli1a:gfp* at 32 hpf. Arrows indicate the location of the endocardium. In the wt endocardium, a lumen is visible, which is absent in *tal1*^{t21384} mutants. **B.** Transversal sections of wt and *tal1*^{t21384} mutant heart ventricles at 56 hpf stained with hematoxylin/eosin. In wt embryos, the endocardium forms an epithelium attached to the myocardium, and blood cells are visible within the heart tube. In the *tal1*^{t21384} mutant heart, the endocardium fails to form an epithelium and is only present in the heart ventricle. **C.** Rescue of endocardial defects. Maximum z-projection of a stack of confocal images of embryos carrying the *kdrl:gfp* transgene. Embryos were divided into three classes based on their endocardial phenotype. Class 1: wt length of the endocardium with normal tube formation (wt phenotype). Class 2: wt length of the endocardium but no tube formation (intermediate phenotype). Class 3: short endocardium with no tube formed (mutant phenotype). All embryos homozygous or heterozygous for the wt allele are in class 1, whereas all embryos homozygous for the *tal1*^{t21384} allele are in class 3, showing the high penetrance of this phenotype. In 43 out of 54 embryos homozygous for the *tal1*^{t21384} allele (83%), the endocardial phenotype can be rescued to class 1 through injection of low amounts of wt *tal1* mRNA (20 pg per embryo), whereas most of the remaining (8/54, 15%) display an intermediate phenotype (class 2).

type was always found in combination with the loss of primitive hematopoiesis, and both aspects of the phenotype could be efficiently rescued by injecting wt *tal1* mRNA, showing the specificity of both phenotypes to the loss of *tal1* function (Figure 2C).

Early Endocardial Precursors Express a VEGF Receptor Gene That Has Been Lost during Mammalian Evolution

To be able to examine the early endocardial defects observed in *tal1*^{t21384} mutants, we aimed to develop several markers for endocardial morphogenesis. A previous study used the expression of a zebrafish vascular endothelial growth factor (VEGF) receptor homologue to delineate early endocardial development in the zebrafish [106], which was pro-

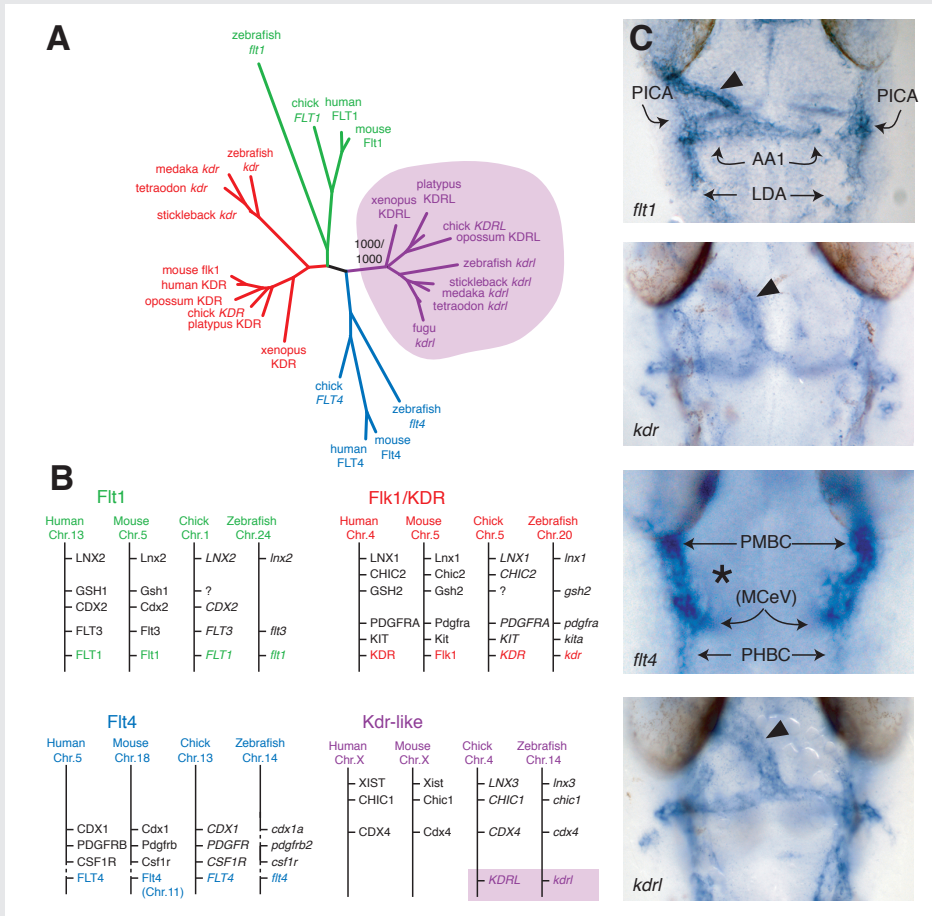

Figure 3. Zebrafish *kdrl (flk1)* Represents a New Class of Nonmammalian VEGF receptors. A. Rooted neighbor-joining tree of vertebrate VEGF receptors. Different colors represent different classes of VEGF receptors. Note the clear separation of zebrafish and other teleost fish *kdrl*, and the novel frog, chick, opossum and platypus VEGF receptor genes from the three other classes of vertebrate VEGF receptors. Bootstrap value of the *kdrl* node is indicated (1,000 times out of 1,000 iterations). **B.** Synteny analysis of vertebrate VEGF receptors using human, mouse, chick and zebrafish genome assemblies. Colors used are similar to those in (A). Question marks represent missing orthologous genes, potentially due to gaps in the chick genome assembly. Clear syntenic relationships of all vertebrate VEGF receptors were observed, indicating duplication from a primordial gene cluster in a primitive chordate. Mammals have lost the zebrafish *kdrl* orthologue, coninciding with the emergence of the X-chromosome inactivation center XIST in the same genomic locus. **C.** Expression of zebrafish VEGF receptors in the heart region at 26 hpf, dorsal view, anterior to the top. Three VEGF receptors are expressed in the endocardium: *kdrl, kdr* and *flt1* (arrowheads). Note the absence of *flt4* expression in the endocardium (asterisk). At this stage, both *kdrl* and kdr are expressed at high levels in all endothelial cells, whereas *flt1* and flt4 have a mutually exclusive expression pattern: *flt1* is expressed in all arteries whereas *flt4* is expressed in all veins.

posed to be the zebrafish Flk1/KDR ortholog. However, the murine Flk1 gene is expressed in multiple non-endothelial cells [112,113] and Flk1$^+$ progenitors give rise to beating cardiomyocytes [83]. The observed endothelial-specific expression of zebrafish *flk1/kdra* at early developmental stages is therefore surprising. This prompted us to reassess the phylogenetic relationship of the zebrafish VEGF receptors.

We obtained the full length sequence for all zebrafish VEGF receptors: *flk1/kdra, flt1, flt4* and *kdrb* [70,106,114,115], of which *flk1/kdra* and *kdrb* were proposed to be the result of a whole-genome duplication event in teleost fish [115]. However, we identified likely orthologs for all four zebrafish genes, including both *flk1/kdra* and *kdrb* in the genomes of *Xenopus tropicalis*, chick, platypus and opossum. Phylogenetic and synteny analysis of the three human VEGF receptors FLT1, KDR and FLT4 and the four receptors of zebrafish, chick and opossum both supported the hypothesis that zebrafish *flk1/kdra* and the novel chick and opossum VEGF receptor genes in fact represent a separate VEGF receptor class that was lost during mammalian evolution (Figure 3A and 3B). In addition, this showed that the gene previously published as *kdrb* is in fact the KDR ortholog. Given these results, we propose the use of *kdr-like* (*kdrl*) to designate the novel class of vertebrate VEGF receptors and will use *kdrl* instead of *flk1/kdra* and *kdr* instead of *kdrb* for the remainder of this thesis.

Expression analysis revealed that *kdr* was the first VEGF receptor expressed during development (Supplementary Figure 1). *kdrl, flt1* and *kdr* but not *flt4* are expressed in the endocardium of the heart at 26hpf (Figure 3C). Importantly, and consistent with earlier results, the expression of *kdrl* was restricted to endothelial precursors and blood vessels during all stages examined and could be used as a marker for endocardial development.

Early Endocardial Development in the Zebrafish

To understand the endocardial defects in *tal1*^{t21384} mutants, we first characterized normal endocardial development in the zebrafish. We used time-lapse confocal microscopy in the *kdrl:gfp* transgenic background [21] to analyze the morphogenetic movements during early endocardial development. Consistent with *kdrl* mRNA expression, this transgene was expressed in the all endothelial cells including the endocardium, but not the myocardium, of the primitive heart tube and therefore was used to follow endocardial precursors during their migration, although it is important to note here that higher resolution tracking of single cells or fate mapping will be required to definitely address the origin and migratory path of endocardial precursors.

The earliest time point at which fluorescence was detected was between the 10- and 12-somite stage (14–15 hpf). At this stage, the transgene was expressed in the anterior and posterior lateral plate mesoderm, representing the endothelial and hematopoietic precursors. Between the 12- and 14-somite stage (15–16 hpf), the anterior lateral plate

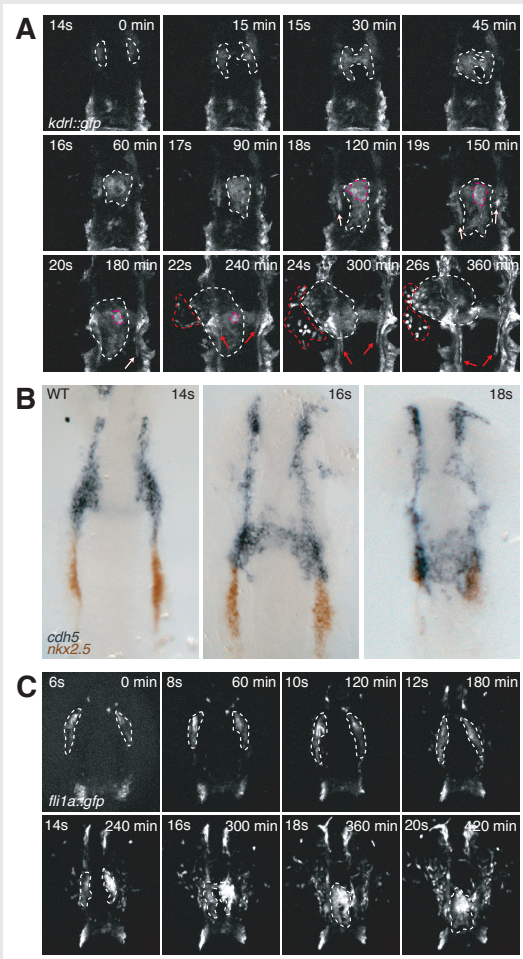

Figure 4. Migration of Endocardial Precursors in wt Embryos A. Embryos transgenic for *kdrl:gfp* were subjected to time-lapse confocal microscopy, revealing rapid endocardial migration prior to heart tube formation. A movie demonstrating this process can be viewed in Supplementary Movie 1. Twelve individual frames from this movie at indicated stages and time-points are shown seen in (A), with white dashed lines indicating the position of (pre-) endocardial cells. Frames 1–5 show the fusion of the bilateral endocardial precursors between the 14- and 16-somite stages. Frames 5–8 indicate the posterior migration of endocardial cells to cover the lateral and posterior regions of the cardiac disc; note the posterior migration of the paired lateral dorsal aortas between the 18- and 22-somite stages (white arrows). The apex of the endocardial disc (pink dashed line) appears to be constricted below the aortic arches between the 18- and 22-somite stages (frames 7–10). A leftward movement of the endocardium is visible between the 20- and 26-somite stages (frames 9–12), and is coinciding with the appearance of single kdrl:gfp-positive cells lateral to the remaining endocardium (red dashed line). Also note the migration of the venous posterior hindbrain channels (red arrows) between the 22- and 26-somite stage (frames 10–12). **B.** Relative locations of endocardial and myocardial precursors during fusion of endocardial precursor populations, revealed by two-color *in situ* hybridization showing *cdh5* (blue, endocardium) and *nkx2.5* (red, myocardium) expression. The bilateral populations of endocardial precursors (arrows) are located anterior to the myocardial precursors until the 14-somite stage, then migrate medially and posteriorly to assume a position in between the myocardial precursors at the 18-somite stage. **C.** Embryos transgenic for *fli1a:gfp* were subjected to time-lapse confocal microscopy, revealing slow medial movement of gfp-positive cells between the six- and 12-somite stage (frames 1–4) and rapid migration starting at the 14-somite stage. A movie demonstrating this process can be viewed in the Supplementary Movie 2.

mesoderm moved medially with more gfp-positive cells in the posterior region of the anterior lateral plate mesoderm. This region later formed part of the head vasculature, the primitive myeloid cells, the anterior dorsal aortas and, importantly, the endocardium and aortic arches (see Supplementary Movie 1 and Figure 4A). The co-expression of *kdrl:gfp*

in both the endocardium as well as the head vasculature suggests a respective origin of these cell populations within the anterior lateral plate mesoderm. Both our marker analysis and the time-lapse imaging are consistent with that notion; however, in the absence of single-cell tracking, it is not completely conclusive. Both of these lineages seem to arise as bilateral populations at the 14-somite stage (dashed lines in Figure 4A). The presumed endocardial precursors then rapidly migrated posterior and fused between the 15- and 18-somite stage (16.5–18 hpf). Fusion of these endocardial precursor populations initiated at the anterior side, progressed in a posterior direction, and was finished by 18 hpf. At the same time, further posterior migration of endocardial cells occurred. Finally, a complex leftward movement of the endocardial primordium occurred to position the endocardial component of the primary heart tube at the left side of the embryo between the 22-and 26-somite stage. Although most endocardial cells moved slowly and as an epithelial sheet at these stages, additional single *kdrl:gfp*-positive cells that are separate from the endocardium were rapidly moving lateral and anterior (Figure 4A).

To assess the relative positions of endocardial and myocardial precursors during fusion of the endocardial precursor populations, we performed two-color in situ hybridization using precisely staged embryos and small time intervals. The endocardial precursors as well as precursors of the head vasculature were marked by expression of VE-cadherin (*cdh5*) and the myocardium by expression of *nkx2.5* (Figure 4B). In this way, we showed that *VE-cadherin* expressing cells, which include the endocardial precursors, do not express *nkx2.5* and are found immediately anterior to the myocardial precursors in the lateral plate mesoderm at the 14-somite stage, when migration begins. In addition, these data confirmed that endocardial and not myocardial cells are the first to arrive in the midline.

Finally, to confirm the results obtained in the *kdrl:gfp* transgenic line and to analyze the movements of endocardial precursors before the 14-somite stage, we used the *fli1a:gfp* transgenic line that also expresses a transgene specifically in endothelial cells, including the endocardium (Figure 4C and Supplementary Movie 2). GFP fluorescence in this line can be detected from before the six-somite stage and thus can be used to follow tissue movements prior to endocardial migration. In addition to the endocardium, this transgene is expressed in the developing primitive myeloid population, as well as the pharyngeal mesoderm. Time-lapse imaging of this line confirmed the results obtained with the *kdrl:gfp* transgenic line between the 14- and 20-somite stage. Before this stage, the anterior lateral plate mesoderm gradually moved medially. This analysis also suggests a close association of endocardial and primitive myeloid cell populations, as macrophages (identified based on their motility and being *fli1a:gfp* positive) start migrating from the 12-somite stage from a region that also includes the endocardial precursors.

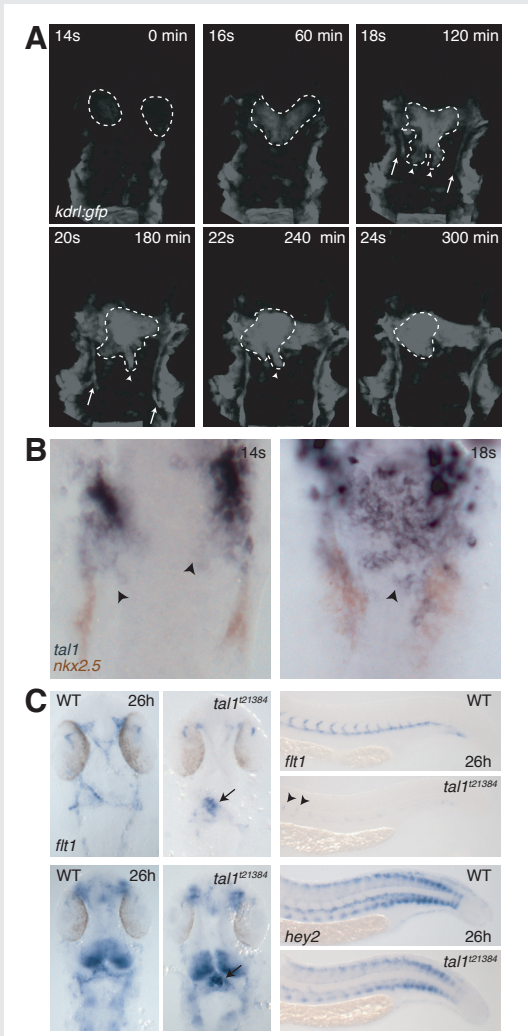

Figure 5. Migration of Endocardial Precursors and Heart Tube Formation in wt and *tal1*^{t21384} Mutant Embryos A. *tal1*^{t21384} mutant embryos transgenic for *kdrl:gfp* were subjected to time-lapse confocal microscopy, revealing defects during early endocardial precursor migration. A movie demonstrating this process can be viewed in the Supplementary Movie 3. Six individual frames from this movie are shown in (A). Whereas the initial formation of bilateral endocardial precursors is not affected, posterior migration is disturbed, and endocardial precursors remain attached in a relative anterior position. Note that migration of the paired lateral dorsal aortae (arrows) proceeds normally. **B.** *tal1* expression in endocardial precursors. Two-color *in situ* hybridization revealing *tal1* (blue) and *nkx2.5* (red) expression in wt embryos at the 14- and 18-somite stage. *tal1* expression is observed in endocardial but not myocardial precursors during their posterior migration (arrowheads). **C.** Expression of the arterial markers *flt1* and *hey2* is retained in *tal1*^{t21384} mutant endocardium, but severely reduced in endothelium, as revealed by *in situ* hybridization. Dorsal view of *flt1* and *hey2* expression in the head, anterior to the top, and lateral view of *flt1* and *hey2* in the tail (28 hpf). In wt embryos, *flt1* expression is observed in all head arteries, the aortic arches and the endocardium (arrow). In *tal1*^{t21384} mutant embryos, expression of *flt1* is observed in a few remaining head arteries and the aortic arches. High levels are seen in the endocardium (arrow). In wt embryos, *flt1* expression is observed in the dorsal aorta and the developing intersegmental vessels. In the tail of *tal1*^{t21384} mutant embryos, expression of *flt1* is abolished, except for a few remaining cells that express *flt1* at low levels (arrowheads). In wt embryos, *hey2* expression is observed in the endocardium and the aortic arches and in some parts of the brain and spinal cord. In *tal1*^{t21384} mutant embryos, expression in the endocardium (arrow) is increased. In wt embryos, *hey2* expression is observed in the dorsal aorta and the developing intersegmental vessels, spinal chord neurons, and in ventral and dorsal cells of the somites. In *tal1*^{t21384} mutant embryos, expression in the dorsal aorta and intersegmental vessels is severely reduced, although some anterior intersegmental vessels and aortic cells retain low levels of *hey2* expression (arrowheads).

Early Endocardial Development in the tal1^{t21384} Mutant

To assess the timing of endocardial defects in *tal1^{t21384}* mutants, we analyzed mutant embryos carrying the *kdrl:gfp* transgene and performed time-lapse confocal microscopy, similar to wt embryos (Figure 5A and Supplementary Movie 3). In mutant embryos, fluorescence was first detected between the ten- and 12-somite stage, indistinguishable from wt embryos. The bilateral presumptive endocardial precursors initiated migration at the 14-somite stage normally, but there was a severe defect in the continued posterior migration of endocardial precursors. Whereas wt endocardial precursors migrated rapidly and formed a single cell layer in the embryonic midline, endocardial precursors in *tal1^{t21384}* mutants aggregated in an anterior position (Figure 5A and Supplementary Movie 3).

Tal1 Expression in Zebrafish Endocardial Precursors

Previous reports have indicated Tal1 expression in the endocardium of the mouse [93]. However, a previous study did not identify *tal1* expression in endocardial cells in the zebrafish [102]. We analyzed *tal1* expression during early endocardial development using two-color *in situ* hybridization and showed *tal1* expression during all stages of endocardial cell migration (10–20-somite stage) (Figure 5B), consistent with a cell-autonomous role for *tal1* in this process. In the trunk, *tal1* expression was detected in angioblasts and primitive erythrocytes. Expression is downregulated during endothelial differentiation and only maintained in erythrocytes. Similarly, expression of *tal1* in the endocardium was downregulated during early migration and maintained in the primitive myeloid lineage.

Endocardial Differentiation in tal1^{t21384} Mutants

Results obtained using morpholino knockdown have shown an important role for *tal1* in the differentiation of arterial and venous endothelial cells [98-100] This suggested that failure of endocardial differentiation could be the primary defect in *tal1^{t21384}* mutant hearts. Using the genetic mutant, we reassessed the role of tal1 during arteriovenous differentiation and showed that indeed most arterial gene expression was lost and venous gene expression expanded (Figure 5C and Supplementary Figure 2). In addition, we resolved a difference between previous data [98,99] and showed migration of angioblasts to the region of the dorsal aorta not to be affected. Endothelial cells were present in their correct location ventral to the notochord (Figure 3).

Many arterial markers, such as *flt1, hey2* and *dll4* but not venous markers such as *flt4* and *dab2* are also expressed in the endocardium at 24–28 hpf, suggesting common regulation of gene expression. Importantly, we observed that *tal1* differentially regulates arterial and endocardial gene differentiation as expression of *flt1* and *hey2* is severely reduced in the

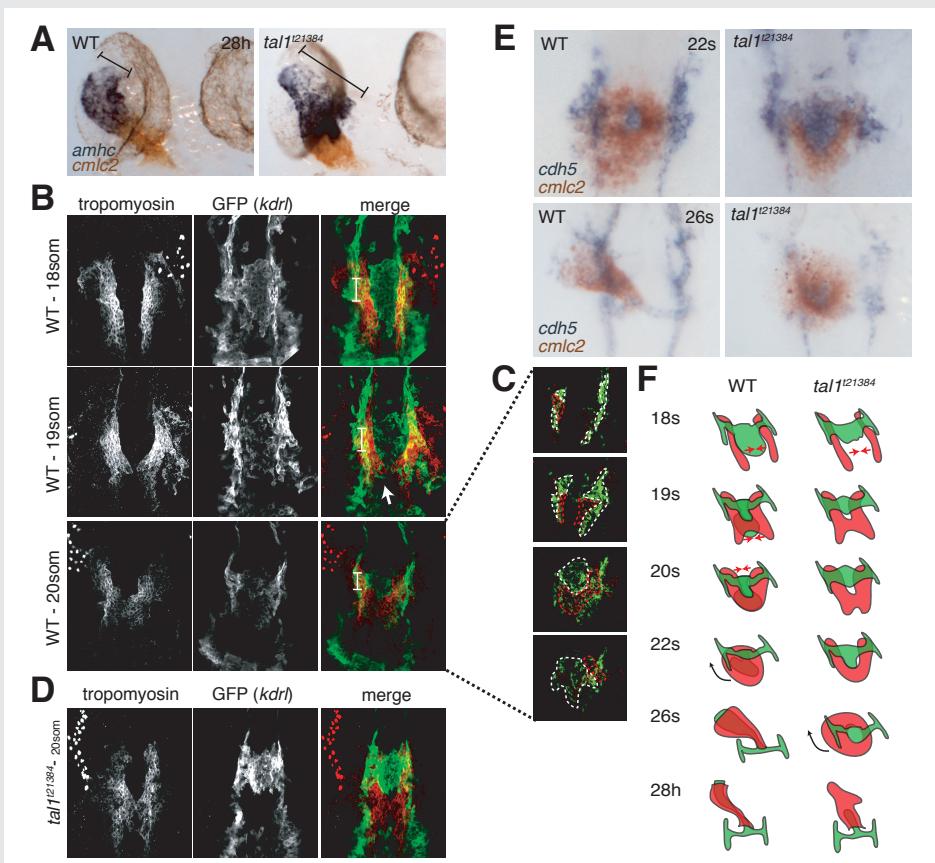

Figure 6. Defective Heart Tube Formation in *tal1*^{t21384} Mutant Embryos Despite Normal Fusion of Bilateral Myocardial Precursor Populations A. Chamber differentiation in wt and *tal1*^{t21384} mutant embryos revealed by two-color *in situ* hybridization showing *amhc* (atrium) and *cmlc2* (atrium and ventricle) at 28 hpf. Chamber differentiation proceeds normal in mutant embryos, but the primary heart tube is malformed with an enlarged atrial inflow region (brackets). **B-D.** Two-color immunohistochemistry using anti-tropomyosin (red, myocardium) and anti-gfp (green, *kdrl*, endocardium) antibodies. Images were generated as maximum projections of confocal z-stacks (ventral views, anterior to the top). Some yolk platelets show intense autofluorescence at the wavelength used for anti-tropomyosin detection (647 nm). **B.** Heart morphogenesis during heart field fusion in wt embryos. The bilateral heart fields fuse dorsal to the endocardium between the 18- and 20-somite stage. Fusion is initiated in the posterior region of the heart. At the 18-somite stage, tropomyosin-positive cells are located ventral to the first aortic arches. **C.** Endocardial precursors are ventral to the myocardium in the lateral and posterior regions of the heart. Endocardial and myocardial sheets are closely associated, as relative positions were only revealed after deconvolution of confocal stacks. Four deconvolved images of the confocal image stack in (B) are shown in (C). **D.** In *tal1*^{t21384} mutant embryos, initial fusion of the myocardial precursor populations occurs normally, although endocardial precursors are absent in the posterior region of the heart field. Continues on next page.

head and trunk arteries, but expression is maintained in the endocardium (Figure 5C). In the absence of more specific endocardial marker genes, these results suggest that defects during migration rather than during endocardial differentiation are the cause of the heart defects observed in *tal1*^{t21384} mutant embryos.

Assembly of Endocardium and Myocardium during Early Heart Tube Formation

Heartbeat initiated normally in *tal1*^{t21384} mutant embryos, indicating normal myocardial differentiation in the absence of an endocardial lining. Indeed, differentiation of atrial and ventricular myocardium was observed at 28 hpf (Figure 6A). However, at this stage, the atrial side of the heart appeared abnormally enlarged, suggesting early defects during heart tube morphogenesis. Therefore, we performed two-color immunohistochemistry labeling the myocardium (tropomyosin) and endocardium (*kdrl:gfp*) in single embryos. Using this method, we confirmed the observation that fusion of the myocardial primordia is initiated in a relative posterior position to form a butterfly-like shape that changes to a horseshoe-shaped myocardium through fusion of the most posterior part of the myocardial primordium between the 18- and 20-somite stages (Figure 6B) [90]. At the onset of myocardial fusion, most of the endocardium is positioned medially to the bilateral myocardial precursors. Connection between the endocardium and the lateral dorsal aortas is persistent throughout development and occurs through the developing first aortic arches. These cells represent the endocardial cells located dorsal to the myocardium as described by Trinh et al. [90] (Figure 6B). Fusion of the myocardium occurs dorsal to the endocardium and is initiated just anterior to the most posterior endocardial cells (Figure 6B). Indeed, around this stage, movement of endocardial cells occurs ventrally relative to the myocardial cells, and by the 20-somite stage, most endocardial cells are located ventral to the myocardium—especially in the lateral and posterior regions of the heart (Figure 6C). However, the region of the endocardium that connects to the aortic arches is

Figure 6. (cont.) E. Primary heart tube formation from myocardial and endocardial precursors in wt and *tal1*^{t21384} mutant embryos revealed by two-color in situ hybridization showing *cdh5* (endocardium, blue) and *cmlc2* (myocardium, red) expression. Dorsal views, anterior is to the top. At the 22-somite stage, wt embryos have formed a cardiac disc, with endocardial cells underlying the circular myocardial primordium. The medial endocardium within the ring of myocardium forms the connection between the endocardium and the aortic arches. In *tal1*^{t21384} mutant embryos, anterior closure of the myocardial primordium is defective due to aggregation of endocardial precursors. At the 26-somite stage, wt embryos have formed the primary heart tube and rhythmical contractions begin. In *tal1*^{t21384} mutant embryos, heart tube formation is delayed. By this stage, myocardial cells have completed fusion formation at the anterior side of the cardiac disc. **F.** Schematic overview of fusion of myocardial precursor regions and heart tube formation in wt and *tal1*^{t21384} mutant embryos. Endocardium and aortic arches are in green, myocardium in red.

still positioned medially to the myocardium.
In *tal1*^{t21384} mutant embryos, fusion of the bilateral myocardial precursors is initiated normally, and thus appears independent of the endocardium or *tal1* function. Endocardial cells at the 22-somite stage remain located anterior to the myocardium, leading to defects in the anterior fusion of the myocardium, which in wt embryos has occurred at this stage (Figure 6D,E). Anterior fusion of the myocardium is delayed until the 26-somite stage (Figure 6E). The medial region of the myocardium at the 22-somite stage gives rise to the ventricle of the heart, whereas the lateral and posterior myocardium gives rise to the atrium [92]. Therefore, absence of atrial endocardial cells can be explained by an early migration defect of endocardial precursors. A summary of heart tube assembly from endocardial and myocardial precursors in wt and *tal1*^{t21384} mutant embryos is provided in Figure 6F.

Discussion

A Second Genetic Vertebrate Model for Loss of tal1 Function

We have identified a truncating mutation in the zebrafish *tal1* gene, making this the second species for which a genetic mutation for this important hematopoietic transcription factor is available. The *tal1*^{t21384} allele contains a truncating mutation that deletes the conserved bHLH domain of the protein. Functional interaction of *Tal1* and *Lmo2* is required for the early stages of vascular and hematopoietic lineages in the zebrafish [116], and this interaction occurs at the second helix, a region that is deleted by the *tal1*^{t21384} mutation. Moreover, expression of only the helix-loop-helix domain was sufficient to rescue hematopoietic and endothelial development in *tal1* morphants [116], indicating that the N-terminal part of the *Tal1* protein is dispensable for early hematopoietic and endothelial development. Therefore, we conclude that the *tal1*^{t21384} mutation leads to a complete loss of *tal1* function during early cardiovascular and hematopoietic development.

Loss of a Fourth VEGF Receptor Gene during Mammalian Evolution

We used a transgenic line under the control of the zebrafish *kdrl* promoter to follow endocardial development. Surprisingly, *kdr*l represents a fourth VEGF receptor class with orthologs in all vertebrates – except placental mammals – for which sufficient genome information is available. This fourth VEGF receptor class most likely arose as a consequence of the two proposed whole-genome duplication events that occurred before vertebrate divergence [117]. This is evidenced by the phylogenetic tree of the vertebrate VEGF receptors, which places the emergence of this fourth class prior to the divergence of teleost fish and terrestrial vertebrates. Linkage of class III receptor tyrosine kinases (which includes the VEGF receptors) to a caudal-type homeobox gene is conserved in the basal chordate

Amphioxus [118], suggesting that this configuration represents the ancestral state.
Our data strongly suggest the loss of a fourth VEGF receptor within the mammalian lineage, as we identified an ortholog of *kdrl* in the genome of the opossum *Monodelphis domestica*, tightly linked to the Cdx4 gene. This implies that the loss of a mammalian *kdrl* ortholog occurred relatively recently – after the divergence of the placental (eutherian) and marsupial mammals ~180 million years ago, but before the mammalian radiation. Interestingly, the human and mouse Cdx4 genes are found adjacent to the XIST noncoding RNA that regulates X-chromosome inactivation. XIST originated through pseudogenization of the LNX3 gene [119], of which an ortholog is also found in the zebrafish *kdrl-cdx4* locus. The differences between marsupial and placental mammals in the mechanism of X-chromosome inactivation [120], together with the observation that Cdx4 has a role during placental development [121], and the absence of a fourth VEGF receptor in placental mammals present in other vertebrate species (this chapter) suggest that the *cdx4-kdrl* locus has been an important hotspot during mammalian evolution.
The observation that non-eutherian vertebrates have a fourth VEGF receptor has consequences for understanding the relationship of *tal1* and the VEGF receptors. The murine KDR ortholog, Flk1, was found to function upstream of Tal1, and Tal1 expression was not detected in Flk1$^{-/-}$ embryos [122]. However, the putative zebrafish *flk1* ortholog was found to be downstream of *tal1* during zebrafish hematopoietic development [102], leading to controversy in the understanding of their interactions. Here we redefine the orthology among the different VEGF receptor classes, and importantly, we identify the true Flk1/KDR ortholog in the zebrafish (*kdr*). We find that early non-endothelial *kdr* expression, which starts 3-4 h before the onset of *tal1* expression, is not affected in *tal1*^{t21384} mutants. Therefore, we conclude that *tal1* does not function as an essential factor for the initiation of *kdr* expression. Rather maintenance of high-level endothelial expression of this gene is dependent on *tal1*.

Morphogenesis and Embryonic Origins of the Endocardium

Lough and Sugi [82] reviewed data on endocardial morphogenesis in higher vertebrates and proposed that endocardial and myocardial precursors are both derived from the same anatomic location: the cardiogenic mesoderm. From there, endocardial precursors migrate as single cells in between the myocardium and the underlying endoderm. Subsequently, endocardial precursors assemble in two bilateral vascular chords that later on fuse to form the inner lining of the primitive heart tube. Our data show that endocardial morphogenesis in the zebrafish embryo differs in at least two important aspects from that found in higher vertebrates. First, endocardial precursors appear to be derived from a distinct anterior region of the cardiogenic mesoderm, and require posterior migration

to the site of heart tube formation. This difference is potentially due to the lack of dynamic observations of endocardial precursor migration in higher vertebrates. Indeed, some data indicate that in higher vertebrates, the endocardium arises from a specific region of the cardiogenic mesoderm [123]. Our results give a first look at the origin of endocardial cells during early development. However, to obtain conclusive evidence regarding the cell movements and origins of the endocardium, higher-resolution fate mapping and cell tracing will be required. Second, zebrafish endocardial precursors do not assemble into bilateral vascular chords, but form a sheet medial to the myocardial precursors. The bilayered disc that is formed through fusion of the myocardial primordia over the endocardium is then converted into the primitive heart tube. This last difference is potentially due to differences in developmental timing between fusion of bilateral primordia and heart tube morphogenesis in zebrafish and higher vertebrates.

Using the *kdrl:gfp* and *fli1a:gfp* lines and two-color *in situ* hybridization, we suggest that the endocardium of the primitive heart tube forms from two bilateral precursor populations that are located immediately anterior to the bilateral myocardial precursor populations that express *nkx2.5*. The finding that the endocardium might arise from a region anterior to the myocardial primordia is surprising, given the lineage-tracing experiments performed by Serbedzija and coworkers [124]. In their study, cells were labeled anterior to the *nkx2.5*-expressing myocardial primordia at the ten- to 12-somite stage. At 33 hpf, these cells were found to contribute to the "head mesenchyme" and no cells were found in the heart. One explanation for this finding is that only cells were labeled immediately anterior to the *nkx2.5*-expressing region. Our time-lapse imaging indicates that these cells give rise to the aortic arches and the head vasculature, whereas endocardial precursors originate from a position within the part of the anterior lateral plate mesoderm that is slightly more anterior and ventral. Therefore, Serbedzija and coworkers most likely have not labeled the cells that we show here constitute the endocardial precursors.

Recently, Kattman et al. [83] used the differentiation of murine embryonic stem cells to show the existence of a cell population expressing Flk1, with the potential to form both myocardial and endocardial cells in vitro. Our data indicate that in the zebrafish embryo, there are anatomically separate populations of endocardial and myocardial precursor cells during early developmental stages. We show that during normal development both lineages undergo different morphogenetic movements that are suggestive of early lineage separation of endocardium and myocardium. However, this does not imply that these precursors are restricted to one particular differentiation fate at this stage, and given alternative (*ex vivo*) cues they can still contribute to both lineages. Our data also indicate that anatomically, the endocardial precursors are found in close association with a particular subset of the hematopoietic lineage in the zebrafish: the anterior population of primitive myeloid cells. Lineage tracing experiments will identify whether there exists a lineage re-

lationship with a common endocardial–myeloid progenitor, or whether endocardial and myeloid precursors are simply intermingled during one stage of their development. While resolving this specific question is beyond the scope of this paper, it is worth noting that we observed migrating cells with macrophage morphology that have low levels of *kdrl:gfp* expression originating from the same bilateral populations of cells as those giving rise to the endocardium and the head vasculature (Figure 4A). This transgene is not expressed in differentiated primitive myeloid cells, and so the signal potentially represents residual gfp protein from a previous stage of their development.

How the endocardial lining of the primitive heart tube becomes established is one of the least-understood aspects of cardiac morphogenesis [82]. In recent years, studies on zebrafish embryos have provided significant insight into the genetic regulation of myocardial development. We show here that a similar approach can be taken to study endocardial development. Given the many interactions between the myocardium and endocardium, both during development as well as in adult physiology and disease [125], our findings will provide a more comprehensive understanding of the morphogenesis and genetic regulation of the heart development.

Acknowledgments

We thank Christine Mummery and Ben Hogan for editorial review, Youri Adolfs and Jeroen Korving for immunohistochemistry and tissue processing, Josi Peterson-Maduro and Hinrich Habeck for cloning the zebrafish VEGF receptors, and the Tübingen 2000 screen consortium for identifying the *t21374* allele. The allele was identified while S. Schulte-Merker was working at Exelixis Deutschland GmbH. We also thank members of the Schulte-Merker laboratory for comments and scientific discussions.

Supplementary Information

Supplementary information, including 3 figures and 3 movies, can be found online at http://www.plosgenetics.org/article/info%3Adoi%2F10.1371%2Fjournal.pgen.0030140.

Supplementary Table. Oligo Sequences

Name	Sequence
tal1_ex3_fw	CAACATTAATGCACATCTTGG
tal1_ex3_rev	TCTACCTGGTGGTCTTCCTC
tal1_ex3_seq	TGGGCGAACAATCAATTTAG

Chapter 4

In vivo imaging of endothelial diversity in transgenic zebrafish

Jeroen Bussmann[1] and Stefan Schulte-Merker[1]

[1]Hubrecht Institute, Developmental Biology and Stem Cell Research, Utrecht, The Netherlands

Abstract

The arteries, veins and lymphatic vessels of the vertebrate circulatory system assemble into complex networks, with a tissue-dependent network structure. How organ-specific vascular networks arise is incompletely understood. A first step towards understanding is the visualization of vascular networks in vivo. We have generated a transgenic line that expresses red fluorescent protein (RFP) under control of enhancer elements from the zebrafish *flt1* gene (*flt1*^{enh}*:rfp*) that captures endothelial diversity in embryonic, larval and adult zebrafish. This line allows the separate identification of arteries, veins and lymphatic vessels based on their relative RFP expression levels. A large variety of network structures in the zebrafish was identified. Interestingly, a fourth vessel type (lymph-arteries) was observed on the skin and scales of the adult zebrafish. These vessels branch from the dorsal aorta, follow the course of the arterial system to the body surfaces, where they connect to the terminal branches of the lymphatic capillaries. We suggest that these vessels constitute the afferent component of the lymphatic system in zebrafish.

Introduction

The circulatory system of higher vertebrates can be divided in two components: a blood vascular system required for the transport of oxygen, nutrients and wastes to and from the tissues, and a lymphatic vascular system, required for the regulation of fluid balance, absorption of fatty acids, and in the regulation of the immune response [126,127]. The blood vasculature consists of afferent vessels, the arteries, and efferent vessels, the veins. In contrast, the lymphatic vasculature in mammals only consists of blunt-ended efferent vessels, which eventually drain into large venous vessels.

Historically, it was thought that the lymphatic vasculature is a common feature of all vertebrates [3]. This view was challenged with the identification of a so-called secondary vascular system in teleost fish [128]. The secondary vascular system is a vascular system parallel to the blood vascular system. Uniquely, there is a direct connection with the arterial system, which in teleost fish presents as interarterial anastomoses: small caliber vessels that originate from the large arteries, and converge into secondary arteries. These form capillary beds mainly on the internal and external body surfaces (fins, skin, gills and intestine) and drain in secondary veins, which connect to the blood venous system [129].

Although the secondary vascular system has been identified morphologically, a lack of molecular markers has precluded direct *in vivo* identification of secondary vessels. In fact, the existence of a secondary vascular system has been recently challenged with the sug-

gestion that the connections between the arterial system and the secondary vasculature are an artifact caused by the morphological methods used to identify them [130]. Recently, a functional lymphatic system was described in zebrafish embryos, with molecular requirements similar to that of higher vertebrates [6,7]. The relationship between the lymphatic vascular system identified molecularly and morphologically in embryonic zebrafish and the various secondary vascular systems identified morphologically in several lower vertebrate species [4,128] is unknown.

Here we show that the arterial component of the secondary vascular system is present in adult zebrafish, and is a molecularly distinct vessel type. This vessel system originates from the dorsal aorta and connects the aorta to the terminal branches of the lymphatic vascular system. The functional and morphological homology of the venous component of the secondary vascular system in the zebrafish and mammalian lymphatic vessels suggests that during evolution of the lymphatic system the afferent component of the lymphatic system –the "lymph-arteries" – as observed in zebrafish, have been lost leaving the blunt-ended lymphatic system of land vertebrates.

Methods

Zebrafish strains

All zebrafish strains were maintained in the Hubrecht Institute using standard husbandry conditions. Animal experiments were approved by the Animal Experimentation Committee of the Royal Netherlands Academy of Arts and Sciences (DEC). Published transgenic lines used were *TG(fli1a:gfp)^{y1}* [15], *TG(kdrl:gfp)^{s843}* [16] and *TG(kdrl:mem-rfp)^{s916}* [23].

Recombineering

The Citrine (yellow fluorescent protein, *yfp*) [132] coding sequence was amplified using primers BamHI_GFPfw and XbaI_GFPrev and directionally cloned in the BamHI and XbaI sites of pCS2+ to generate pCS2+_Citrine. A kanamycin resistance cassette was amplified from pCDNA3 using primers NotI_Em7_fw and ApaI_Kan_rev and directionally cloned in the NotI and ApaI sites downstream of the SV40 late 3'UTR in pCS2+_Citrine to generate pCS2+_Citrine_kan. A bacterial artificial chromosome (BAC), DKEY-256I8, was identified based on BAC clone end sequences in the UCSC genome browser, assembly March 2006 (Zv6). Presence of the *flt1* transcription start site was confirmed by colony PCR using primers flt1_HA1_cont_fw and flt1_HA2_cont_rev. Positive colonies were used for recombineering using Red/ET Recombination Technology (Gene Bridges GmbH, Dresden) according to the manufacturers' protocol.
In a first recombineering step a citrine-SV40polyA-kanamycin cassette was inserted at the start codon of *flt1*. This was done through recombineering with a PCR fragment that was amplified from pCS2+_Citrine_kan using recombineering primers with 50bp homology arms (flt1_HA1_gfp_fw and flt1_HA1_kan_rev). Correct insertions were confirmed by colony PCR using primers flt1_HA1_control_fw with gfp_control_rev and kan_control_fw with flt1_HA2_control_rev. In a second recombineering step, a cassette containing an I-*Sce*I meganuclease site, an *attB* site for *phiC31* mediated transgenesis and an ampicillin resistance cassette was integrated into the clone backbone in place of a *loxP* site. This was done through recombineering with a PCR fragment amplified from pBluescript SK+ using primers pIndigo_I-SceI_amp_fw and pIndigo_attB_amp_rev. Correct insertion was confirmed by colony PCR using primers pIndigo_control_fw with amp_control_rev and amp_control_fw with pIn-

digo_control_rev. BAC DNA was isolated using HiPure Plasmid midiprep kit (Invitrogen, Carlsbad, CA, USA) with the following modifications to the manufacturers protocol: 100 ml of overnight culture was used as starting material, and bacterial lysis was scaled up by doubling the volumes of the respective buffers used. BAC DNA was eluted from the column with elution buffer heated to 50 °C, and precipitated with ice-cold isopropanol. DNA was very briefly allowed to dry and then dissolved in 100µl milliQ water.

BAC transgenesis

An injection mix was prepared containing 0.5 µl phenol red, 1µl 10x meganuclease buffer (Roche) 0.5 µl MgCl2 (1M) and 250 ng/µl BAC DNA. Volume was adjusted to 9µl with milliQ water. Shortly before injection, 1µl I-SceI enzyme was added. 1-cell embryos from paired matings were collected rapidly after laying and injected with 1-2 nl injection mix/embryo. Embryos were allowed to develop for 5 days, and those 10% of larvae with highest YFP expression were grown to adulthood. Germline transmission of the transgene was identified by outcrossing and screening for YFP expression. 3 adults from 50 screened displayed germline transmission (~10% of YFP+ embryos).

Identification and cloning of conserved flt1 enhancers

Promoter-YFP-polyA fragments were amplified from the modified BAC DKEY-256I8 described above using primers SpeI_p181_fw or SpeI_p2.2kb_fw with HinD3_SV40_rev and directionally cloned into the SpeI and HinDIII sites of the pMiniTol2 [133] vector to generate pTol2_flt1p2.2kb and pTol2_flt1p181. pMiniTol2 contains the long terminal repeats of the Tol2 transposable element. Enhancer elements were directionally cloned into pTol2_flt1p181 using primers NotI_CNE9_fw and SpeI_CNE9b_rev; NotI_CNE9_fw and SpeI_CNE9a_rev; NotI_CNE11_fw and SpeI_CNE11_rev to generate pTol2_flt1CNE9a+b_p181, pTol2_flt1CNE9a_p181 and pTol2_flt1CNE11_p181.

Tol2 transgenesis

Promoter/enhancer constructs described above were injected at 25 ng/µl with tol2 transposase RNA (25 ng/µl) into embryos obtained from paired matings. Embryos were selected at 3 dpf for high transient expression and grown to adulthood. Germline transmission was identified by outcrossing and screening for fluorescent protein expression.

Imaging

Embryos and dissected adult organs were mounted for imaging in 0.5% low melting point agarose (Invitrogen, Carlsbad, CA, USA) in E3 buffer or phosphate buffered saline. Confocal image stacks were collected on SPE, SP2 or SP5 confocal microscopes with 10x or 20x objectives (Leica Microsystems, Wetzlar, Germany). Images were processed in ImageJ.

Results

Generation and characterization of flt1^{BAC}:yfp transgenic zebrafish

In an effort to visualize the endothelial diversity of zebrafish, we selected several genes with restricted endothelial expression patterns during early development for the generation of transgenic reporter lines. One of the genes selected was *flt1*, a gene we had observed previously to exhibit an expression pattern highly restricted to arterial endothelial cells at 24 hours post fertilization (hpf) (see Chapter 3).

The zebrafish *flt1* gene has 30 exons spanning 58 kb on chromosome 24, and based on expressed sequence tag (EST) evidence, encodes two major splice isoforms. One is pre-

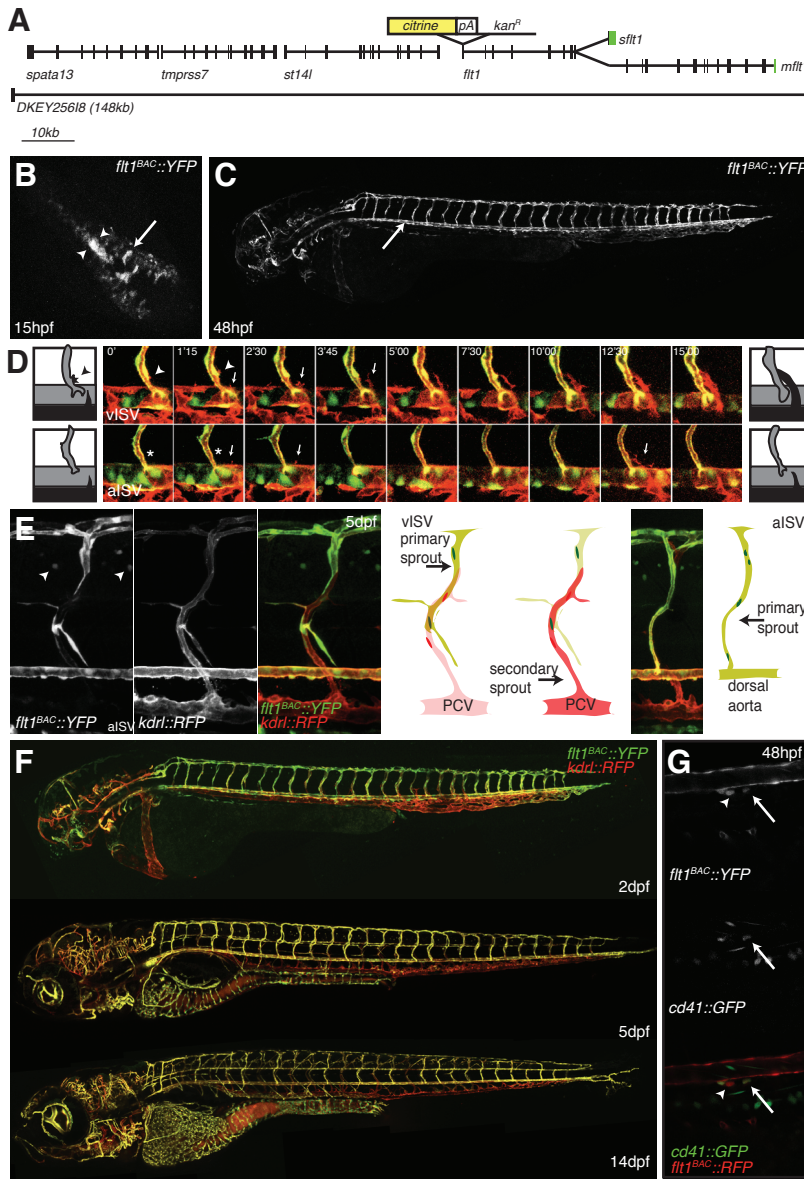

Figure 1. Generation and characterization of *flt1*^{BAC}*:yfp* transgenic zebrafish. A. Overview of the zebrafish *flt1* locus contained within BAC DKEY-256l6. There are 4 genes on this 148kb BAC, namely *spermatogenesis associated 13* (*spata13*), *transmembrane protease, serine 7* (*tmprss7*) a gene similar to *suppressor of tumorigenicity 14* (*st14l*) and *flt1*. (continues on next page)

dicted to encode full-length membrane-bound *flt1*(*mflt1*), the other, secreted *flt1* (*sflt1*) terminates on an alternative exon 11, and lacks the transmembrane and tyrosine kinase domains. These two major isoforms have also been observed in higher vertebrates, where the secreted isoform is generated by skipping a splice donor site of exon 13 and termination in the intron between exon 13 and 14.

To generate a *flt1* reporter line, a bacterial artificial chromosome (BAC) clone was identified containing the *flt1* gene (DKEY-256I8) including 86 kb of upstream and 4 kb of downstream sequence (Figure 1A). Also on this BAC are three other predicted genes, namely *spermatogenesis associated 13* (*spata13*), *transmembrane protease, serine 7* (*tmprss7*) and a gene similar to *suppressor of tumorigenicity 14* (*st14l*). Homologous recombination in *E.coli* (recombineering) was used to insert a YFP reporter cassette at the start ATG of *flt1*. This insertion is predicted to abolish *flt1* expression by removing the endogenous start codon. Both *mflt1* and *sflt1* use the same translation start site, therefore this construct acts as a reporter for both isoforms. The line with the highest expression was used for further analysis (called *flt1^{BAC}:yfp* hereafter). *Flt1^{BAC}:yfp* transgenic fish are viable and fertile and do not display obvious phenotypes due to the presumed overexpression of three other genes on the BAC.

Expression from the *flt1^{BAC}:yfp* transgene is initiated at 15hpf, when angioblasts that will

Figure 1 (cont.) The *flt1* gene has two major splice variants: a secreted isoform (*sflt1*) and a full length isoform containing the tyrosine kinase domain (*mflt1*). For the generation of the *flt1^{BAC}:yfp* transgenic line, the yellow fluorescent protein Citrine, a SV40 3'UTR and a kanamycin resistance cassette (not to scale) was inserted at the start ATG of *flt1*. **B-E.** Characterization of *flt1^{BAC}:yfp* transgenic zebrafish. **B.** The onset of YFP expression is at 15hpf, when migrating angioblasts (arrow) and the forming dorsal aorta (arrowheads) express YFP. **C.** At 48hpf, high YFP expression is observed in the dorsal aorta (arrow), intersegmental arterial network and head arteries. Low YFP expression is observed in the veins. **D.** Images from a timelapse movie comparing *flt1^{BAC}:yfp* (green) and *kdrl:rfp-caax* (red) expression. The dorsal aorta and intersegmental vessels are YFP and RFP positive (yellow), whereas the posterior cardinal vein and sprouts derived from it are RFP positive only (red). During remodelling of the trunk vascular network, sprouts (arrows) from the PCV can make a connection to the existing intersegmental artery and convert it into a vein. Two sprouts are compared, in the first sequence the sprout emerging from the PCV makes a connection to the ISV, in the second sequence the sprout is unsuccesful, and the ISV remains arterial. Note the presence of filopodia emerging from the ISV in the first sequence (arrowhead) and absence in the second sequence (asterisk). **E.** At 5 dpf, the trunk vascular network has been remodelled. *flt1^{BAC}:yfp* marks only the cells in the network that were derived from the dorsal aorta, whereas *kdrl:rfp-caax* marks all blood endothelial cells. Therefore, arterial ISVs are positive for both YFP and RFP. In venous ISVs the cells derived from the PCV are positive for RFP only. Also note the expression of *flt1^{BAC}:yfp* in a subset of spinal chord neurons (arrowheads). **F.** YFP expression is largely restricted to arteries during the first 3 days of development but then gradually expands to the veins, and later is coincident with the *kdrl:rfp-caax* transgenic line. **G.** The *flt1^{BAC}:yfp* transgenic line also marks developing hematopoietic stem cells as they emerge from the dorsal aorta. Non-endothelial *flt1^{BAC}:yfp* cells are observed ventral to the dorsal aorta at 48hpf, some of these cells co-express the hematopoietic stem cell marker *cd41:gfp* (arrow). Note the presence of a YFP positive, *cd41:gfp* negative cell (arrowhead).

eventually form the dorsal aorta are seen to migrate from the lateral plate mesoderm to the midline (Figure 1B). Weak expression is observed in the forming cardinal vein, however, this expression gradually extinguishes, and YFP expression is then restricted to the dorsal aorta and the sprouting primitive intersegmental arteries in the trunk from 48hpf to 5dpf (Supplementary Figure). In the head, YFP expression is observed in head arteries, and in the ventricular endocardium (Figure 1C).

Initially, all trunk intersegmental vessels are connected to the dorsal aorta, and can all be considered intersegmental arteries. Between 36 and 60 hours, the primitive vascular network in the zebrafish trunk is remodeled by secondary angiogenic sprouts from the posterior cardinal vein (PCV) that make a connection to ~50% of preexisting intersegmental vessels, thereby converting them into intersegmental veins. Primary sprouts that do not connect will maintain their connection to the dorsal aorta and will maintain their arterial identity [2]. Secondary sprouts from the PCV that do not make a connection instead migrate to the parachordal region, and recent work has shown that these are the precursors to the lymphatic system [131].

A previously established transgenic line, *kdrl:rfp*, labels all blood endothelial cells [131]. Since the *flt1^{BAC}:yfp* transgene only labels the cells derived from the primitive intersegmental arteries, but not the venous sprouts from the PCV, the *flt1^{BAC}:yfp* transgene in combination with *kdrl:rfp* can be used to distinguish the different cellular origins of the intersegmental veins (Figure 1E). Time-lapse imaging of the double transgenic embryos revealed the dynamic behavior of intersegmental vessels during the establishment of connections with the secondary sprouts. More specifically, sprouts emerging from the PCV send out filopodia in the direction of the intersegmental vessels. The endothelial cells of the intersegmental vessels can also send out filopodia in the direction of the venous sprout. If they do, a connection will be established, and the intersegmental vessel is converted into an intersegmental vein. Interestingly, presumptive intersegmental arteries remain quiescent and do not send out filopodia (Figure 1D). This suggests that at least some of the selection for intersegmental identity is determined within the intersegmental vessels themselves.

Although the *flt1^{BAC}:yfp* transgene is highly specific for arterial endothelial cells during early stages, later reporter expression becomes upregulated in all blood endothelial cells. This upregulation is first apparent in the venous endothelial cells in the brain. Later venous endothelial cells in the trunk also express the transgene. This becomes especially apparent in the *kdrl:rfp|flt1^{BAC}:yfp* double transgenic embryos, where YFP and RFP expression become almost indistinguishable from 2 weeks of development (Figure 1D).

The *flt1^{BAC}:yfp* transgene is also expressed in single cells ventral to the wall of the dorsal aorta. This is the location from where the first definitive hematopoietic stem cells emerge in the zebrafish embryo. Consistently, a subset of *flt1^{BAC}:yfp^{+}* cells also expresses *cd41:gfp,* a

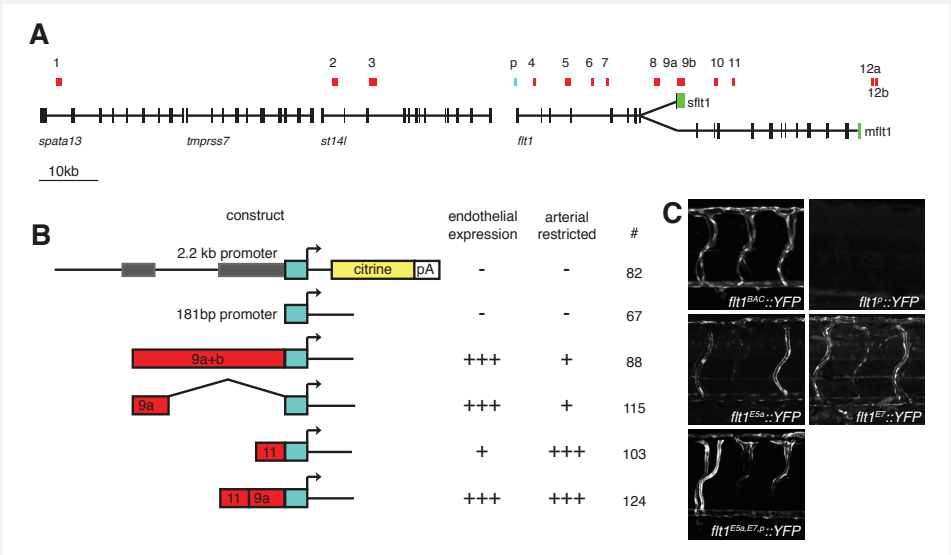

Figure 2. Identification of conserved *flt1* enhancers. A. Overview of the *flt1* locus. Conserved noncoding elements (indicated in red) were identified using VISTA. **B.** Overview of enhancer constructs generated. Two promoter (2.2kb promoter, and 181b promoter) constructs failed to drive endothelial gene expression. Of the CNE constructs tested, CNE 9a+b, CNE 9a and CNE11 resulted in restricted endothelial expression, analyzed at 3dpf. Only CNE11 drove restricted arterial expression. A combination of CNE9a and CNE11 resulted in high-level arterial-restricted expression. # indicates number of injected embryos analysed. **C.** Trunk segmental vasculature in transgenic lines derived from the injections in B.

marker for definitive hematopoietic stem cells (Figure 1E). Other non-endothelial *flt1*^{BAC}*:yfp* expression is observed in a subpopulation of spinal cord neurons (arrowheads in Supplementary figure (A)).

Identification of conserved flt1 enhancers

The upregulation of venous expression of the *flt1*^{BAC}*:yfp* transgene suggested that separate regulatory elements were responsible for different aspects of *flt1* expression. To obtain a general *in vivo* marker for arterial endothelial cells in adult zebrafish, the transcriptional regulation of *flt1* was analyzed in more detail. Cloning of upstream sequence in front of a YFP reporter failed to drive endothelial expression when introduced into zebrafish embryos. The proximal promoter contains a large number of repetitive elements and has very little sequence conservation. This suggested that *flt1* transcription is largely regulated by distant enhancer elements. We therefore aimed to identify conserved sequences in the *flt1* locus that might act as enhancers.

Twelve conserved non-coding elements (CNEs) were identified when five different fish

species (zebrafish, two pufferfish species, medaka and stickleback) were compared (Figure 2A). Three of these showed very strong sequence conservation and were also found in mammalian genomes. Interestingly, part of the 3'UTR of human *sflt1* was found to be conserved as CNE 9a in fish, even though this sequence is not used as 3'UTR in these species. This suggested that the 3'UTR of mammalian *sflt1* provides a second independent function as an enhancer element. Similarly, the 3'UTR of fish *sflt1* was found to be conserved in mammals as CNE 11, where it is not used as a 3'UTR.

Enhancer activity of the CNEs was initially tested by cloning the region from the zebrafish in front of a minimal promoter (*e1b:yfp*). For none of the cloned enhancer fragments this resulted in endothelial reporter expression. Therefore the *e1b* promoter was replaced by a short fragment (400bp) of the endogenous *flt1* promoter (*flt1^{p}:yfp*). This element did not contain regulatory elements sufficient for endothelial expression by itself. However, for several CNEs the combination with the endogenous *flt1* promoter resulted in endothelial reporter expression in transgenic lines (Figure 2C). More specifically, endothelial expression was found to be regulated by the two highly conserved CNEs found in the fish (CNE9a) and mammalian (CNE11) 3'UTRs. Interestingly, these enhancers showed complementary regulation: the CNE9a enhancer showed very high endothelial specific expression, but expression was not completely arterial-restricted. The CNE11 enhancer showed relatively weak endothelial expression, but within the endothelium was restricted to arterial endothelial cells. Therefore, a combined construct was generated containing both the CNE9a and CNE11 enhancers. The transgenic line generated with this construct displayed strong arterial-restricted expression (Figure 2C).

flt1^{enh}:rfp is a general marker for arterial endothelial cells

Most of the previously established vascular transgenic lines in the zebrafish use GFP as a reporter. These include the *kdrl:gfp* transgenic line, which labels blood endothelial (but not lymphatic) cells in the embryo and most adult tissues (Chapter 5), and the *fli1a:gfp* transgenic line, which is a general marker for endothelial cells throughout development and in adults [15]. In order to make a direct comparison between reporter expression from the *flt1* enhancer/promoter construct, a coding sequence of the bright red fluorescent protein tdTomato was cloned behind the *flt1* promoter-enhancer construct to generate the *flt1^{enh}:rfp* transgenic line. Similar to the *flt1^{BAC}:yfp*, this transgenic line labels arterial endothelial cells in embryos, including the pectoral artery, intersegmental arteries and brain arterial network (Supplementary Figure). Differences also exist between the two lines, as expression of the *flt1^{enh}:rfp* reporter is reduced in the dorsal aorta, and its associated hematopoietic stem cells. This line also does not label the spinal cord neurons that can be observed in the *flt1:yfp* transgenic line (Supplementary Figure).

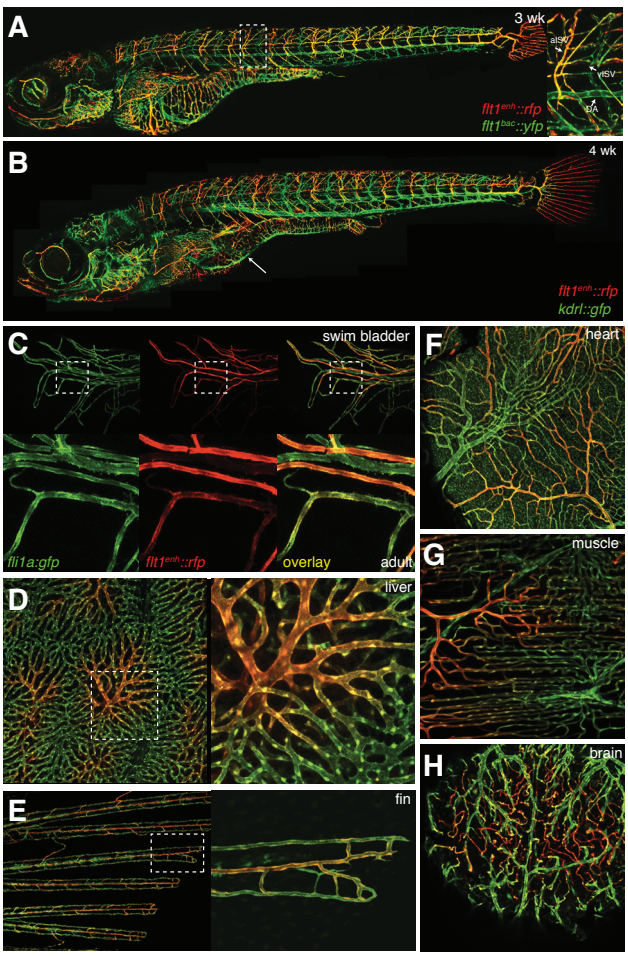

Figure 3. *flt1*^{enh}*:rfp* expression in larvae and adult organs. A. Comparison of *flt1*^{BAC}*:yfp* and *flt1*^{enh}*:rfp* expression, 3 weeks after fertilization. Note high-level expression of *flt1*^{BAC}*:yfp*, but not *flt1*^{enh}*:rfp*in venous intersegmental vessels (vISV) and the dorsal aorta (DA). Expression of *flt1*^{enh}*:rfp* is observed in arterial intersegmental vessels (aISVs). **B.** Comparison of *kdrl:gfp* and *flt1*^{enh}*:rfp* expression, 4 weeks after fertilization. Note high-level expression of *kdrl:gfp*, but not *flt1*^{enh}*:rfp* expression in the hepatic portal vein (arrow). **C-H.** Comparison of *flt1*^{enh}*:rfp* and *fli1a:gfp* expression in various adult organs. **C.** Transgene expression in the swim bladder. *fli1a:gfp* expression is uniform over the swim bladder. Expression of *flt1*^{enh}*:rfp* is high in the arteries, but low in the veins. A gradient of expression levels is observed in the swim bladder capillaries. **D.** Transgene expression in the dense endothelial network of the liver. Note the gradients of *flt1*^{enh}*:rfp* expression (inset). **E.** Transgene expression in the fin rays. A central artery with high *flt1*^{enh}*:rfp* expressions drains into 2 veins in each fin ray. **F.** Transgene expression in the heart. On the surface of the heart, tree-like coronary arterioles and capillaries are observed that drain into the venules and larger veins of the heart. **G.** Transgene expression in the skeletal muscle. A dense network of capillaries is observed in the fast skeletal muscle. Gradients of *flt1*^{enh}*:rfp* expression are observed throughout this network. **H.** Transgene expression in the brain (optic tectum). Arteries from deep within the brain express high levels of *flt1*^{enh}*:rfp* and are found to drain to veins on the surface of the brain.

Importantly, arterial restricted expression in the *flt1*^{enh}*:rfp* reporter line persists until adulthood. One example is the elaborate vascular network of the adult swim bladder. Several swim bladder arteries and veins run in parallel, with terminal branches that loop over its surface. A direct comparison in the *fli1a:gfp/flt1*^{enh}*:rfp* double transgenic line revealed that *fli1a:gfp* expression is uniform over the swim bladder vascular network, but *flt1*^{enh}*:rfp* var-

ies between vessel type. The swim bladder arteries express the *flt1^{enh}*:rfp transgene at high levels, whereas the swim bladder veins have only low expression. The terminal loops display a gradient of RFP expression (Figure 3A). Similar observations were made in other organs examined, including the liver (Figure 3B), fins (3C), coronary vasculature (3D), skeletal muscle (3E) and brain (3F). Arterial restricted *flt1^{enh}:rfp* expression is independent of network density, branching and relative orientation of vessel. Hence, vascular networks of various organs with different morphology, can be divided in an arterial and a venous half based on *flt1^{enh}:rfp* expression.

Identification of lymphatic vessels and a fourth vessel type in adult zebrafish

flt1^{enh}:rfp expression is relatively low in venous endothelial cells compared to arteries, but can be detected in all adult blood vessels. By comparing *flt1^{enh}:rfp* and *fli1a:gfp* expression, a third vessel type was observed which expresses *GFP*, but has a complete lack of *RFP* expression. This vessel type was observed in the intestine and ovaries and was especially pronounced on the skin and scales. The scale vascular network can be observed through life imaging of adult zebrafish, which allows simultaneous determination of blood flow. This identified the third vessel type as lymphatic vessels based on the absence of blood circulation and their morphology (wide vessels containing valve-like structures).

Interestingly, yet another vessel type was identified in the scale vascular network. These vessels were bloodless, but displayed intermediate levels of *flt1^{enh}:rfp* expression. Their caliber and general morphology was similar to the arteries and veins on the scales, and their initial path after they penetrated the skin was adjacent to arteries (Figure 4A). Strikingly, these vessels branched into a capillary network on the lateral edges of the scales, were they formed cellular connections with the terminal branches of the lymphatic vessels (Figure 4B). On most of these connections, the lumen appeared to be constricted, but several points of direct communication between the lymphatic network and this fourth vessel type were observed. This fourth vessel type was also observed in the skin, where connections with the lymphatic vascular system were abundant (Figure 4C). In the skin, blunt-ended lymphatic capillaries were also observed (Figure 4C). The fourth vessel type was usually found in close association with *flt1^{enh}:rfp^{hi}* arteries (Figure 4D). Sparse, cellular connections between the arteries and *flt1^{enh}:rfp^{mid}* vessels were observed (inset in Figure4D). Tracing back the *flt1^{enh}:rfp^{mid}* vessels to their point of origin revealed a direct connection with the arterial system at the dorsal aorta. Surrounding this vessel a branched network of *flt1^{enh}:rfp^{mid}* cells was identified. In the skin, some shunt-like structures between smaller arteries and the *flt1^{enh}:rfp^{mid}* vessels were found.

The structural features of the *flt1^{enh}:rfp^{mid}* vessels, including point of origin along the dorsal aorta, small caliber and connection to the lymphatic vascular system, identify these ves-

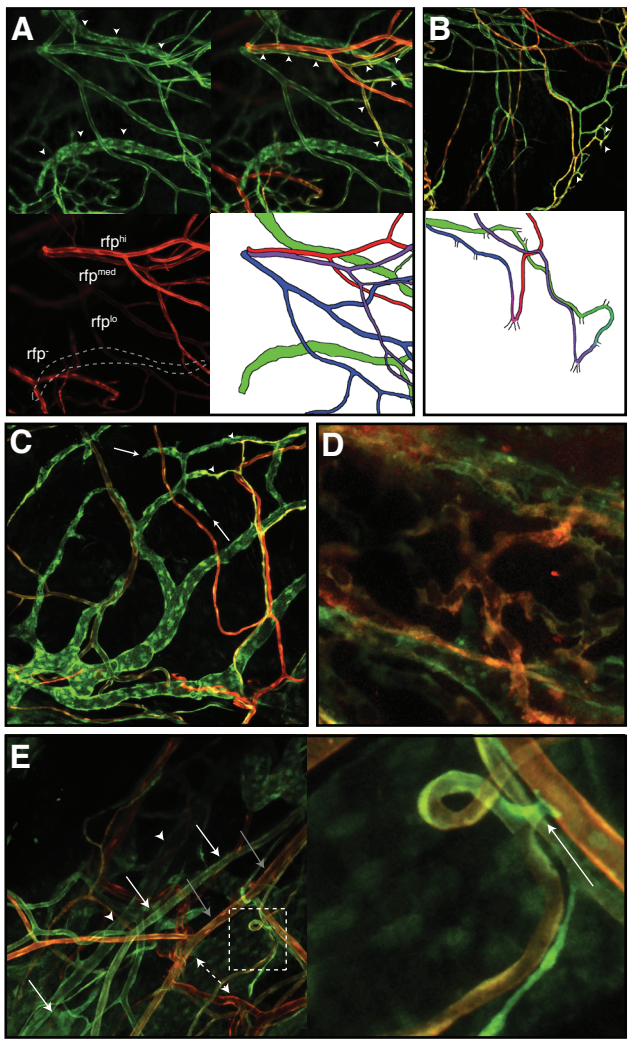

Figure 4. Identification of a fourth vessel type in adult zebrafish. A. Comparison of *flt1*^{enh}*:rfp* and *fli1a:gfp* expression in the scales of adult zebrafish. Uniform *fli1a:gfp* expression is observed in endothelial cells in the scale vascular network. Note the presence of wide vessels resembling the morphology of mammalian skin lymphatic vessels. These vessels have no detectable *flt1*^{enh}*:rfp* expression (rfp^{-}). Vessels expressing three different levels of *flt1*^{enh}*:rfp* expression are observed, which can be identified as arteries (rfp^{hi}), veins (rfp^{lo}) and a novel vessel type, lymph-arteries (rfp$^{int(ermediate)}$, arrowheads). The scheme displays the various vessel types in different colors (lymphatics: green; arteries, red; veins, blue; lymph-arteries are indicated in purple. **B.** rfp-mid lymph-arteries drain into lymphatic capillaries on the lateral edges of the scales (arrowheads). **C.** All four vessel types are observed in the skin. Note the presence of blunt-ended lymphatic capillaries (arrows) and connections between lymphatic vessels and lymph-arteries (arrowheads). **D.** Lymph-arteries originate from the dorsal aorta, where finger-like projections of rfp^{mid} vessels are observed on the surface of the dorsal aorta. **E.** Larger-calliber vessels in the dermis. Large arteries (grey arrows), veins (white arrowheads) and lymph-arteries (white arrows) are observed within the deeper layers of the dermis. Also note the presence of collecting lymphatic vessesl with very large diameter (dashed arrow), and the presence of cellular connections between lymph-arteries and arterioles (arrow in inset).

sels as the secondary arteries. Since they are molecular and morphologically distinct from lymphatic vessels and appear to originate as a separate vessel type during embryonic development, we propose to name these vessels lymph-arteries.

Discussion

Regulation of flt1 expression

In this study, we used regulatory elements from the zebrafish *flt1* locus to generate a artery-restricted transgenic line. We chose *flt1* as an arterial marker, since we found previously that *flt1* expression is restricted to arterial endothelial cells (Chapter 3). This was rather surprising, since Flt1 is not considered to be an arterial marker in higher vertebrates. In this study, we found YFP expression from the *flt1*^{BAC}*:yfp* expands to venous endothelial cells during larval development. It appears likely therefore, that Flt1 expression is similar during mammalian development, initially enriched in arterial endothelial cells and subsequently expressed in all blood endothelial cells. Consistently, expression of Flt1 was found to be restricted to a subset of endothelial cells, and absent from lymphatic endothelial cells. Significantly, *flt1* expression was found to be especially pronounced in the dorsal aorta during mouse development.

Similarities and differences between the zebrafish and mammalian lymphatic system

Several features of the mammalian lymphatic vasculature appear to be conserved in the zebrafish. Probably the most conserved function is in the regulation of tissue fluid balance. Lymph flow is observed through zebrafish lymphatic vessels, and dyes injected in the interstitial space are taken up by the lymphatic system [6,7]. Also, zebrafish embryos lacking lymphatic vessels develop edema, similar to that observed in mammals [131]. The presence of lymphatic vessels in the intestine, suggests that they function in the dietary uptake of fatty acids, although this remains to be shown definitively. The function of the zebrafish lymphatic system in the regulation of the immune response, as observed in mammals, are unclear. There is no evidence for the existence of lymph nodes so far. Also, no blood cells are observed in embryonic or adult lymphatic vessels, although it is possible that lymphoid cells enter the lymphatic vascular system during infection.

Morphologically, the zebrafish lymphatic system appears very similar to that of higher vertebrates, including wide-diameter lymphatic capillaries with what appear to be valve-like structures. The collecting lymphatic vessel network contains many of the vessels observed in mammals, including the jugular lymph sac and the thoracic duct. Also the drainage of lymph into the jugular vein is conserved. The presence of smooth muscle cells surrounding the collecting lymphatic vessels is unknown.

One of the major differences is the presence of a fourth vessel type connecting the lymphatic system to arteries. This connection has been described morphologically as the afferent component of the secondary vascular system, but no molecular markers have been

identified so far. Here we describe the first molecular identification of this vessel type in the *flt1*^{enh}*:rfp* transgenic line. The identification of this vessel type in the zebrafish, a model organism which is highly amenable to experimental manipulation, will allow the functional characterization of this enigmatic vessel type.

Supplementary Information

Supplementary Table
Oligo Sequences

Name	Sequence
BamHI_GFPfw	GCGCGGATCCACCATGGTGAGCAAGGGCGAGGAG
XbaI_GFPrev	GCGCTCTAGATTACTTGTACATGCTCGTCCATG
SacII_Em7fw	GCGCCCGCGGCGACCTGCAGCCTGTTGA
ApaI_Kan_rev	GCGCGGGCCCTCAGAAGAACTCGTCAAGAAGGCG
flt1_HA1_cont_fw	CGTTGTGAGGTGAACTGATTC
flt1_HA2_cont_rev	CATTCCAGACCTGTATTTCATC
flt1_HA1_gfp_fw	tccataggtattccttcatctccaaacaaacaccctcaagcaagaccaag ACCATGGTGAGCAAGGGCGAGGAG
flt1_HA2_kan_rev	gtcagaacacgtcctgacagtccaaatatcatcacaaataatatatcgaa TCAGAAGAACTCGTCAAGAAGGCG
gfp_control_rev	GCCCTCGAACTTCACCTC
kan_control_fw	GTCAAGACCGACCTGTCC
pIndigo_I-SceI_amp_fw	ttctctgtttttgtccgtggaatgaacaatggaagtccgagctcatcgct ATTACCCTGTTATCCCTAAGAGTTGGTAGCTCTTGATC
pIndigo_attB_amp_rev	agccccgacacccgccaacacccgctgacgcgaacccctgcggccgcat GGAGTACGCGCCCGGGGAGCCCAAGGGCACGCCCTGGCA CCCGCACCGCGGCATTCAAATATGTATCCGCTC
pIndigo_cont_fw	AAGAAAGGAAACGACAGGTG
Amp_cont_rev	CTGAGATAGGTGCCTCACTG
Amp_cont_fw	TTTACTTTCACCAGCGTTTC
pIndigo_cont_rev	TGGTGCACTCTCAGTACAATC
SpeI_p181_fw	GCGCACTAGTCAACTGTACACCAGTAAACAGG
SpeI_p2.2kb_fw	GCGCACTAGTAATAAAGGCCCAACTGAAAGTGG
HinDIII_SV40_rev	GCGCAAGCTTTTAAAAAACCTCCCACACCTC
NotI_CNE9_fw	GAGAGCGGCCGCCCAGGGAGAGTGGAGTTG
SpeI_CNE9a_rev	GCGCACTAGTACGGAGGGTGTGTGAGTG
SpeI_CNE9b_rev	GCGCACTAGTTTTGCCAACATTTCAGCTAC
NotI_CNE11_fw	GAGAGCGGCCGCACAGATGCGGAAAGAGAAAC
SpeI_CNE11_rev	GCGCACTAGTGATGCGTACTATTGCTTTGG
BamHI_CNE11_fw	GCGCGGATCCGGTCCTTGGGAACTGGGTCCCTTAGC
NotI_CNE11_rev	GAGAGCGGCCGCCTGACTTCTGTTTCAGATATTGTCC

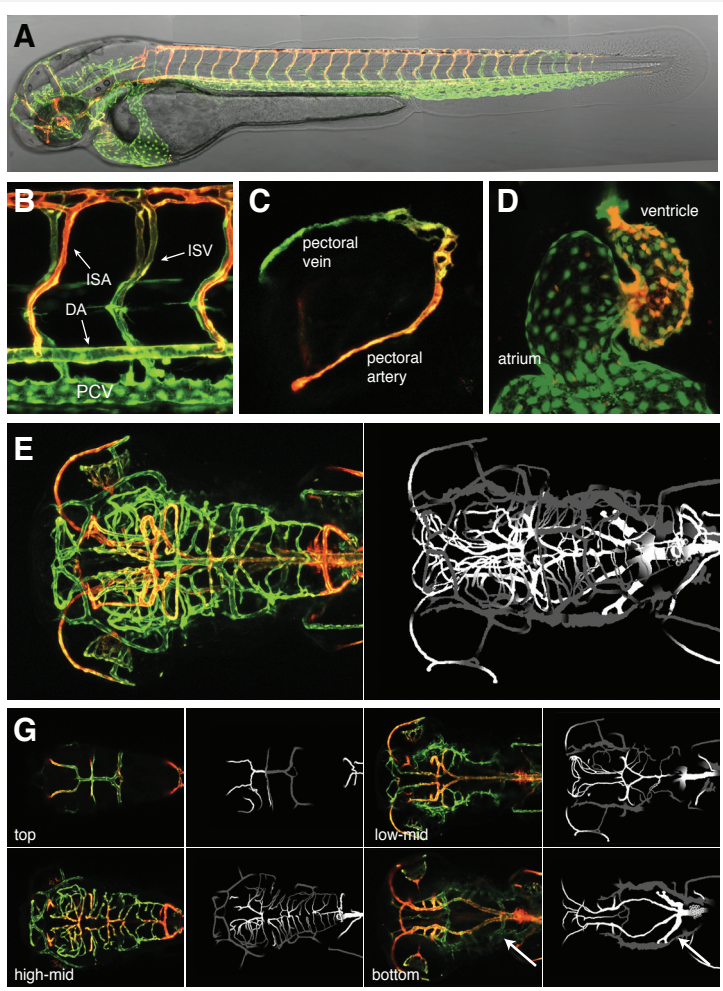

Supplementary Figure Comparison of *flt1^{enh}:rfp* and *kdrl:gfp* transgene expression. A. Double transgenic embryo at 48hpf. **B.** Trunk expression at 72hpf. Note high-level expression of *flt1^{enh}:rfp* in intersegmental arteries (ISA), but not in intersegmental veins (ISV), dorsal aort (DA) or posterior cardinal vein (PCV). **C.** Pectoral fin vascular network. High-level rfp expression is observed in the pectoral artery, but not in the pectoral vein. A gradient of transgene expression is observed in the capillary vessels that connect them. **D.** *flt1^{enh}:rfp* expression is observed in the ventricle, but only at low levels in the atrium of the heart. **E.** Head vascular network. Head arteries are identified by high-level *flt1^{enh}:rfp* expression (compare with a scheme of the head vasculature derived by analysing blood-flow patterns in the head vessels **F.** Adapted from [119], in this scheme arteries are in white, and veins in gray. **G.** Different optical sections through the confocal z-stack in (E), comparing *flt1^{enh}:rfp* expression with head arteries identified by blood flow. All arteries have high rfp expression. The only exception are the afferent arteries of the gill vasculature (arrow).

Chapter 5

ccbe1 is required for embryonic lymphangiogenesis and venous sprouting

Benjamin M. Hogan[1], Jeroen Bussmann[1,], Frank L. Bos[1,2,*], Merlijn Witte[1,*], Henricus J. Duckers[2] and Stefan Schulte-Merker[1]*

Nature Genetics 41 (4): 396-398 (2009)

[1]Hubrecht Institute, Developmental Biology and Stem Cell Research, Utrecht, The Netherlands
[2]Experimental Cardiology, Erasmus University Medical Centre, Rotterdam, The Netherlands
* These authors contributed equally

Abstract

Lymphatic vessels play important roles in tissue fluid balance, fatty acid absorption, inflammation, immunity and cancer metastasis. During development or pathogenesis, lymphatic vessels develop from pre-existing vessels in a dynamic process involving budding, migration and proliferation of lymphangioblasts. The molecular control of lymphangiogenesis remains to be elucidated. Here we identify a zebrafish mutant that lacks lymphatic vessels, while maintaining a functional, patterned blood vasculature. The responsible gene, *collagen and calcium binding EGF domain-1 (ccbe1)*, encodes a predicted secreted protein that is expressed along embryonic lymphangioblast migration routes. We identify *ccbe1* as a novel factor critically required for embryonic lymphangiogenesis, which acts at the same stage as *Vegfc/Vegfr3* signaling, being required for both venous angiogenic sprouting and lymphangioblast budding from venous endothelium.

The zebrafish lymphatic vasculature has recently been identified in early larvae with the molecular, functional and morphological characterization of the thoracic duct [6,7]. The thoracic duct is found immediately ventral to the dorsal aorta from 3.5 days post fertilization (dpf) and develops via the function of conserved molecular pathways including the vegfc/vegfr3 signalling pathway [6,7,134]. Consistent with the venous origin of lymphatic vessels [135], endothelial precursors of the zebrafish thoracic duct are derived from venous endothelium [2,6].

To identify novel regulators of lymphangiogenesis, we performed a forward genetic screen and isolated one mutant, *full of fluid* (*fof* ^{hu30613}), which failed to form a thoracic duct while retaining a patterned and functional blood vasculature (Fig. 1a-f). *fof* mutants also lacked previously unidentified, bloodless intersegmental (ISLVs) and dorsal longitudinal lymphatic vessels (DLLVs) (Fig. 1c-f). Mutants displayed severe edema initiating in the lower intestine and around the eyes from 6 dpf (Fig. 1 g and h, Supplementary Fig. 1) and very few mutants survived past the second week of life, with surviving 36 day old mutants displaying marked edema (Fig. 1i and j).

Genetic mapping of *fof* localized the mutation to chromosome 21 in an interval containing a single gene, c*ollagen and calcium binding EGF domain 1* (*ccbe1*) (Fig. 2a). *ccbe1* encodes a predicted secreted protein containing a signal peptide, collagen domain and calcium binding EGF domain. Sequencing revealed a single coding mutation in the fourth exon of *ccbe1* changing an aspartic acid (D) to glutamic acid (E) in the calcium binding EGF domain (Fig. 2 b-c). The residue mutated (D162) is completely conserved in *Ccbe1* proteins (Fig. 2d). Significantly, an equivalent mutation (D1479E) in a calcium-binding EGF domain of Fibrilin1 is associated with loss-of-function phenotypes in humans [136]. We injected

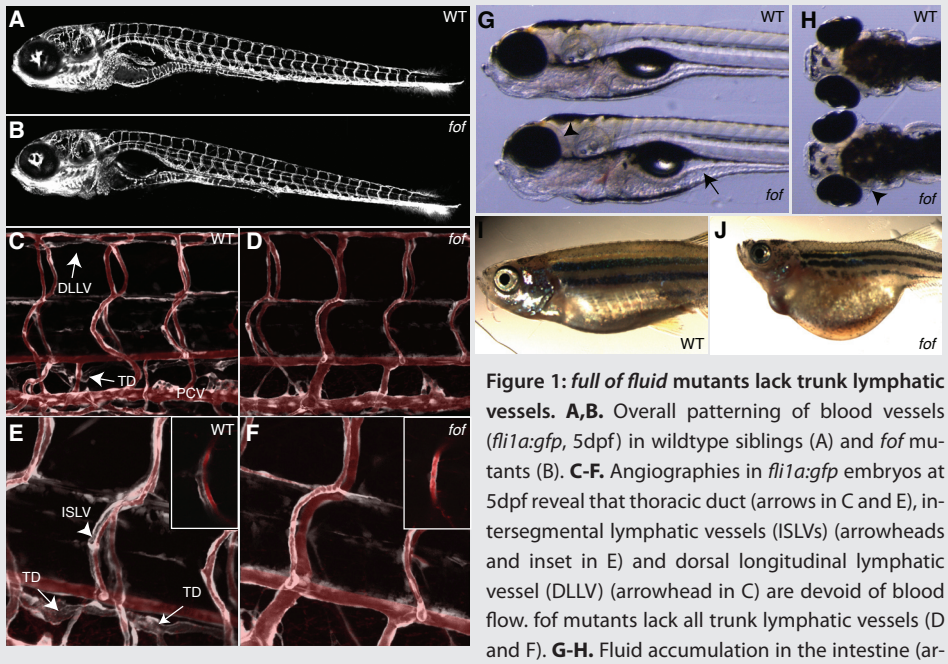

Figure 1: *full of fluid* mutants lack trunk lymphatic vessels. A,B. Overall patterning of blood vessels (*fli1a:gfp*, 5dpf) in wildtype siblings (A) and *fof* mutants (B). **C-F.** Angiographies in *fli1a:gfp* embryos at 5dpf reveal that thoracic duct (arrows in C and E), intersegmental lymphatic vessels (ISLVs) (arrowheads and inset in E) and dorsal longitudinal lymphatic vessel (DLLV) (arrowhead in C) are devoid of blood flow. fof mutants lack all trunk lymphatic vessels (D and F). **G-H.** Fluid accumulation in the intestine (arrow in G) and around the eyes (arrowheads in G and H) in mutants (lower) compared with wildtype siblings (upper) at 6dpf. **I,J.** *fof* mutants (J) that survive to 36dpf (n=3/28, see Supplementary Fig. 1) display severe edema.

ccbe1 targeting morpholinos (MOs), which efficiently phenocopied *fof* at 5 dpf (Fig. 2 e and f). Furthermore, the injection of *ccbe1* mRNA was sufficient to rescue lymphatic deficiency in a blind, genotype based assay (Fig. 2g), together demonstrating that *fof* ^{hu30613} is a loss-of-function allele.

We examined *ccbe1* expression during development and observed restricted expression in pre-pronephric mesoderm, ventral mesoderm, otic vesicles, epiphysis, the early pharyngeal region and the skin (Supplementary Fig. 2). In the 24 hpf trunk, expression was detected in the pronephros, the region of the posterior cardinal vein (PCV) and ventral mesenchyme (Fig. 3a). By 36 hpf, expression was detected in discrete zones along each somitic boundary, between the PCV and the horizontal myoseptum, as well l as along the horizontal myoseptum itself (Fig. 3b and c). This expression was non-endothelial as it was retained in *cloche* ^{hu30613} mutant embryos pre-selected for the absence of trunk endothelial cells (Fig. 3d). At 48 hpf, *ccbe1* expression was restricted along the horizontal myoseptum (Fig. 3e). Intriguingly, this highly dynamic expression pattern correlates spatially and temporally with the migration routes of endothelial cells which bud from the PCV and seed the horizontal myoseptum [2].

To determine whether non-endothelial expression was responsible for the lymphangiogenic role of *ccbe1,* we performed transplantation assays. When *ccbe1* morphant (MO injected) donor cells contributed to somitic mesoderm, thoracic duct formation from host cells was interrupted in the region of the transplanted cells (Fig. 3f). Reciprocally, wildtype contributions to somitic mesoderm were sufficient for morphant cells to form a thoracic duct in the region of the graft (Fig. 3g). We controlled for MO efficacy and endothelial cell origin by determining that wildtype embryos contained normal lymphatic vessels and morphant embryos were lymphatic deficient in non-grafted regions, and in addition transplanted endothelial cells were readily detectable (Supplementary Fig. 3). Additionally, muscle pioneer cells, which contribute to venous budding [137,138], were readily identifiable in all embryos (n=87) produced from heterozygous matings. Taken together, the domain structure of Ccbe1 (signal peptide, collagen domain, calcium binding-EGF domain), non-endothelial expression and transplantation assays indicate that *ccbe1* acts non-autonomously from somitic mesoderm during lymphangiogenesis.

To directly observe embryonic lymphangiogenesis, we developed a transgenic line with YFP expression enriched in embryonic veins and lymphatic vessels. We utilized regulatory elements from the *stabilin1 (stab1)* locus, which is expressed in lymphatic vessels [139,140] and which we found to be expressed in the same manner as *lyve1* [141] in ze-

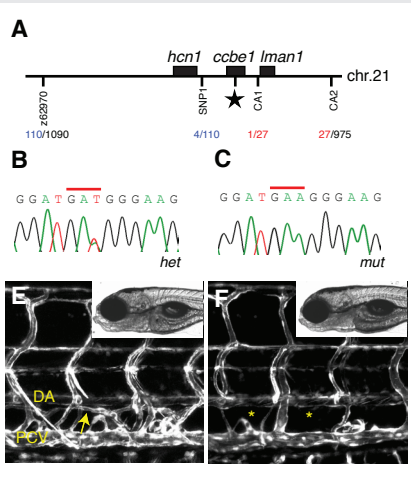

Figure 2: *fof*^{hu30613} encodes *ccbe1*. A. Meiotic map of the *fof* locus. Recombinant events for each polymorphic marker are depicted in red (proximal) and blue (distal). Recombinants for SNP1 and CA1 exclude neighboring genes *lman1* and *hcn1*. **B,C.** Sequencing of *ccbe1* identified a transversion (T to A) corresponding to position 162 of the predicted protein, replacing aspartic acid (D) with glutamic acid (E) (affected codon underlined). **D.** Multiple sequence alignment of Ccbe1 proteins demonstrating the conservation of zebrafish D162. **E,F.** Injection of a *ccbe1* ATG morpholinos phenocopies fof (F); wildtype control in (E). Arrow=thoracic duct,asterisk=absence of thoracic duct. **G.** *ccbe1* mRNA rescued the *fof* phenotype. An incross of heterozygous adult *fof* carriers was injected with *ccbe1* mRNA (wt or mutant), and scored for the absence of the TD (phenotype). Subsequently, the embryos with a TD were genotyped, and homozygous *fof* mutants were scored (genotype).

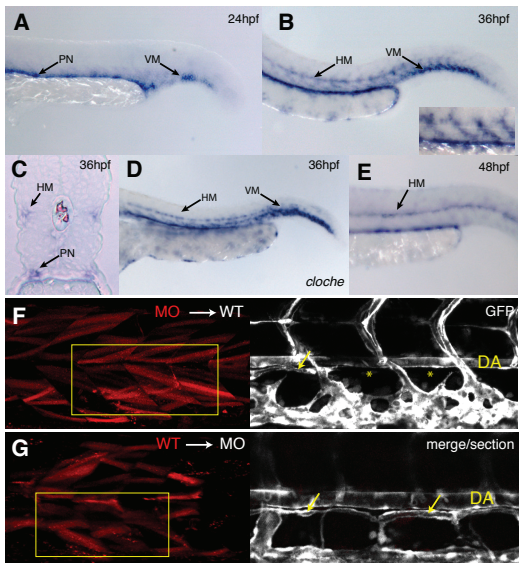

Figure 3. *ccbe1* is expressed within somitic mesoderm and required non-autonomously for lymphangiogenesis. A-E. *ccbe1* trunk expression is restricted to ventral mesenchyme (vm), pronephros (pn) and weakly in the region surrounding the PCV at 24 hpf (A). At 36hpf, expression extends along somitic boundaries (inset A) and the horizontal myoseptum (hm) (B and C). Expression in *cloche* mutant embryos is unaltered (D). *ccbe1* trunk expression is restricted to the horizontal myoseptum at 48hpf, when lymphangioblasts populate this region (E). **F.** Morpholino injected cells (rhodamine labeled, left) transplanted into wildtype embryos disrupt thoracic duct formation (GFP, right, boxed area) when contributing to somitic mesoderm. In a total of 92 transplants, n=7/7 disrupted thoracic ducts were immediately ventral to labeled muscle cells (5dpf). **G.** Wildtype donor cells (rhodamine labeled, left) rescued thoracic duct formation by morphant cells (GFP/rhodamine in single confocal section, right, boxed area) when contributing to somatic mesoderm. n=134 embryos transplanted, n=7/7 with lymphaatic fragments immediately ventral to grafted muscle. Arrows = presence, asterix = absence of thoracic duct fragments. See also Supplementary Figure 3.

brafish (Supplementary Fig. 4). Expression of *stab1*^{BAC}*:yfp* was vascular restricted, enriched in the PCV and venous derived endothelial cells (36hpf) and included endothelial cells at the horizontal myoseptum by 48hpf. At later stages, expression was largely restricted to lymphatic and venous endothelium, with arterial expression weakening progressively (Fig. 4a). Using live imaging, *stabilin1* positive cells were observed to bud directly from the PCV to the horizontal myoseptum from approximately 36 hpf (Supplementary Movie 1). Between 48 and 72 hpf, these cells remained in this region before migrating dorsally, to contribute to the DLLV, or ventrally, to contribute to the thoracic duct (Supplementary Movie 2). In *ccbe1* morphants, *stab1*^{BAC}*:yfp* expressing cells failed to bud from the PCV (Fig. 4a, Supplementary Movie 3). In mammals, Vegfc/Vegfr3 signaling is required for the initiation of lymphangioblast budding [142,143,144,145]. Zebrafish *vegfc* but not *vegfd* expression is found immediately dorsal to the PCV prior to and concurrent with the budding and dorsal migration of *stab1* expressing cells (Supplementary Fig. 5) [99]. We injected *vegfc* targeting MOs [121] and found that *vegfc* was required for the initiation of budding of *stabilin1* positive cells from the PCV at precisely the stage requiring *ccbe1* (Fig. 4a, Supplementary Movie 4).

Previous studies have described the budding of *fli1a:gfp* expressing cells from the PCV

Figure 4. *ccbe1* and *vegfc* are required for lymphangioblast budding and angiogenic sprouting from venous endothelium. A. *stabilin1:yfp* expression marks the PCV (blue bars=PCV, red bars=DA) and derived lymphangioblasts (arrows indicate bilateral cells) at 48hpf, and the lymphatic vasculature (arrowheads) and PCV at 7dpf, with progressively weakening arterial expression. *stabilin1* expressing cells fail to bud in *ccbe1* and *vegfc* morphants. **B.** Endothelial cells in the region of the horizontal myoseptum express *fli1a* (arrow) but do not sustain blood flow (asterisk, angiogram in red) (52hpf). **C.** *fli1a* positive lymphangioblasts in the region of the horizontal myospetum are migratory and contribute to the lymphatic vasculature as visualized in *kdrl:rfp*, *fli1a:gfp* double transgenic animals (arrows indicate lymphangioblasts (52hpf and 3.5dpf) and lymphatic vessels (5dpf), asterisk indicates absence of parachordal endothelial cells) (see also Supplementary Movie 4). **D.** Lymphangioblasts (*fli1a:gfp*) fail to bud and migrate in fof mutants, *vegfc* morphants, fof/plcg double morphants and *vegfc/plcg* double morphants but not in *plcg* single morphants at 48hpf. Arrows indicate lymphangioblasts, asterix indicate their absence. **E.** *tie2* is expressed in PCV sprouts in wildtype embryos which are absent in *fof* mutants, *vegfc* morphants or *plcg* morphants at 48hpf. **F.** In wildtype embryos, venous sprouts *flt1:yfp* negative at 48 hpf in *kdrl:rfp, flt1:yfp* double transgenic embryos. In *ccbe1* and *vegfc* morphants, venous sprouts are absent. Bracket indicates venous derived sprouts, arrows indicate arterial connections.

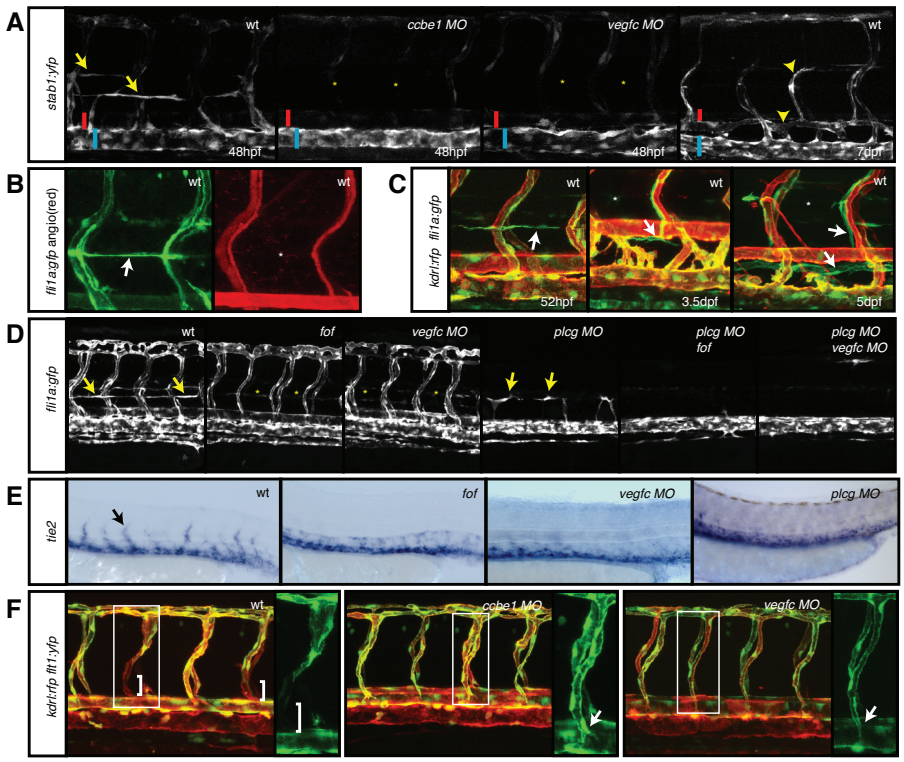

to the horizontal myoseptum to form a structure dubbed the parachordal vessel [2]. Cells from this putative vessel later migrate ventrally to form the thoracic duct [6] at the same

time as we observe movements of *stab1*^{BAC}*:yfp* expressing cells. We examined the parachordal region in detail and found that the *fli1a:gfp* expressing cells are not part of a conventional blood vessel as they do not form a vascular tube or support blood flow (Fig. 4b). Rather, by taking advantage of the absence of *kdrl:rfp* [146] expression in lymphatic vessels (Supplementary Fig. 6), we found that the majority of these cells migrate away from the horizontal myoseptum to contribute to the lymphatic vasculature in *kdrl:rfp* [23], *fli1a:gfp* double transgenic embryos (Fig. 4c, Supplementary Movie 5). Therefore, these cells do not constitute a vessel and function primarily as lymphatic vascular precursors. We hereafter refer to these cells as lymphangioblasts. We next examined *fli1a:gfp* expressing lymphangioblasts in an experimental scenario in which arteries and derivatives are absent due to loss of *phospholipase C gamma 1* (*plcg1*) function [34]. In *plcg1* morphants, *fli1a:gfp* positive lymphangioblasts clearly budded from the PCV even in the absence of intersegmental vessels, but this budding was absent in both *fof* mutants and in *vegfc* morphants (Fig. 4d).

Next, we examined the expression of the venous marker *tie2* [147]. *tie2* expression identified venous derived sprouts in wildtype embryos (48hpf) that were absent in *fof* mutants and *vegfc* morphants, however, these sprouts were also absent in *plcg* morphants selected for the presence of lymphangioblasts, indicating that they are a distinct cellular population (Fig. 4e). Hence, we investigated other venous sprouting populations by developing a double transgenic line (*flt1*^{BAC}*:yfp*, *kdrl:mem-rfp)*, which unmasks the venous or arterial origins of individual cells of the trunk vasculature. We found that the venous derived sprouts of the intersegmental vasculature were absent in *ccbe1* or *vegfc* morphants. In the absence of venous sprouts, a functional circulation was established due to increased intersegmental vessel connections with the dorsal aorta (Fig. 4f).

Taken together, these data demonstrate that, during embryogenesis, *ccbe1* and *vegfc* act at the level of both angiogenic sprouting and lymphangiogenic budding from venous endothelium. Angiogenic sprouting from the PCV to the intersegmental vessels additionally requires *plcg* function, genetically separating the two processes. The structure of *Ccbe1* suggests an extracellular role (possibly in association with the ECM) while its expression implies a requirement for *ccbe1* function along the lymphangioblast migration pathway. Alongside *vegfc* [145] and *prox1* [148,149] knockout mice, the *full of fluid* mutant represents just the third vertebrate loss-of-function mutant which leads to the specific loss of the embryonic lymphatic vasculature.

Acknowledgements

BMH was supported by an EMBO long term fellowship and an NH&MRC CJ Martin Fellowship, and JB by the Stichting Vrienden van het Hubrecht. The authors thank the Hubrecht

Screen Team, Jeroen Korving for sectioning, Rik Korswagen, Alyson MacInnes and Hans Clevers for critical reading of the manuscript.

Supplementary Information

Supplementary information, including 6 figures, 2 tables, 5 movies and supplementary mehtods can be found online at http://www.nature.com/ng/journal/v41/n4/suppinfo/ng.321_S1.html

Supplementary Table 1. DNA Oligo Sequences

Name	Sequence
z62970_fw	ACACTGTAAACCAGACGGCC
z62970_rev	TCAGTCAAGCGCACGTAATC
SNP1_fw	GCCTCCACACCTGGATAAC
SNP1_rev	CCTGGGATATTAGCTTGCAG
CA1_fw	ACTGACCCCAAACTTTTGAC
CA1_rev	CATGTCTACAGCCTGAATGC
CA2_fw	ATTTGCGTCAATGCTAACAC
CA2_rev	CAGTCTGCTCAGGTTGGAG
ccbe1_cDNA_fw1	GCGCTGAACTTCAAGACTG
ccbe_cDNA_rev1	ATCATCCTCCAGGTAGAAGC
ccbe1_cDNA_fw2	AGAAACCATATTGCCTGGAC
ccbe_cDNA_rev2	TTTGATATGCGACAGGTCAG
ccbe_cDNA_fw3	GGCTCTCCTGGACAGATG
ccbe_cDNA_rev3	ATTCAGCCTTCTTTCCTCAG
CA3_fw	CAACTTTCTGTCCCTCACAC
CA3_rev	GCGTGTCCTCATTTACTTTG
EcoRI_ccbe1_fw	GCGCGAATTCACCATGATCTACCCGGGCAGAGG
XhoI_ccbe1_rev	GCGCCTCGAGTCAAACCGGCCAATCGGGAT
stab1_gfp_fw	tgtttgttgttacatgtttatctgactaattctctggctttgagggagta ACCATGGTGAGCAAGGGCGAGGAG
stab1_neo_rev	tgaatctgtgcagtccacagtactgtaagtcccaaaacgagaagataaga TCAGAAGAACTCGTCAAGAAGGCG
stab1_ cont_fw	TGAGCGAGAAGATCAGAAGAG
stab1_cont_rev	TAAATGGCAATACCATGCTC
EcoRI_vegfc_fw	GCGCGAATTCACCATGCACTTATTTGGATTTTC
XhoI_vegfc_rev	GCGCCTCGAGTTAGTCCAGTCTTCCCCAGT
EcoRI_vegfd_fw	GCGCGAATTCACCATGAAGAAACAGAAATGTGC
XhoI_vegfd_rev	GCGCCTCGAGTCACGTATAGTGTAGTCTGT
Stab1_p_fw	CACTGATGTAGTGCTGGTTG
T3_stab1_p_rev	GGATCCATTAACCCTCACTAAAGGGAACA CAGAAGGGCTGTCAAAC

Supplementary Table 2.
Morpholino Oligo Sequences

Name	Sequence
ccbe1 ATG	CGGGTAGATCATTTCAGACACTCTG
ccbe1 splice	ACAGCACAGCACTTTACCTGTCTAC
plcg1	ATTAGCATAGGGAACTTACTTTCG
vegfc	GAAAATCCAAATAAGTGCATTTTAG

Chapter 6

General Discussion

Vertebrate genome duplication and the evolution of the vertebrate circulatory system

The evolution of a closed circulatory system is one of the key distinguishing features of vertebrates. In this thesis, we use the zebrafish as a model organism to study the development of the circulatory system. Although the study of the zebrafish vasculature has already provided important new insights into the genetic regulation of human vascular development, it is important to keep in mind that the human and zebrafish lineages diverged ~450 million years ago, and therefore are separated by 900 million years of evolution. Therefore I would like to conclude by discussing some evolutionary aspects of the circulatory system, and providing a new hypothesis on the evolution of the vascular system in early vertebrates.

In 1968, Sasumo Ohno proposed that large transitions in evolution could arise through genome duplication [152]. The argument he put forward is that most genes fulfill important roles in an organism, and therefore genetic mutations usually lead to selective disadvantages that cause the elimination of these mutations from the population. In a genome duplication event, potentially deleterious mutations are compensated for by a functional duplicate, providing a large degree of freedom for evolution to occur.
After a genome duplication event, duplicated genes can undergo several changes [153]. One of the possibilities that occurs most frequently is the loss – or pseudogenization – of one of the duplicated genes. Since two copies are present, loss of one of the copies is usually selectively neutral. There are two ways for a gene pair to escape from pseudogenization. In the first – subfunctionalization - both duplicated genes take up only part of the function of the original gene. One important case of when this occurs is in the division of a gene expression pattern. If a gene, prior to gene duplication, is expressed in two different tissues, the duplicated genes are expressed in only one of those tissues, and both copies need to be maintained. The second way to avoid pseudogenization is neofunctionalization of one of the duplicated gene copies. This in turn can lead to the development of new functions – with potentially strong selective advantages – for the organism.
The example used by Ohno used to illustrate his hypothesis was the occurrence of two rounds of whole-genome duplication at the base of the vertebrate lineage (the 2R hypothesis). Although the 2R hypothesis has been much debated, the sequencing of several vertebrate genomes has provided strong evidence that two genome duplication events indeed occurred in the vertebrate ancestor about 450 million years ago [117]. Sequencing of several fish species additionally identified a third round of genome duplication, also suggested by Ohno, at the base of the teleost radiation (3R) [154]. Most support for the

2R/3R hypothesis has been provided by the conservation of chromosomal gene order between sets (also called *Ohno*logs) of duplicated genes. Although intra- and interchromosomal rearrangements gradually erase the evidence of genome duplications, comparisons of neighboring genes in several vertebrate species allow the identification of ancient chromosomal rearrangements and the reconstruction of gene order in early vertebrates.
One example is provided in Chapter 3, where the evolutionary history of vertebrate VEGF receptors was reconstructed. Four homologous VEGF receptor genes were identified in the genomes of teleost fish (zebrafish and fugu) and several other vertebrates. Gene order within these loci is exceptionally conserved with ohnologs of several other genes also present within this locus. These include the *kit/csf1r/flt3/pdgfra/b* receptor tyrosine kinases that are evolutionary related to the VEGF receptors, the *cdx*, *gsh*, *chic* and *lnx* genes. A similar locus containing a VEGF/PDGF receptor, a *cdx* and a *chic* gene has been identified in the primitive chordate *Amphioxus*. *Amphioxus* diverged from the vertebrate lineage before the whole genome duplication events and serves as an outgroup. By comparing gene orders in several species, a hypothetical evolutionary history of this locus can be obtained. The simplest explanation of this history is provided by the 2R hypothesis combined with several segmental duplications and pseudogenization events.
Although this example is exceptional in respect to the relatively low number of chromosomal rearrangements and gene losses, similar reconstructions can be built for almost all human genes. This is important, not only in the analysis of vertebrate evolution, but also for the correct interpretation of experimental results in model organisms such as the zebrafish. Interpretations critically depend on the correct assignment of orthologs (i.e. genes in different organisms that evolved from a common ancestor through speciation). The identification of orthologs usually occurs through gene phylogenies – the reconstruction of evolution based on sequence divergence. This analysis can result in ambiguous orthology assignments, especially when there is a lineage-specific loss of one of the ohnologs. As shown in Chapter 3, the incorrect assignment of orthology for one of the zebrafish VEGF receptors, has led to confusion in the interpretation of the function of *Kdr* in vascular development. Table 1 provides several other examples of lineage-specific losses for genes involved in vascular development. In most cases the analysis of gene order (synteny analysis) results in the correct ortholog identification. As more vertebrate genome sequences from different lineages become available, it becomes likely that complete reconstructions of early vertebrate chromosomes will eventually be obtainable. Several initial reports based on currently available genome sequences have shown that this is feasible [155-158].
Although some examples were given that suggest a lineage specific loss, it is important to note that most genes known to be involved in vascular development in mammals are conserved in zebrafish. Although only a few genes have been functionally analyzed in the

Gene Family	Ohnologs in human	Ohnologs in zebrafish
VEGF receptor	*FLT1, KDR, FLT4*	*flt1, kdr, flt4, kdrl*
Nitric oxide synthase	*NOS1, NOS2, NOS3*	*nos1, nos2a, nos2b*
bHLH – Hand class	HAND1, HAND2	*hand2*
Forkhead Class C	FOXC1, FOXC2	*foxc1a, foxc1b*

Table 1. Missing orthologues of vascular specific genes. The gene missing in the respective other species is underlined. Teleost duplicates are indicated by a or b (For example, *nos2a* and *nos2b*). Lineage-specific loss of ohnologs mostly occured at the base of vertebrate evolution, before the radiation of teleost fish or land vertebrates. Exceptions are *kdrl,* which was lost during early mammalian evolution and *hand1*, which was lost in zebrafish, but not in other teleost fish.

zebrafish so far, it appears that most genes have at least a partially conserved function. In cases where orthologs are missing in the zebrafish genome this appears due to subfunctionalization of duplicated genes within the human lineage: although *Nos3* and *FoxC2* are missing in the zebrafish genome, the function of nitric oxide synthases or forkhead C class genes in the zebrafish vasculature appears conserved [159,160].

Presence of a closed vascular system is one of the defining features of vertebrates. Extant relatives of the vertebrate phylum, such as *Amphioxus* and the tunicates have a heart and some large blood vessels, but lack capillaries. Circulation occurs through body cavities without endothelial lining. The evolution of the circulatory system in early vertebrates probably occurred together with the increase in body size and resulting rise in oxygen demand. At this stage of vertebrate circulatory evolution 3 - 4 new cell types appeared (arterial, venous, lymphatic and possibly lymph-arterial cells). I hypothesize that the whole-genome duplication at the base of vertebrate evolution provided the substrate to generate these various cell types. According to this hypothesis, a closed primitive vascular system in an early vertebrate ancestor was composed of undifferentiated endothelial cells. An increase in body size led to an increase in systemic blood pressure, especially in the blood vessels closest to the heart. The first round of whole-genome duplication allowed the differentiation of two types of endothelial cells – arterial and venous. Arteries with elastic walls compensated the increase in blood pressure, whereas veins adapted to return blood to the heart along a relatively shallow pressure gradient. A further size increase of the primitive vertebrate, with accompanying increase in systemic blood pressure would cause a buildup of tissue fluid. A second round of whole-genome duplication now allowed the emergence of a second (or lymphatic) vascular system with differentiated lymphatic (and lymph-arterial) endothelial cells.

The functional divergence of *Flt1* and *Flt4* provides support for this hypothesis. Both genes are receptors for different members of the VEGF family of ligands: *Flt1* is a receptor for *Vegfa*, *Vegfb* and *Pgf*, *Flt4* is a receptor for *Vegfc* and *Vegfd* [161]. The vertebrate ancestor most likely had 2 ligands (*Vegfa/Pgf/Vegfb* and *Vegfc/d*) that could bind to one receptor.

Two rounds of whole-genome duplications resulted in the 4 receptors present in most vertebrates (Chapter 3). At least one of the receptors (Kdr) retained the ability to bind to all of the *Vegf* ligands. However, two of the receptors, *Flt1* and *Flt4*, diverged in function to bind only to one of the original ligands. The expression of *Flt1* and *Flt4* also diverged, they are mutually exclusive in the vascular system: in embryos, *Flt1* is expressed primarily in arterial endothelial cells whereas *Flt4* is expressed mostly in venous endothelial cells. As the expression of *Flt1* expands to all blood endothelial cells, *Flt4* expression becomes restricted to the lymphatic endothelial cells. *Vegfc* is required for lymphangiogenesis in the murine embryo and for lymphangiogenesis and venous angiogenesis in the zebrafish. Although *Flt4* has an additional *Vegfc* independent role during sprouting angiogenesis, its main function is to act as a *Vegfc* receptor in lymphangiogenesis. The kinase domain of *Flt*1 is only weakly active, therefore its main role is to restrict sprouting (arterial) angiogenesis by acting as a decoy receptor for *Vegfa*.

The further analysis of gene function in distantly related vertebrate model organisms such as the mouse and the zebrafish, but also of the vasculature in other vertebrate lineages and of our closest non-vertebrate relatives will lead to a more comprehensive understanding of the evolutionary history of the vertebrate circulatory system. (Un)fortunately, I was not there when it happened, but the astonishing conservation of vascular development between animals as distantly related as zebrafish and humans suggest that the evolution of the circulatory system was one of the key events in human evolution.

References

1. Lawson ND, Weinstein BM (2002) Arteries and veins: making a difference with zebrafish. Nat Rev Genet 3: 674-682.

2. Isogai S, Lawson ND, Torrealday S, Horiguchi M, Weinstein BM (2003) Angiogenic network formation in the developing vertebrate trunk. Development 130: 5281-5290.

3. Hewson WH, W (1769) An Acount of the Lymphatic System in Fish. By the Same. Philosophical Transactions of the Royal Society of London 59: 204-215.

4. Vogel WC, M (1981) Vascular specialization in fish, but no evidence for lymphatics. Zeitschrift fur Naturforschung 36C: 490-492.

5. Steffensen JF, Lomholt JP, Vogel AM (1986) In vivo observations on a specialized microvasculature, the primary and secondary vessels in fishes. Acta Zoologica 67: 193-200.

6. Yaniv K, Isogai S, Castranova D, Dye L, Hitomi J, et al. (2006) Live imaging of lymphatic development in the zebrafish. Nat Med 12: 711-716.

7. Kuchler AM, Gjini E, Peterson-Maduro J, Cancilla B, Wolburg H, et al. (2006) Development of the zebrafish lymphatic system requires VEGFC signaling. Curr Biol 16: 1244-1248.

8. Stainier DY (2001) Zebrafish genetics and vertebrate heart formation. Nat Rev Genet 2: 39-48.

9. Beis D, Bartman T, Jin SW, Scott IC, D'Amico LA, et al. (2005) Genetic and cellular analyses of zebrafish atrioventricular cushion and valve development. Development 132: 4193-4204.

10. Carradice D, Lieschke GJ (2008) Zebrafish in hematology: sushi or science? Blood 111: 3331-3342.

11. Vogeli KM, Jin SW, Martin GR, Stainier DY (2006) A common progenitor for haematopoietic and endothelial lineages in the zebrafish gastrula. Nature 443: 337-339.

12. Kissa K, Murayama E, Zapata A, Cortes A, Perret E, et al. (2008) Live imaging of emerging hematopoietic stem cells and early thymus colonization. Blood 111: 1147-1156.

13. Cha YR, Weinstein BM (2007) Visualization and experimental analysis of blood vessel formation using transgenic zebrafish. Birth Defects Res C Embryo Today 81: 286-296.

14. Isogai S, Horiguchi M, Weinstein BM (2001) The vascular anatomy of the developing zebrafish: an atlas of embryonic and early larval development. Dev Biol 230: 278-301.

15. Lawson ND, Weinstein BM (2002) In vivo imaging of embryonic vascular development using transgenic zebrafish. Dev Biol 248: 307-318.

16. Jin SW, Beis D, Mitchell T, Chen JN, Stainier DY (2005) Cellular and molecular analyses of vascular tube and lumen formation in zebrafish. Development 132: 5199-5209.

17. Kamei M, Saunders WB, Bayless KJ, Dye L, Davis GE, et al. (2006) Endothelial tubes assemble from intracellular vacuoles in vivo. Nature 442: 453-456.

18. Herzog W, Muller K, Huisken J, Stainier DY (2009) Genetic evidence for a noncanonical function of seryl-tRNA synthetase in vascular development. Circ Res 104: 1260-1266.

19. Roman BL, Pham VN, Lawson ND, Kulik M, Childs S, et al. (2002) Disruption of acvrl1 increases endothelial cell number in zebrafish cranial vessels. Development 129: 3009-3019.

20. Cross LM, Cook MA, Lin S, Chen JN, Rubinstein AL (2003) Rapid analysis of angiogenesis drugs in a live fluorescent zebrafish assay. Arterioscler Thromb Vasc Biol 23: 911-912.

21. Jin SW, Beis D, Mitchell T, Chen JN, Stainier DY (2005) Cellular and molecular analyses of vascular tube and lumen formation in zebrafish. Development.

22. Choi J, Dong L, Ahn J, Dao D, Hammerschmidt M, et al. (2007) FoxH1 negatively modulates flk1 gene expression and vascular formation in zebrafish. Dev Biol 304: 735-744.

23. Chi NC, Shaw RM, De Val S, Kang G, Jan LY, et al. (2008) Foxn4 directly regulates tbx2b expression and atrioventricular canal formation. Genes Dev 22: 734-739.

24. Blum Y, Belting HG, Ellertsdottir E, Herwig L, Luders F, et al. (2008) Complex cell rearrangements during intersegmental vessel sprouting and vessel fusion in the zebrafish embryo. Dev Biol 316: 312-322.

25. Zhu H, Traver D, Davidson AJ, Dibiase A, Thisse C, et al. (2005) Regulation of the lmo2 promoter during hematopoietic and vascular development in zebrafish. Dev Biol 281: 256-269.

26. Motoike T, Loughna S, Perens E, Roman BL, Liao W, et al. (2000) Universal GFP reporter for the study of vascular development. Genesis 28: 75-81.

27. Long Q, Meng A, Wang H, Jessen JR, Farrell MJ, et al. (1997) GATA-1 expression pattern can be recapitulated in living transgenic zebrafish using GFP reporter gene. Development 124: 4105-4111.

28. Traver D, Paw BH, Poss KD, Penberthy WT, Lin S, et al. (2003) Transplantation and in vivo imaging of multilineage engraftment in zebrafish bloodless mutants. Nat Immunol 4: 1238-1246.

29. Huang CJ, Tu CT, Hsiao CD, Hsieh FJ, Tsai HJ (2003) Germline transmission of a myocardium-specific GFP transgene reveals critical regulatory elements in the cardiac myosin light chain 2 promoter of zebrafish. Dev Dyn 228: 30-40.

30. Mably JD, Mohideen MA, Burns CG, Chen JN, Fishman MC (2003) heart of glass regulates the concentric growth of the heart in zebrafish. Curr Biol 13: 2138-2147.

31. Hsu K, Traver D, Kutok JL, Hagen A, Liu TX, et al. (2004) The pu.1 promoter drives myeloid gene expression in zebrafish. Blood 104: 1291-1297.

32. Stainier DY, Fouquet B, Chen JN, Warren KS, Weinstein BM, et al. (1996) Mutations affecting the formation and function of the cardiovascular system in the zebrafish em-

bryo. Development 123: 285-292.
33. Chen JN, Haffter P, Odenthal J, Vogelsang E, Brand M, et al. (1996) Mutations affecting the cardiovascular system and other internal organs in zebrafish. Development 123: 293-302.
34. Lawson ND, Mugford JW, Diamond BA, Weinstein BM (2003) phospholipase C gamma-1 is required downstream of vascular endothelial growth factor during arterial development. Genes Dev 17: 1346-1351.
35. Jin SW, Herzog W, Santoro MM, Mitchell TS, Frantsve J, et al. (2007) A transgene-assisted genetic screen identifies essential regulators of vascular development in vertebrate embryos. Dev Biol 307: 29-42.
36. Habeck H, Odenthal J, Walderich B, Maischein H, Schulte-Merker S (2002) Analysis of a zebrafish VEGF receptor mutant reveals specific disruption of angiogenesis. Curr Biol 12: 1405-1412.
37. Lawson ND, Vogel AM, Weinstein BM (2002) sonic hedgehog and vascular endothelial growth factor act upstream of the Notch pathway during arterial endothelial differentiation. Dev Cell 3: 127-136.
38. Covassin LD, Siekmann AF, Kacergis MC, Laver E, Moore JC, et al. (2009) A genetic screen for vascular mutants in zebrafish reveals dynamic roles for Vegf/Plcg1 signaling during artery development. Dev Biol 329: 212-226.
39. Siekmann AF, Lawson ND (2007) Notch signalling limits angiogenic cell behaviour in developing zebrafish arteries. Nature 445: 781-784.
40. Siekmann AF, Covassin L, Lawson ND (2008) Modulation of VEGF signalling output by the Notch pathway. Bioessays 30: 303-313.
41. Torres-Vazquez J, Gitler AD, Fraser SD, Berk JD, Van NP, et al. (2004) Semaphorin-plexin signaling guides patterning of the developing vasculature. Dev Cell 7: 117-123.
42. Alvarez Y, Cederlund ML, Cottell DC, Bill BR, Ekker SC, et al. (2007) Genetic determinants of hyaloid and retinal vasculature in zebrafish. BMC Dev Biol 7: 114.
43. Anderson MJ, Pham VN, Vogel AM, Weinstein BM, Roman BL (2008) Loss of unc45a precipitates arteriovenous shunting in the aortic arches. Dev Biol 318: 258-267.
44. David L, Mallet C, Mazerbourg S, Feige JJ, Bailly S (2007) Identification of BMP9 and BMP10 as functional activators of the orphan activin receptor-like kinase 1 (ALK1) in endothelial cells. Blood 109: 1953-1961.
45. Park SO, Lee YJ, Seki T, Hong KH, Fliess N, et al. (2008) ALK5- and TGFBR2-independent role of ALK1 in the pathogenesis of hereditary hemorrhagic telangiectasia type 2. Blood 111: 633-642.
46. Knoll R, Postel R, Wang J, Kratzner R, Hennecke G, et al. (2007) Laminin-alpha4 and integrin-linked kinase mutations cause human cardiomyopathy via simultaneous defects in cardiomyocytes and endothelial cells. Circulation 116: 515-525.
47. Buchner DA, Su F, Yamaoka JS, Kamei M, Shavit JA, et al. (2007) pak2a mutations cause cerebral hemorrhage in redhead zebrafish. Proc Natl Acad Sci U S A 104: 13996-14001.
48. Liu J, Fraser SD, Faloon PW, Rollins EL, Vom Berg J, et al. (2007) A betaPix Pak2a signaling pathway regulates cerebral vascular stability in zebrafish. Proc Natl Acad Sci U S A 104: 13990-13995.
49. Santoro MM, Samuel T, Mitchell T, Reed JC, Stainier DY (2007) Birc2 (clap1) regulates endothelial cell integrity and blood vessel homeostasis. Nat Genet 39: 1397-1402.
50. Pendeville H, Winandy M, Manfroid I, Nivelles O, Motte P, et al. (2008) Zebrafish Sox7 and Sox18 function together to control arterial-venous identity. Dev Biol 317: 405-416.
51. Weinstein BM, Stemple DL, Driever W, Fishman MC (1995) Gridlock, a localized heritable vascular patterning defect in the zebrafish. Nat Med 1: 1143-1147.
52. Zhong TP, Rosenberg M, Mohideen MA, Weinstein B, Fishman MC (2000) gridlock, an HLH gene required for assembly of the aorta in zebrafish. Science 287: 1820-1824.
53. Leslie JD, Ariza-McNaughton L, Bermange AL, McAdow R, Johnson SL, et al. (2007) Endothelial signalling by the Notch ligand Delta-like 4 restricts angiogenesis. Development 134: 839-844.
54. Lawson ND, Scheer N, Pham VN, Kim CH, Chitnis AB, et al. (2001) Notch signaling is required for arterial-venous differentiation during embryonic vascular development. Development 128: 3675-3683.
55. Childs S, Chen JN, Garrity DM, Fishman MC (2002) Patterning of angiogenesis in the zebrafish embryo. Development 129: 973-982.
56. Fukui H, Hanaoka R, Kawahara A (2009) Noncanonical activity of seryl-tRNA synthetase is involved in vascular development. Circ Res 104: 1253-1259.
57. Labauge P, Denier C, Bergametti F, Tournier-Lasserve E (2007) Genetics of cavernous angiomas. Lancet Neurol 6: 237-244.
58. Hilder TL, Malone MH, Bencharit S, Colicelli J, Haystead TA, et al. (2007) Proteomic identification of the cerebral cavernous malformation signaling complex. J Proteome Res 6: 4343-4355.
59. Voss K, Stahl S, Schleider E, Ullrich S, Nickel J, et al. (2007) CCM3 interacts with CCM2 indicating common pathogenesis for cerebral cavernous malformations. Neurogenetics 8: 249-256.
60. Zawistowski JS, Serebriiskii IG, Lee MF, Golemis EA, Marchuk DA (2002) KRIT1 association with the integrin-binding protein ICAP-1: a new direction in the elucidation of cerebral cavernous malformations (CCM1) pathogenesis. Hum Mol Genet 11: 389-396.
61. Zawistowski JS, Stalheim L, Uhlik MT, Abell AN, Ancrile BB, et al. (2005) CCM1 and CCM2 protein interactions in cell signaling: implications for cerebral cavernous malformations pathogenesis. Hum Mol Genet 14: 2521-2531.
62. Zhang J, Clatterbuck RE, Rigamonti D, Chang DD, Dietz

HC (2001) Interaction between krit1 and icap1alpha infers perturbation of integrin beta1-mediated angiogenesis in the pathogenesis of cerebral cavernous malformation. Hum Mol Genet 10: 2953-2960.

63. Gunel M, Laurans MS, Shin D, DiLuna ML, Voorhees J, et al. (2002) KRIT1, a gene mutated in cerebral cavernous malformation, encodes a microtubule-associated protein. Proc Natl Acad Sci U S A 99: 10677-10682.

64. Beraud-Dufour S, Gautier R, Albiges-Rizo C, Chardin P, Faurobert E (2007) Krit 1 interactions with microtubules and membranes are regulated by Rap1 and integrin cytoplasmic domain associated protein-1. FEBS J 274: 5518-5532.

65. Glading A, Han J, Stockton RA, Ginsberg MH (2007) KRIT-1/CCM1 is a Rap1 effector that regulates endothelial cell cell junctions. J Cell Biol 179: 247-254.

66. Whitehead KJ, Plummer NW, Adams JA, Marchuk DA, Li DY (2004) Ccm1 is required for arterial morphogenesis: implications for the etiology of human cavernous malformations. Development 131: 1437-1448.

67. Mably JD, Chuang LP, Serluca FC, Mohideen MA, Chen JN, et al. (2006) santa and valentine pattern concentric growth of cardiac myocardium in the zebrafish. Development 133: 3139-3146.

68. Amsterdam A, Nissen RM, Sun Z, Swindell EC, Farrington S, et al. (2004) Identification of 315 genes essential for early zebrafish development. Proc Natl Acad Sci U S A 101: 12792-12797.

69. Bussmann J, Bakkers J, Schulte-Merker S (2007) Early endocardial morphogenesis requires Scl/Tal1. PLoS Genet 3: e140.

70. Thompson MA, Ransom DG, Pratt SJ, MacLennan H, Kieran MW, et al. (1998) The cloche and spadetail genes differentially affect hematopoiesis and vasculogenesis. Dev Biol 197: 248-269.

71. Covassin L, Amigo JD, Suzuki K, Teplyuk V, Straubhaar J, et al. (2006) Global analysis of hematopoietic and vascular endothelial gene expression by tissue specific microarray profiling in zebrafish. Dev Biol 299: 551-562.

72. Turner DL, Weintraub H (1994) Expression of achaete-scute homolog 3 in Xenopus embryos converts ectodermal cells to a neural fate. Genes Dev 8: 1434-1447.

73. Ho RK, Kane DA (1990) Cell-autonomous action of zebrafish spt-1 mutation in specific mesodermal precursors. Nature 348: 728-730.

74. Shaner NC, Campbell RE, Steinbach PA, Giepmans BN, Palmer AE, et al. (2004) Improved monomeric red, orange and yellow fluorescent proteins derived from Discosoma sp. red fluorescent protein. Nat Biotechnol 22: 1567-1572.

75. Sehnert AJ, Huq A, Weinstein BM, Walker C, Fishman M, et al. (2002) Cardiac troponin T is essential in sarcomere assembly and cardiac contractility. Nat Genet 31: 106-110.

76. Murayama E, Kissa K, Zapata A, Mordelet E, Briolat V, et al. (2006) Tracing hematopoietic precursor migration to successive hematopoietic organs during zebrafish development. Immunity 25: 963-975.

77. Denier C, Gasc JM, Chapon F, Domenga V, Lescoat C, et al. (2002) Krit1/cerebral cavernous malformation 1 mRNA is preferentially expressed in neurons and epithelial cells in embryo and adult. Mech Dev 117: 363-367.

78. Petit N, Blecon A, Denier C, Tournier-Lasserve E (2006) Patterns of expression of the three cerebral cavernous malformation (CCM) genes during embryonic and postnatal brain development. Gene Expr Patterns 6: 495-503.

79. Seker A, Pricola KL, Guclu B, Ozturk AK, Louvi A, et al. (2006) CCM2 expression parallels that of CCM1. Stroke 37: 518-523.

80. le Noble F, Moyon D, Pardanaud L, Yuan L, Djonov V, et al. (2004) Flow regulates arterial-venous differentiation in the chick embryo yolk sac. Development 131: 361-375.

81. Olson EN (2006) Gene regulatory networks in the evolution and development of the heart. Science 313: 1922-1927.

82. Lough J, Sugi Y (2000) Endoderm and heart development. Dev Dyn 217: 327-342.

83. Kattman SJ, Huber TL, Keller GM (2006) Multipotent flk-1(+) cardiovascular progenitor cells give rise to the cardiomyocyte, endothelial, and vascular smooth muscle lineages. Dev Cell 11: 723-732.

84. Schultheiss TM, Burch JB, Lassar AB (1997) A role for bone morphogenetic proteins in the induction of cardiac myogenesis. Genes Dev 11: 451-462.

85. Nemer G, Nemer M (2002) Cooperative interaction between GATA5 and NF-ATc regulates endothelial-endocardial differentiation of cardiogenic cells. Development 129: 4045-4055.

86. Cohen-Gould L, Mikawa T (1996) The fate diversity of mesodermal cells within the heart field during chicken early embryogenesis. Dev Biol 177: 265-273.

87. Lee RK, Stainier DY, Weinstein BM, Fishman MC (1994) Cardiovascular development in the zebrafish. II. Endocardial progenitors are sequestered within the heart field. Development 120: 3361-3366.

88. Keegan BR, Meyer D, Yelon D (2004) Organization of cardiac chamber progenitors in the zebrafish blastula. Development 131: 3081-3091.

89. Chen JN, Fishman MC (1996) Zebrafish tinman homolog demarcates the heart field and initiates myocardial differentiation. Development 122: 3809-3816.

90. Glickman NS, Yelon D (2002) Cardiac development in zebrafish: coordination of form and function. Semin Cell Dev Biol 13: 507-513.

91. Stainier DY, Lee RK, Fishman MC (1993) Cardiovascular development in the zebrafish. I. Myocardial fate map and heart tube formation. Development 119: 31-40.

92. Yelon D, Horne SA, Stainier DY (1999) Restricted expression of cardiac myosin genes reveals regulated aspects of heart tube assembly in zebrafish. Dev Biol 214: 23-37.

93. Drake CJ, Fleming PA (2000) Vasculogenesis in the day 6.5 to 9.5 mouse embryo. Blood 95: 1671-1679.

94. Gering M, Yamada Y, Rabbitts TH, Patient RK (2003) Lmo2 and Scl/Tal1 convert non-axial mesoderm into haemangioblasts which differentiate into endothelial cells in the absence of Gata1. Development 130: 6187-6199.
95. Shivdasani RA, Mayer EL, Orkin SH (1995) Absence of blood formation in mice lacking the T-cell leukaemia oncoprotein tal-1/SCL. Nature 373: 432-434.
96. Robb L, Lyons I, Li R, Hartley L, Kontgen F, et al. (1995) Absence of yolk sac hematopoiesis from mice with a targeted disruption of the scl gene. Proc Natl Acad Sci U S A 92: 7075-7079.
97. Visvader JE, Fujiwara Y, Orkin SH (1998) Unsuspected role for the T-cell leukemia protein SCL/tal-1 in vascular development. Genes Dev 12: 473-479.
98. Patterson LJ, Gering M, Patient R (2005) Scl is required for dorsal aorta as well as blood formation in zebrafish embryos. Blood 105: 3502-3511.
99. Dooley KA, Davidson AJ, Zon LI (2005) Zebrafish scl functions independently in hematopoietic and endothelial development. Dev Biol 277: 522-536.
100. Juarez MA, Su F, Chun S, Kiel MJ, Lyons SE (2005) Distinct roles for SCL in erythroid specification and maturation in zebrafish. J Biol Chem 280: 41636-41644.
101. Prince VE, Moens CB, Kimmel CB, Ho RK (1998) Zebrafish hox genes: expression in the hindbrain region of wild-type and mutants of the segmentation gene, valentino. Development 125: 393-406.
102. Liao EC, Paw BH, Oates AC, Pratt SJ, Postlethwait JH, et al. (1998) SCL/Tal-1 transcription factor acts downstream of cloche to specify hematopoietic and vascular progenitors in zebrafish. Genes Dev 12: 621-626.
103. Detrich HW, 3rd, Kieran MW, Chan FY, Barone LM, Yee K, et al. (1995) Intraembryonic hematopoietic cell migration during vertebrate development. Proc Natl Acad Sci U S A 92: 10713-10717.
104. Lieschke GJ, Oates AC, Paw BH, Thompson MA, Hall NE, et al. (2002) Zebrafish SPI-1 (PU.1) marks a site of myeloid development independent of primitive erythropoiesis: implications for axial patterning. Dev Biol 246: 274-295.
105. Kalev-Zylinska ML, Horsfield JA, Flores MV, Postlethwait JH, Vitas MR, et al. (2002) Runx1 is required for zebrafish blood and vessel development and expression of a human RUNX1-CBF2T1 transgene advances a model for studies of leukemogenesis. Development 129: 2015-2030.
106. Liao W, Bisgrove BW, Sawyer H, Hug B, Bell B, et al. (1997) The zebrafish gene cloche acts upstream of a flk-1 homologue to regulate endothelial cell differentiation. Development 124: 381-389.
107. Song HD, Sun XJ, Deng M, Zhang GW, Zhou Y, et al. (2004) Hematopoietic gene expression profile in zebrafish kidney marrow. Proc Natl Acad Sci U S A 101: 16240-16245.
108. Berdougo E, Coleman H, Lee DH, Stainier DY, Yelon D (2003) Mutation of weak atrium/atrial myosin heavy chain disrupts atrial function and influences ventricular morphogenesis in zebrafish. Development 130: 6121-6129.
109. Dong PD, Munson CA, Norton W, Crosnier C, Pan X, et al. (2007) Fgf10 regulates hepatopancreatic ductal system patterning and differentiation. Nat Genet 39: 397-402.
110. Lejeune F, Maquat LE (2005) Mechanistic links between nonsense-mediated mRNA decay and pre-mRNA splicing in mammalian cells. Curr Opin Cell Biol 17: 309-315.
111. Chang CP, Neilson JR, Bayle JH, Gestwicki JE, Kuo A, et al. (2004) A field of myocardial-endocardial NFAT signaling underlies heart valve morphogenesis. Cell 118: 649-663.
112. Ema M, Takahashi S, Rossant J (2006) Deletion of the selection cassette, but not cis-acting elements, in targeted Flk1-lacZ allele reveals Flk1 expression in multipotent mesodermal progenitors. Blood 107: 111-117.
113. Motoike T, Markham DW, Rossant J, Sato TN (2003) Evidence for novel fate of Flk1+ progenitor: contribution to muscle lineage. Genesis 35: 153-159.
114. Rottbauer W, Just S, Wessels G, Trano N, Most P, et al. (2005) VEGF-PLCgamma1 pathway controls cardiac contractility in the embryonic heart. Genes Dev 19: 1624-1634.
115. Covassin LD, Villefranc JA, Kacergis MC, Weinstein BM, Lawson ND (2006) Distinct genetic interactions between multiple Vegf receptors are required for development of different blood vessel types in zebrafish. Proc Natl Acad Sci U S A 103: 6554-6559.
116. Patterson LJ, Gering M, Eckfeldt CE, Green AR, Verfaillie CM, et al. (2006) The transcription factors, Scl and Lmo2, act together during development of the haemangioblast in zebrafish. Blood.
117. Dehal P, Boore JL (2005) Two rounds of whole genome duplication in the ancestral vertebrate. PLoS Biol 3: e314.
118. Ferrier DE, Dewar K, Cook A, Chang JL, Hill-Force A, et al. (2005) The chordate ParaHox cluster. Curr Biol 15: R820-822.
119. Duret L, Chureau C, Samain S, Weissenbach J, Avner P (2006) The Xist RNA gene evolved in eutherians by pseudogenization of a protein-coding gene. Science 312: 1653-1655.
120. Cooper DW (1993) X-inactivation in marsupials and monotremes. Seminars in Developmental Biology 4: 117-128.
121. van Nes J, de Graaff W, Lebrin F, Gerhard M, Beck F, et al. (2006) The Cdx4 mutation affects axial development and reveals an essential role of Cdx genes in the ontogenesis of the placental labyrinth in mice. Development 133: 419-428.
122. Ema M, Faloon P, Zhang WJ, Hirashima M, Reid T, et al. (2003) Combinatorial effects of Flk1 and Tal1 on vascular and hematopoietic development in the mouse. Genes Dev 17: 380-393.
123. Sugi Y, Markwald RR (1996) Formation and early morphogenesis of endocardial endothelial precursor cells and the role of endoderm. Dev Biol 175: 66-83.
124. Serbedzija GN, Chen JN, Fishman MC (1998) Regulation in the heart field of zebrafish. Development 125: 1095-1101.
125. Hsieh PC, Davis ME, Lisowski LK, Lee RT (2006) Endothe-

lial-cardiomyocyte interactions in cardiac development and repair. Annu Rev Physiol 68: 51-66.

126. Saharinen P, Tammela T, Karkkainen MJ, Alitalo K (2004) Lymphatic vasculature: development, molecular regulation and role in tumor metastasis and inflammation. Trends Immunol 25: 387-395.

127. Alitalo K, Carmeliet P (2002) Molecular mechanisms of lymphangiogenesis in health and disease. Cancer Cell 1: 219-227.

128. Vogel WO (1981) [Structure and principles of organization of the vascular system in bony fishes]. Gegenbaurs Morphol Jahrb 127: 772-784.

129. Steffensen JF, Lomholt JP (1992) The Secondary Vascular System. In: Hoar WS, Randall DJ, Farrell AP, editors. Fish Physiology. San Diego: Academic Press, Inc. . pp. 185-217.

130. Isogai S, Hitomi J, Yaniv K, Weinstein BM (2009) Zebrafish as a new animal model to study lymphangiogenesis. Anat Sci Int.

131. Hogan BM, Bos FL, Bussmann J, Witte M, Chi NC, et al. (2009) Ccbe1 is required for embryonic lymphangiogenesis and venous sprouting. Nat Genet 41: 396-398.

132. Griesbeck O, Baird GS, Campbell RE, Zacharias DA, Tsien RY (2001) Reducing the environmental sensitivity of yellow fluorescent protein. Mechanism and applications. J Biol Chem 276: 29188-29194.

133. Balciunas D, Wangensteen KJ, Wilber A, Bell J, Geurts A, et al. (2006) Harnessing a high cargo-capacity transposon for genetic applications in vertebrates. PLoS Genet 2: e169.

134. Alitalo K, Tammela T, Petrova TV (2005) Lymphangiogenesis in development and human disease. Nature 438: 946-953.

135. Srinivasan RS, Dillard ME, Lagutin OV, Lin FJ, Tsai S, et al. (2007) Lineage tracing demonstrates the venous origin of the mammalian lymphatic vasculature. Genes Dev 21: 2422-2432.

136. Collod-Beroud G, Beroud C, Ades L, Black C, Boxer M, et al. (1998) Marfan Database (third edition): new mutations and new routines for the software. Nucleic Acids Res 26: 229-223.

137. Wilson BD, Ii M, Park KW, Suli A, Sorensen LK, et al. (2006) Netrins promote developmental and therapeutic angiogenesis. Science 313: 640-644.

138. Navankasattusas S, Whitehead KJ, Suli A, Sorensen LK, Lim AH, et al. (2008) The netrin receptor UNC5B promotes angiogenesis in specific vascular beds. Development 135: 659-667.

139. Prevo R, Banerji S, Ni J, Jackson DG (2004) Rapid plasma membrane-endosomal trafficking of the lymph node sinus and high endothelial venule scavenger receptor/homing receptor stabilin-1 (FEEL-1/CLEVER-1). J Biol Chem 279: 52580-52592.

140. Salmi M, Koskinen K, Henttinen T, Elima K, Jalkanen S (2004) CLEVER-1 mediates lymphocyte transmigration through vascular and lymphatic endothelium. Blood 104: 3849-3857.

141. Banerji S, Ni J, Wang SX, Clasper S, Su J, et al. (1999) LYVE-1, a new homologue of the CD44 glycoprotein, is a lymph-specific receptor for hyaluronan. J Cell Biol 144: 789-801.

142. Makinen T, Veikkola T, Mustjoki S, Karpanen T, Catimel B, et al. (2001) Isolated lymphatic endothelial cells transduce growth, survival and migratory signals via the VEGF-C/D receptor VEGFR-3. Embo J 20: 4762-4773.

143. Kukk E, Lymboussaki A, Taira S, Kaipainen A, Jeltsch M, et al. (1996) VEGF-C receptor binding and pattern of expression with VEGFR-3 suggests a role in lymphatic vascular development. Development 122: 3829-3837.

144. Veikkola T, Jussila L, Makinen T, Karpanen T, Jeltsch M, et al. (2001) Signalling via vascular endothelial growth factor receptor-3 is sufficient for lymphangiogenesis in transgenic mice. Embo J 20: 1223-1231.

145. Karkkainen MJ, Haiko P, Sainio K, Partanen J, Taipale J, et al. (2004) Vascular endothelial growth factor C is required for sprouting of the first lymphatic vessels from embryonic veins. Nat Immunol 5: 74-80.

146. Bussmann J, Lawson N, Zon L, Schulte-Merker S (2008) Zebrafish VEGF receptors: a guideline to nomenclature. PLoS Genet 4: e1000064.

147. Lyons MS, Bell B, Stainier D, Peters KG (1998) Isolation of the zebrafish homologues for the tie-1 and tie-2 endothelium-specific receptor tyrosine kinases. Dev Dyn 212: 133-140.

148. Wigle JT, Harvey N, Detmar M, Lagutina I, Grosveld G, et al. (2002) An essential role for Prox1 in the induction of the lymphatic endothelial cell phenotype. Embo J 21: 1505-1513.

149. Wigle JT, Oliver G (1999) Prox1 function is required for the development of the murine lymphatic system. Cell 98: 769-778.

150. Herpers R, van de Kamp E, Duckers HJ, Schulte-Merker S (2008) Redundant roles for sox7 and sox18 in arteriovenous specification in zebrafish. Circ Res 102: 12-15.

151. Wienholds E, Schulte-Merker S, Walderich B, Plasterk RH (2002) Target-selected inactivation of the zebrafish rag1 gene. Science 297: 99-102.

152. Ohno S, Wolf U, Atkin NB (1968) Evolution from fish to mammals by gene duplication. Hereditas 59: 169-187.

153. Zhang J (2003) Evolution by gene duplication: an update. Trends Ecol Evol 18: 292-298.

154. Postlethwait JH (2007) The zebrafish genome in context: ohnologs gone missing. J Exp Zoolog B Mol Dev Evol 308: 563-577.

155. Kohn M, Hogel J, Vogel W, Minich P, Kehrer-Sawatzki H, et al. (2006) Reconstruction of a 450-My-old ancestral vertebrate protokaryotype. Trends Genet 22: 203-210.

156. Naruse K, Tanaka M, Mita K, Shima A, Postlethwait J, et al. (2004) A medaka gene map: the trace of ancestral vertebrate proto-chromosomes revealed by comparative gene mapping. Genome Res 14: 820-828.

157. Kasahara M, Naruse K, Sasaki S, Nakatani Y, Qu W, et al. (2007) The medaka draft genome and insights into vertebrate

genome evolution. Nature 447: 714-719.
158. Jaillon O, Aury JM, Brunet F, Petit JL, Stange-Thomann N, et al. (2004) Genome duplication in the teleost fish Tetraodon nigroviridis reveals the early vertebrate proto-karyotype. Nature 431: 946-957.
159. De Val S, Chi NC, Meadows SM, Minovitsky S, Anderson JP, et al. (2008) Combinatorial regulation of endothelial gene expression by ets and forkhead transcription factors. Cell 135: 1053-1064.
160. North TE, Goessling W, Peeters M, Li P, Ceol C, et al. (2009) Hematopoietic stem cell development is dependent on blood flow. Cell 137: 736-748.
161. Olsson AK, Dimberg A, Kreuger J, Claesson-Welsh L (2006) VEGF receptor signalling - in control of vascular function. Nat Rev Mol Cell Biol 7: 359-371.

Samenvatting in het Nederlands

De bloedcirculatie bij de mens bestaat uit het hart, het bloed en de bloedvaten. Samen met de lymfevaten vormen deze componenten een orgaansysteem dat al vanaf het vroegste begin essentieel is voor de overleving en groei van het mensenlijk embryo. In dit proefschrift worden verschillende aspecten van de ontwikkeling van dit orgaansysteem onderzocht. Hiervoor is gebruik gemaakt van een relatief nieuw onderzoeksmodel: de zebravis.

De zebravis is een kleine, van oorsprong Indiase vis die veel in aquaria wordt gehouden. Een volwassen zebravis is ongeveer 3-4 cm groot, met kenmerkende donkerblauwe strepen die in lengterichting over het lichaam lopen. Sinds de jaren tachtig wordt de zebravis gebruikt als modelorganisme in de biologie. Een van de voornaamste redenen om de zebravis hiervoor uit te kiezen was het gemak om zebravissen te kweken: een paartje zebravissen produceert tot 1000 eitjes per week die binnen 2-3 maanden uitgroeien tot geslachtsrijpe visjes. Ze stellen weinig eisen aan voedsel en leefomgeving waardoor grote aantallen goedkoop te houden zijn. Maar waarschijnlijk de voornaamste reden - zeker in vergelijking met andere modelorganismen zoals bijvoorbeeld de muis - is dat zebravis-eitjes buiten het lichaam bevrucht worden. Bovendien zijn zebravis-embryos doorzichtig, waardoor vanaf het allereerste begin de ontwikkeling onder een microscoop gevolgd kan worden. Die ontwikkeling gaat ook nog eens razendsnel: binnen een dag zijn de eerste organen gevormd, en na een dag of 5 zorgt een zebravisembryo voor zijn eigen voedsel.

Deze eigenschappen maken de zebravis tot een ideaal organisme om de ontwikkeling van het hart- en vaatsysteem te bestuderen. Ondanks dat het onderzoek naar het hart en vaatsysteem bij zebravissen nog in de kinderschoenen staat, zijn er al verschillende belangrijke ontdekkingen gedaan. Zo is bijvoorbeeld bij zebravissen ontdekt hoe slagaders en aders zich tijdens de vroegste ontwikkeling van elkaar onderscheiden en hoe de allereerste bloedvaten van een rij cellen een doorlopende buis – het bloedvat – vormen. Op dit moment is de zebravis het enige modelsysteem waarbij de groei van bloedvaten in 'real time' gevolgd kan worden.

In dit proefschrift worden verschillende nieuwe ontdekkingen beschreven Zo gaat hoofdstuk 4 over een zebravis waarin voor het eerst in een levend dier de slagaders, aders en lymfevaten onderscheiden kunnen worden. Dit wordt gedaan door twee verschillend gekleurde lichtgevende eiwitten, rood en groen, in de bloedvaten te laten produceren. De ene (groen) wordt in alle vaten gemaakt, terwijl de andere (rood) op verschillende niveaus in slagaders (hoog niveau), aders (laag niveau) en lymfevaten (niet) wordt geproduceerd. Hierbij ontdekten we een nieuw soort vaten in volwassen zebravissen die het rode eiwit op middelmatig niveau maken. Deze vaten vormen een directe verbindingen tussen slag-

aders en lymfevaten – iets unieks bij vissen.
De andere hoofdstukken gaan vooral over de rol van specifieke genen bij de vorming van het hart en vaatstelsel. In hoofdstuk 2 wordt de functie van de zogenaamde *CCM*-genen bestudeerd. Mensen met een mutatie in één van deze genen hebben een aanleg om op willekeurige plaatsen in het lichaam extreem verwijde bloedvaten te maken. Deze 'caverneuse malformaties' vormen vooral in de hersenen een probleem omdat ze instabiel zijn en kunnen leiden tot hersenbloedingen. We hebben ontdekt dat wanneer deze genen in de zebravis compleet worden uitgeschakeld, alle bloedvaten extreem verwijden. De bloedvatcellen in deze embryos vormen normale contacten met elkaar, maar lijken uitgerekt te worden. We tonen hierbij voor het eerst aan dat het probleem ontstaat in de bloedvatcellen zelf, en niet in de cellen eromheen.
In hoofdstuk 3 wordt de functie van het gen *TAL1* bestudeerd. Mutaties die ervoor zorgen dat dit eiwit te veel wordt geproduceerd komen vaak voor bij acute T-cell leukemie bij kinderen. Zebravissen waarin dit gen is uitgeschakeld hebben een erg sterk defect aan het hart- en vaatstelsel. Ze vormen geen bloed en er is geen onderscheid tussen de slagaders en aders. We ontdekten bovendien dat dit gen een rol speelt bij de vroege hartontwikkeling. In het eerste begin bestaat het hart uit 2 buizen om elkaar heen: een binnenste 'bloedvatlaag' en een buitenste 'spierlaag'. In de zebravisembryos die dit gen missen wordt de spierlaag wel gevormd, maar bestaat de bloedvatlaag niet uit een buis, maar uit een klomp cellen die een soort plug in het hart vormt. Hierdoor wordt bovendien de vorming van de spierlaag beïnvloed, waardoor we de interactie tussen de beide cellagen kunnen bestuderen.
In hoofdstuk 5 tenslotte, wordt de vorming van het lymfevatsysteem in de zebravis bestudeerd. We hebben een zebravis gemaakt waarbij de lymfevatcellen een geel lichtgevend eiwit maken. Hierdoor kunnen we voor het eerst op celniveau de vorming van de lymfevaten in het embryo bestuderen. Bovendien hebben we een tot dusver onbekend gen, *CCBE1*, ontdekt dat essentieel is voor de vorming van de lymfevaten. Zonder dit gen ontbreken de lymfevaten en een aantal aderen compleet. Het eiwit waarvoor dit gen codeert wordt gemaakt door cellen die zich rondom de vormende lymfevaten bevinden, het lijkt er dus op dat het eiwit een signaalstof is om de groei van lymfevaten en adervorming te reguleren, maar verder onderzoek zal moeten uitwijzen wat dit eiwit precies doet. Aangezien de groei van lymfevaten een belangrijke factor vormt bij het uitzaaien van kanker, is *CCBE1* een interessante kandidaat om met medicijnen te remmen. De verwachting is dan dat met zo'n medicijn de groei van lymfevaten stopt, waardoor een tumor niet meer via de lymfe uit kan zaaien.
Onderzoek naar het vaatsysteem in de zebravis staat tussen fundamenteel biologisch en direct geneeskundig gericht onderzoek in. In het onderzoek beschreven in dit proefschrift wordt de onbevooroordeelde aanpak van de genetica, zoals die gebruikt wordt in

bijvoorbeeld fruitvliegen, toegepast op een onderwerp dat direct medische relevantie heeft, maar het is belangrijk te benadrukken dat dit onderzoek nog aan de basis van de toepassing staat. De weg van de ontdekking van een nieuw gen tot de ontwikkeling van een nieuw medicijn of nieuwe therapie is lang, al lijkt dat traject iets te verbeteren.
Tijdens dit onderzoek heb ik me vaak verbaasd hoeveel overeenkomsten er bestaan tussen het vaatsysteem van de mens en de zebravis. Dit terwijl maar liefst 450 miljoen jaar geleden leefden onze laatste gemeenschappelijke voorouders. Toch kan van de meeste bloed- en lymfevaten in de mens een directe kopie in de zebravis gevonden worden. Ook spelen bijna alle genen waarvan bekend is dat deze belangrijk zijn voor de bloedvatvorming bij mensen een vergelijkbare rol bij zebravissen. Waarschijnlijk wordt deze bijzondere overeenkomst veroorzaakt door de essentiële rol die het hart- en vaatsysteem speelt al tijdens de vroegste ontwikkeling. Genetische afwijkingen hebben hierdoor veel minder kans om van de ene generatie op de andere te worden over gedragen, waardoor de evolutie van dit systeem relatief langzaam verloopt.
De zebravis biedt een unieke kans om de vorming van een compleet vaatsysteem cel voor cel en gen voor gen te bestuderen. Belangrijk daarvoor is vooral de mogelijkheid om individuele bloedvatcellen in een levend dier te kunnen volgen. De ontwikkelingen in de microscopie van de laatste jaren maken het nu ook mogelijk om individuele eiwitten binnen of buiten een cel te gaan volgen, waardoor het complexe gedrag van bloedvatcellen op eiwitniveau verklaard kan gaan worden. Tegelijkertijd kunnen we op dit moment de rol van alle genen tegelijkertijd gaan bestuderen om zo een compleet beeld te krijgen van zowel het hele systeem als de rol van de individuele eiwitten. Naar mijn mening zal dit gaan leiden tot belangrijke nieuwe ontdekkingen over de groei van het vaatsysteem en daarmee tot nieuwe toepassingen. Daarbij bedoel ik niet alleen nieuwe medicijnen om vaatgroei te remmen (om bijvoorbeeld tumorgroei te remmen) of te bevorderen (bijvoorbeeld om de bloedcirulatie bij diabetes patiënten te verbeteren), maar ook manieren om het bloedvatsysteem van complete organen in een kweekschaaltje te laten onstaan.

Dankwoord/Acknowledgements

Bladerend door oude proefschiften viel me op dat sommige personen zelden worden genoemd in een dankwoord. Personen die misschien wel de belangrijkste rol spelen in het tot stand komen van een proefschift, al is het vaak ver voor de uiteindelijke promotieplechtigheid. Om ooit te promoveren heb je namelijk allereerst goede, maar vooral inspirerende leraren nodig. Leraren die de nieuwsgierigheid prikkelen waardoor je gefascineerd raakt door de wetenschap en je 4 (of 5) jaar in een heel specifiek onderwerp wil gaan verdiepen. Om deze reden wil ik allereerst Rob Wijting, scheikundeleraar op De Heemgaard, bedanken. Een tweede persoon die ik wil noemen is Henri Stroband, docent ontwikkelingsbiologie aan de unversiteit van Wageningen. Zijn colleges hebben ervoor gezorgd dat ik gefascineerd ben geraakt door de embryologie en speciaal de ontwikkelingsgenetica. Natuurlijk mijn mentoren tijdens afstuderen, Astrid Keijser en Freek van Eeden van het Hubrecht Instituut, die mij de technische kneepjes van het werken met zebravissen hebben bijgebracht en Lisa Steiner van het MIT in Boston, for the stimulation and confidence to follow my own curiosity.

Daarnaast wil ik mijn collega's bedanken, zowel voor de samenwerking als voor de persoonlijke sfeer die promoveren op het Hubrecht Instituut tot zo'n bijzondere ervaring maken. Hopelijk blijft die sfeer gehandhaafd bij de uitbreiding van het instituut. Een aantal mensen wil ik speciaal noemen. Om te beginnen, Stefan, thanks for the opportunity to pursue my PhD in your group, and for the freedom you gave me. Ben, I really enjoyed our many scientific discussions, I am really happy that my defense was just in time before you and Kelly move back to Australia, so you can be one of my 'paranimfen'! Mijn andere 'roommates', Kirsten, voor de vrolijkheid die je met je meebrengt en Robert, voor je veelzijdigheid. Frank, jij hoort ook in dit rijtje, bedankt voor je positivisme en voor de goede samenwerking het afgelopen jaar. Ellen, bedankt voor je vriendschap en advies. Ive, voor de gezelligheid. Evisa, voor je medeleven en Josi, voor je technische tips en persoonlijke woorden. Youri, bedankt voor je inzet tijdens je stage. Bedankt Claudia, Marko, Merlijn, Terhi, Chrissy, Leonie, Jo, Andreas en de andere (ex-) collega's en studenten van het Schulte-Merker lab, de mensen van de andere groepen op het Hubrecht Instituut, met name Fiona, Adele, Chris, John, Vince, Appie, Judith, Marjo en zover niet genoemd, de vrijdagmiddag-borrelaars voor de wekelijkse gezelligheid! Erma, Bert, Rob en de andere dierverzorgers, bedankt voor de super-vissen!

Ten slotte wil ik vrienden en (schoon-)familie bedanken voor jullie belangstelling in mijn onderzoek, en omdat jullie mijn leven naast het lab zo geweldig maken. Maurice, bedankt voor je vriendschap, super dat je een van mijn paranimfen bent! Paul en Marja, ik weet dat jullie trots zijn, bedankt voor de rol die jullie hebben gespeeld om mij zover te brengen, en omdat jullie er altijd voor me zijn.

En als laatste de liefste, Aline, mijn steun en toeverlaat. Je bent er geweest om mijn enthousiasme te delen bij een nieuwe ontdekking - ook al kwam die om 3 uur 's nachts! - en voor relativering bij een mislukte proef. De wetenschap is natuurlijk een beetje een vreemde wereld, en jij houdt me met twee benen in de echte. Bovendien heb je me met Luci het grootste cadeau gegeven dat ik me ooit heb kunnen wensen. Ik vind het fantastisch dat je met me meegaat om met z'n drietjes aan een nieuw avontuur in Duitsland te beginnen!

Curriculum Vitae

Jeroen Bussmann werd op 6 september 1981 geboren in Eindhoven. In 1998 behaalde hij zijn VWO diploma op "De Heemgaard" te Apeldoorn. In hetzelfde jaar begon hij de studie Bioprocestechnologie aan de Landbouwuniversiteit Wageningen. Bij zijn eerste afstudeerstage op het Hubrecht Instituut heeft hij onderzoek gedaan naar de ontwikkeling van het hart van de zebravis onder supervisie van Dr. Freek van Eeden. Zijn tweede afstudeerstage heeft hij gedaan bij op het Massachusetts Institute of Technology in Boston, USA, waar hij onderzoek heeft gedaan naar het immuunsysteem van de zebravis, onder supervisie van Prof. Lisa Steiner. In de herfst van 2003 behaalde hij zijn doctoraal diploma, in de specialisatie cellulaire en moleculaire wetenschappen. Op 1 november 2003 begon hij aan zijn promotie-onderzoek onder begeleiding van Dr. Stefan Schulte-Merker. De resultaten van dit onderzoek staan beschreven in dit proefschrift. Vanaf Januari 2010 zal hij gaan werken als postdoc in de groep van Dr. Arndt Siekmann aan het Max Planck Institute for Molecular Medicine in Muenster.

List of Publications

Hogan BM, **Bussmann J***, Bos FL*, Witte M*, Chi NC, Duckers HJ, and Schulte-Merker S (2009) ccbe1 is required for embryonic lymphangiogenesis and venous sprouting. Nat Genet 41(4):396-398
*equal contribution

Bussmann J, Lawson N, Zon L, Schulte-Merker S and Zebrafish Nomenclature Committee (2008) Zebrafish VEGF receptors: a guideline to nomenclature. PLoS Genet 4(5):e1000064

Hogan BM, **Bussmann J**, Wolburg H and Schulte-Merker S. (2008) ccm1 cell autonomously regulates endothelial cellular morphogenesis and vascular tubulogenesis in zebrafish. Hum Mol Genet 17(16):2424-2432

Smith KA, Chocron S, von der Hardt S, de Pater E, Soufan A, **Bussmann J**, Schulte-Merker S, Hammerschmidt M and Bakkers, J. (2008) Rotation and asymmetric development of the zebrafish heart requires directed migration of cardiac progenitor cells. Dev Cell 14(2):287-297

Besser J, Bagowski CP, Salas-Vidal E, van Hemert MJ, **Bussmann J**, and Spaink HP (2007) Expression analysis of the family of 14-3-3 proteins in zebrafish development. Gene Expr Patterns 7(4):511-520

Bussmann J, Bakkers J, and Schulte-Merker S (2007) Early Endocardial Morphogenesis Requires Scl/Tal1. PLoS Genet 3(8):e140

Bussmann J*, Danilova N*, Jekosch K and Steiner LA (2005) The immunoglobulin heavy-chain locus in zebrafish: identification and expression of a previously unknown isotype, immunoglobulin Z. Nat Immunol 6(3):295-302
* equal contribution

Meijer AH, Verbeek FJ, Salas-Vidal E, Corredor-Adámez M, **Bussmann J**, van der Sar AM, Otto GW, Geisler R and Spaink HP (2005) Transcriptome profiling of adult zebrafish at the late stage of chronic tuberculosis due to Mycobacterium marinum infection. Mol Immunol 42(10):1185-1203

Cover: Processed confocal micrograph of adult skin from a double transgenic zebrafish (*flt1^{enh}:rfp* | *fli1a:gfp*). Arteries in red, lymphatics in green, veins in a color in between. Invitation: confocal micrograph of embryonic brain vasculature (3dpf) from a double transgenic zebrafish (*flt1^{enh}:rfp* | *kdrl:gfp*), dorsal view. Arteries in red/yellow, veins in green.

Printed by: DPP digital printing